UNIVERSITAT POLITÈCNICA DE VALÈNCIA

Desarrollo y evaluación de nuevos métodos de automatización de experimentos con *C. elegans* basados en visión activa

(Development and evaluation of new methods for automating experiments with C. elegans *based on active vision)*

TESIS DOCTORAL

Joan Carles Puchalt

Director

Antonio José Sánchez Salmerón

Septiembre 2021

To my wife, my family and my thesis director

ACKNOWLEDGMENTS

Aunque minúscula, nuestra contribución al mundo y a la historia puede ser significativa con la suma de todas las buenas acciones de miles de personas. Esta creencia hace avanzar al Ser Humano hacia un futuro mejor.

Gracias a Sussane Ayed y mi familia por su gran y querido apoyo, a mis compañeros y a Antonio Sánchez por ser un guía y ayuda fundamental en este fantástico desafío.

RESUMEN

Esta tesis se centra en el desarrollo de nuevas técnicas automatizadas que permiten inspeccionar nematodos *Caenorhabidits elegans* (*C. elegans*) en placas de Petri estándar, para el análisis de sus comportamientos. *C. elegans* es un nemátodo de 1mm de longitud, con el cual se pueden realizar distintos experimentos para analizar los efectos de fármacos, compuestos o alteraciones genéticas en su longevidad, su salud física o su cognición. El campo principal metodológico del presente trabajo para el análisis de esos efectos es la visión por computador; y con ello, el desarrollo completo del sistema de visión activo: sistema de iluminación inteligente, sistema de captura óptimo, procesamiento de las imágenes para detección y clasificación de nematodos. Los campos secundarios en esta investigación son el control y robotización.

Los *C. elegans* son animales sensibles a la luz y por ello el primero de los métodos está en la rama de la iluminación inteligente, con el cual se permite regular la intensidad y las longitudes de onda de la luz que reciben los nematodos. El siguiente método es el procesado para la detección y clasificación de movimiento a partir de las imágenes obtenidas con esa iluminación controlada. Tener el ambiente controlado es fundamental, los nematodos son muy sensibles a las condiciones ambientales por lo que puede alterarse su actividad biológica, y con ello los resultados, así que el tercer método es la integración de las técnicas en un nuevo dispositivo que permite automatizar ensayos de lifespan y validar los resultados automáticos comparándolos con los manuales. El movimiento del animal es clave para poder realizar inferencias estadísticas que puedan mostrar tendencias en sus comportamientos, por ello la estimulación automatizada que provoque una reacción de su movilidad es el cuarto de los métodos. Por último, el aumento de la resolución en las imágenes muestra mayor detalle, mejorando el procesamiento y extracción de características. El quinto método es un robot multivista que posibilita tomar imágenes a distintas resoluciones, lo que permite mantener el seguimiento global de los gusanos, al mismo tiempo que se toman imágenes con un encuadre de mayor detalle del nematodo objetivo.

RESUM

Esta tesi doctoral se centra en el desentrollament de noves tècniques automatitzades que permeten inspeccionar nemàtodes *Caenorhabidits elegans* (*C. elegans*) en plaques de Petri estàndar, per a l'anàlisi dels seus comportaments. *C. elegans* és un nemàtode d'1mm de llargària, ab el qual se poden realitzar distints experiments per a analitzar els efectes de fàrmacs, composts o alteracions genètiques en sa longevitat, la seua salut física o la seua cognició. El camp principal metodològic del present treball per a l'anàlisi d'eixos efectes és la visió per computador; i ab açò, el desentrollament complet del sistema de visió actiu: sistema d'il.luminació inteligent, sistema de captura òptim, processament de les imàtgens per a detecció i classificació de nematode. Els camps secundaris en esta investigació són el control i robotització.

Els *C. elegans* són animals sensibles a la llum i por ello el primer dels mètodes està en la branca de la il.luminació intel.ligent, ab el qual es permet regular la intensitat i les longituds d'ona de la llum que reben els nematodes. El següent mètode és el processat per a la detecció i classificació de moviment a partir de les imàtgens obtinguda ab eixa il.luminació controlada. Tindre l'ambient controlat és fonamental, els nemàtodes són molt sensibles a les condicions ambientals per lo que pot alterar-se la seua activitat biològica, i ab aço els resultats, aixina que el tercer mètode és la integració de les tècniques en un nou dispositiu que permet automatitzar ensajos de lifespan i validar els resultats automàtics comparant-los ab els manuals. El moviment de l'animal és clau per a poder realitzar inferencies estadístiques que puguen mostrar tendències en el seus comportaments, per això la estimulació automatitzada que provoque una reacció de la seua mobilitat és el quart dels mètodes. Per últim, l'augment de la resolució en les imàtgens mostra major detall, millorant el processament i extracció de característiques. El quint mètode és un robot multivista que possibilita prendre imàtgens a distintes resolucions, lo que permet mantindre el seguiment global dels cucs, al mateix temps que se prenguen imàtgens ab un enquadrament de major detall del nematode objectiu.

ABSTRACT

This thesis focuses on the development of new automated techniques that allow the inspection of *Caenorhabidits elegans* nematodes (*C. elegans*) in Petri dishes, for the analysis of their behavior. This nematode is a 1mm long worm, with which different experiments can be carried out to analyze the effects of drugs, compounds or genetic alterations on its longevity, physical health or cognition. The main methodological field of the present work for the analysis of these effects is computer vision; and with it, the complete development of the active vision system: intelligent lighting system, optimal capture system, image processing for detection and classification of nematodes. The secondary fields in this research are control and robotization.

C. elegans are light-sensitive animals and therefore the first method is in the field of intelligent lighting, with which it is possible to regulate the intensity and wavelength of the light that nematodes receive. The next method is the processing for the detection and classification of movement from the images obtained with that controlled lighting. Having a controlled environment is essential, worms are very sensitive to environmental conditions so it can alter biological activity, and with it the results, so the third method is the integration of techniques in a new device that allows automating tests of lifespan and validate the automatic results comparing them with the manual ones. The movement of the animal is key to be able to carry out statistical conferences that can show trends in its behaviors, therefore the automated stimulation that causes a reaction of its mobility is the fourth of the methods. Finally, increasing the resolution in the images shows greater detail, improving the processing and extraction of features. The fifth method is a multiview robot that enables images to be taken at different resolutions, allowing global tracking of worms to be maintained, while at the same time taking images with a more detailed frame of the target worm.

INDEX

UNIVERSITAT POLITÈCNICA DE VALÈNCIA

CHAPTER 1
INTRODUCTION

HISTORY

Introduction to *C. elegans*

Why is it interesting to research with C. elegans?

C. elegans is a nematode, about 1 mm in length. They are inexpensive to maintain and can be grown in vast quantities in the lab. Today this nematode is the world's best understood animal. The genome has been mapped and sequenced. They have many tissues and organs that are present in higher organisms, such as the nervous system, digestive tract, motor (muscles), and reproductive system. These tissues and organs can be easily monitored *in vivo*, using optical methods, because they are transparent throughout their sort life cycle (less than three weeks). They also exhibit behaviours that are modulated by their environment as well as experience. It has since proven to be exquisitely sensitive to its environment, displaying remarkable behavioural plasticity.

Due to these characteristics, *C. elegans* has emerged as one of the premiere model systems in many research fields, including aging, neurobiology and even rudimentary forms of learning. The ease with which *C. elegans* can be grown, manipulated and observed has driven research into new areas and 'the worm' has been a silent collaborator in three Nobel prizes, and thousands of research articles over the last years. Future developments in optical methods will continue to enrich our knowledge and understanding of how biological pathways orchestrate development, learning, memory, behaviour and aging.

How are research labs working with C. elegans nowadays?

Nowadays, most of the research labs cultured *C. elegans* in standard Petri plates, which must be maintained in incubators around 20ºC (depending of the strain). *C. elegans* work in research labs consists of many different processes, such as, (1) autoclaving liquids to avoid contamination, (2) preparing different medias (M9, NGM, HGM, etc.), (3) pipetting M9 or pouring NGM in standard Petri plates, (4) seeding *E. Coli* OP50 on NGM,

(5) chunking plates, (6) transporting plates between incubators and different processing zones, (7) Egg Prep for *C. elegans* synchronization, (8) preparing conditions (9) placing synchronized *C. elegans* in experimental plates, (10) picking and placing *C. elegans,* (11) counting, fixing and monitoring *C. elegans* manually on some microscopes (Fig. 0.1), etc.

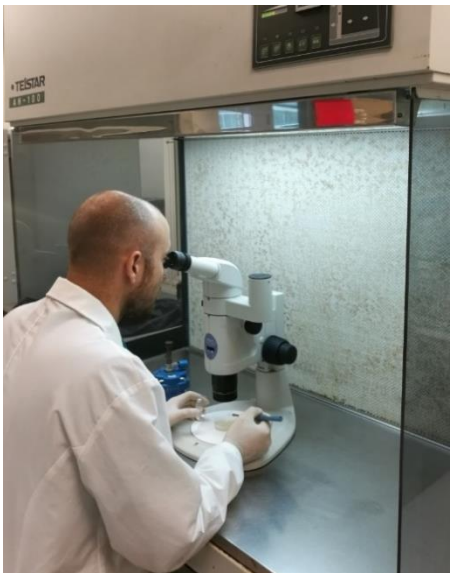

Figure 0.1.- *C. elegans* manual monitoring

Research labs around the world are developing their *C. elegans* experiments mostly manually by experts. However, processes related to handing and monitoring *C. elegans* individually are very time-consuming. Many different assays have been defined based on Petri plates.

Use of C. elegans to study lifespan

Lifespan assays are used for aging analysis. The lifespan assay consists of counting alive worms every day to get survivals curves over time. In lifespan assays, you have to poke each worm on the head to test if is alive. Different synchronized populations (same age) are prepared to which different compounds or genetic modifications are applied, which are called conditions. The survival of these conditions is compared to make statistical analyzes, in order to find, or not, significant statistical differences. In this way, the causes that can alter the survival of these animals can be found, and thus be able to design experiments on other higher animals. Ideally you need less than one hundred, preferably closer to two hundred for each condition. With multiple conditions, mutants etc., it becomes a considerable undertaking. Hence, automation is an attractive proposition. As well as saving researcher time, automated technology also promises objectivity, constant monitoring, and other measures of aging such as decline in movement over time (healthspan). Therefore, research

teams are trying to develop new protocols and tools for automating these processes.

C. elegans research is a young discipline where there is a need of developing mature technologies and using new standards for automating all these processes.

There are different research groups that work with *C. elegans*, one of them is in a company called, ADM Biopolis. We carry out a collaboration project[1] with Biopolis for whom we automate processes. The Cell Biology Laboratory of ADM Biopolis initiated us in the manual processes that they carry out, they provided us with the strains and those who carried out the manual experiments in parallel with which we could evaluate the results.

Use of C. elegans to study healthspan

Another factor that measures health is quality of life, healthspan. To measure healthspan, the nematode movement, factors such as amount of movement and coordination, are evaluated. The amount of movement is usually measured by counting the thrashing number in one minute (in a liquid medium), and good coordination can be related to a greater distance traveled from the origin. This movement degradation can be due to aging, muscular or neurodegenerative problems. Certain compounds or genetic alterations can be the cause of these diseases; therefore, the movement factors of different nematode populations are compared to observe if there are significant statistical differences, and in this way deduce if a certain condition affects the animal health.

The manual inspection of these experiments is even more tedious than the lifespan inspection, since the expert has to be counting the thrashings per minute for each nematode. And on the other hand, observing its initial and final position is difficult if there are no marks in the medium. We have carried out a collaborative project[2] with Health Research La Fe, in order to design new automation methods that can improve the inspection and

[1] Smartfoods CIEN project (in collaboration with Biopolis S. L.) (2014-2017): the goal is to develop an automated C. elegans monitoring system.
[2] CONOCE project (in collaboration with La Fe University and Polytechnic Hospital) (2019-2022): the goal is to develop an automated C. elegans monitoring system.

analysis of these experiments. This research group has provided us with *C. elegans*, experimentation protocols and manual validation.

OBJECTIVES

One of the thesis goals is to carry out a search for the state of the art of experiments with *C. elegans*, the biological factors that affect them and the automated methods that exist to carry out these experiments.

Once this search has been carried out, analyze what are the shortcomings of the existing automated methods, in order to find new methods that improve these techniques or create new ones, always taking into account the biological factors of the nematodes.

Another goal is to analyze, design, develop and validate new automation techniques with special attention to the most complex test, the lifespan, and to try to make the new capture methods flexible to be able to carry out other types of tests such as healthspan, learning and memory and cognitive function. In short, to open new lines that allow perfecting the automation of tests with *C. elegans*.

STRUCTURE

This thesis has the format of an articles compendium, four articles published and one in the revision stage, which correspond to chapter 2, where each one is a section. The articles are complete as they have been published, with the exception of the bibliography, which, in order not to duplicate references, has all been included in the last section of the chapter.

The document is divided into four chapters, the first is the introduction in which the description of the problem is presented. The second is the articles, which is divided into five sections corresponding to the five articles:

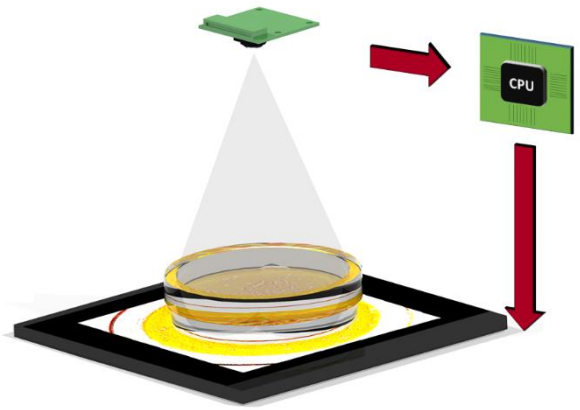

Paper 1: This paper uses a lighting matrix (in our experimentation a display) to illuminate the Petri dishes. This lighting matrix has RGB pixels, so we can illuminate each point with a wavelength (R, G, B) and an intensity. In this way, each nematode receives the type of lighting that we want, being able to be very flexible and thus carry out a wide range of experimentation possibilities. *C. elegans* are sensitive to light, higher intensity or exposure and shorter wavelengths, animals become stressed and even their life is reduced. Therefore, in our study we focus on lighting with a minimum intensity necessary to be able to capture images.

Puchalt JC, Sánchez-Salmerón AJ, Martorell Guerola P, Genovés Martínez S (2019) Active backlight for automating visual monitoring: An analysis of a lighting control technique for Caenorhabditis elegans cultured on standard Petri plates. PLOS ONE 14(4): e0215548. https://doi.org/10.1371/journal.pone.0215548

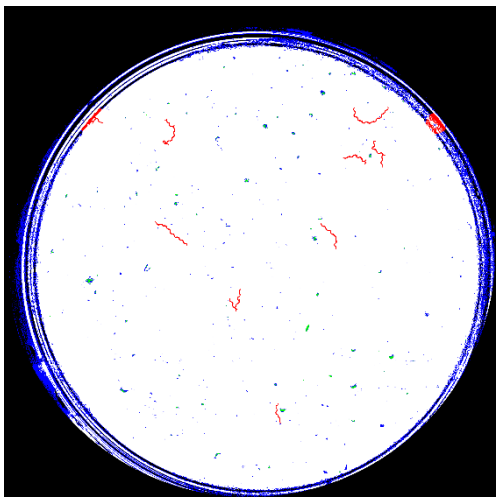

Paper 2: In this paper, the previous type of lighting is applied and image processing techniques are developed to automate lifespan experiments. Lifespan experiments measure survival with a sampling period over time until an entire sample of animals dies. So, an algorithm is developed for the detection of nematodes and their alive or dead classification, in order to be able to give as a result survival curves.

Puchalt, J.C., Sánchez-Salmerón, AJ., Ivorra, E. *et al.* Improving lifespan automation for *Caenorhabditis elegans* by using image processing and a post-processing adaptive data filter. *Sci Rep* **10,** 8729 (2020). https://doi.org/10.1038/s41598-020-65619-4

Paper 3: *C. elegans* are very sensitive to environmental conditions such as light or temperature. That is why we carried out an integration of the previous methods in a new device that allows to automate the lifespan test. In this we take the automated survival curves and the traditional manual curves that a laboratory technician produces, to validate the results and check that there are no alterations in the biological activity of the animals.

Puchalt, J.C., Sánchez-Salmerón, AJ., Ivorra, E. *et al*. Small flexible automated system for monitoring *Caenorhabditis elegans* lifespan based on active vision and image processing techniques. Sci Rep **11**, 12289 (2021). https://doi.org/10.1038/s41598-021-91898-6

Paper 4: Movement is essential to be able to detect *C. elegans* and classify them as alive or dead. Manually, the technician

conducting the experiments touches them with a spike and that causes a flight reaction. In order to perform an equivalent and effective stimulation, we apply vibration on the plate that makes the animals move to flee. This can lead to problems due to memory and adaptation.

Puchalt, J.C.; Layana Castro, P.E.; Sánchez-Salmerón, A.-J. Reducing Results Variance in Lifespan Machines: An Analysis of the Influence of Vibrotaxis on Wild-Type *Caenorhabditis elegans* for the Death Criterion. *Sensors* **2020**, *20*, 5981. https://doi.org/10.3390/s20215981

Paper 5: There are very subtle features and movements that require a higher resolution in the image. On the other hand, the study in 55mm Petri dishes gives the animals more freedom in movement, but at the same time it does not make it possible to capture images of nematodes with high resolution. For this reason, we designed a new method that allows images to be taken at different resolutions, a high-resolution one that frames a nematode and a low-resolution one that captures the entire Petri dish. This simultaneous double capture enables image sequences of a nematode to be captured in high resolution, while tracking all worms on the plate at low resolution.

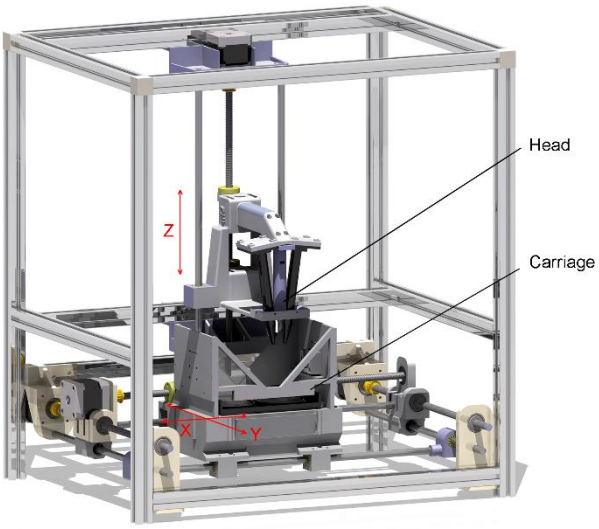

Puchalt, J.C.; Gonzalez-Rojo, J.F.; Gómez-Escribano, A.P.; Vázquez-Manrique, R.P.; Sánchez-Salmerón, A.-J. Multi-view cartesian robot-based movement tracking to monitor *Caenorhabditis elegans* Healthspan in standard Petri dishes.

The last chapters (3 and 4) are respectively **discussion** of all the results in a global way and **conclusions**.

RELATED WORKS

Other works (three articles) have been published in which the author of this Thesis has participated, but not as the main author, and therefore these manuscripts are not part of the thesis, although we are going to name them in this section. Another related work is a patent application, with reference P202130492, of the multi-view robot described in paper 5.

The three articles are based on image processing, which improve the detection and classification techniques of *C. elegans*. For these works, the images were captured with the described techniques in the articles that make up this doctoral thesis.

The first article improves the traditional method for obtaining the skeleton:

"*This is a challenge given the marked flexibility that their bodies present and the different poses that can be performed during their behaviour individually, which become even more complicated when worms aggregate with others while moving. This work proposes a simple solution by combining some computer vision techniques to help to determine certain worm poses and to identify each one during aggregation or in coiled shapes. This new method is based on the distance transformation function to obtain better worm skeletons. Experiments were performed with 205 plates, each with 10, 15, 30, 60 or 100 worms, which totals 100,000 worm poses approximately. A comparison of the proposed method was made to a classic skeletonisation method to find that 2196 problematic poses had improved by between 22% and 1% on average in the pose predictions of each worm.*"

Layana Castro, P.E., Puchalt, J.C. & Sánchez-Salmerón, AJ. Improving skeleton algorithm for helping *Caenorhabditis elegans* trackers. *Sci Rep* **10,** 22247 (2020). https://doi.org/10.1038/s41598-020-79430-8

The second article improves the first one in the skeleton detection for overlapping cases: *"Automatic tracking of* Caenorhabditis elegans *(*C. egans*) in standard Petri dishes is challenging due to high-resolution image*

requirements when fully monitoring a Petri dish, but mainly due to potential losses of individual worm identity caused by aggregation of worms, overlaps and body contact. To date, trackers only automate tests for individual worm behaviors, canceling data when body contact occurs. However, essays automating contact behaviors still require solutions to this problem. In this work, we propose a solution to this difficulty using computer vision techniques. On the one hand, a skeletonization method is applied to extract skeletons in overlap and contact situations. On the other hand, new optimization methods are proposed to solve the identity problem during these situations. Experiments were performed with 70 tracks and 3779 poses (skeletons) of C. elegans*. Several cost functions with different criteria have been evaluated, and the best results gave an accuracy of 99.42% in overlapping with other worms and noise on the plate using the modified skeleton algorithm and 98.73% precision using the classical skeleton algorithm."*

Layana Castro, P.E.; Puchalt, J.C.; García Garví, A.; Sánchez-Salmerón, A.-J. *Caenorhabditis elegans* Multi-Tracker Based on a Modified Skeleton Algorithm. *Sensors* **2021**, *21*, 5622. https://doi.org/10.3390/s21165622

The third uses neural networks to classify *C. elegans* as dead/live: *"Moreover, determining whether a worm is alive or dead can be complex as they barely move during the last few days of their lives. This paper proposes a method combining traditional computer vision techniques with a live/dead* C. elegans *classifier based on convolutional and recurrent neural networks from low-resolution image sequences. In addition to proposing a new method to automate lifespan, the use of data augmentation techniques is proposed to train the network in the absence of large numbers of samples. The proposed method achieved small error rates (3.54% ± 1.30% per plate) with respect to the manual curve, demonstrating its feasibility."*

García Garví, A.; Puchalt, J.C.; Layana Castro, P.E.; Navarro Moya, F.; Sánchez-Salmerón, A.-J. Towards Lifespan Automation for *Caenorhabditis elegans* Based on Deep Learning: Analysing Convolutional and Recurrent Neural Networks for Dead or Live Classification. *Sensors* **2021**, *21*, 4943. https://doi.org/10.3390/s21144943

CHAPTER 2
PAPERS

Paper 1:

Puchalt JC, Sánchez-Salmerón AJ, Martorell Guerola P, Genovés Martínez S (2019) Active backlight for automating visual monitoring: An analysis of a lighting control technique for *Caenorhabditis elegans* cultured on standard Petri plates. PLOS ONE 14(4): e0215548. https://doi.org/10.1371/journal.pone.0215548

Paper 2:

Puchalt, J.C., Sánchez-Salmerón, AJ., Ivorra, E. *et al.* Improving lifespan automation for *Caenorhabditis elegans* by using image processing and a post-processing adaptive data filter. *Sci Rep* **10,** 8729 (2020). https://doi.org/10.1038/s41598-020-65619-4

Paper 3:

Puchalt, J.C., Sánchez-Salmerón, AJ., Ivorra, E. *et al.* Small flexible automated system for monitoring *Caenorhabditis elegans* lifespan based on active vision and image processing techniques. Sci Rep **11**, 12289 (2021). https://doi.org/10.1038/s41598-021-91898-6

Paper 4:

Puchalt, J.C.; Layana Castro, P.E.; Sánchez-Salmerón, A.-J. Reducing Results Variance in Lifespan Machines: An Analysis of the Influence of Vibrotaxis on Wild-Type *Caenorhabditis elegans* for the Death Criterion. *Sensors* **2020**, *20*, 5981. https://doi.org/10.3390/s20215981

Paper 5:

Puchalt, J.C.; Gonzalez-Rojo, J.F.; Gómez-Escribano, A.P.; Vázquez-Manrique, R.P.; Sánchez-Salmerón, A.-J. Multi-view cartesian robot-based movement tracking to monitor *Caenorhabditis elegans* Healthspan in standard Petri dishes.

Paper bibliography

PAPER 1

Active backlight for automating visual monitoring: an analysis of a lighting control technique for *Caenorhabditis elegans* cultured on standard Petri plates

Joan Carles Puchalt[1], Antonio-José Sánchez-Salmerón[1]*, Patricia Martorell Guerola[2], Salvador Genovés Martínez[2]

[1] Universitat Politecnica de Valencia, Instituto de Automatica e Informatica Industrial, Valencia, Spain

[2] Cell Biology Laboratory/ADM Nutrition/Biopolis SL/Archer Daniels Midland, Paterna, Valencia, Spain

Puchalt JC, Sánchez-Salmerón AJ, Martorell Guerola P, Genovés Martínez S (2019) Active backlight for automating visual monitoring: *An analysis of a lighting control technique for Caenorhabditis elegans cultured on standard Petri plates*. PLOS ONE 14(4): e0215548. https://doi.org/10.1371/journal.pone.0215548

Abstract

Lifespan and healthspan machines can undergo *C. elegans* image segmentation errors due to changes in lighting conditions, which produce non-uniform images. Most *C. elegans* monitoring machines use backlight techniques based on the transparency of both the container and media. Backlight illumination obtains high-contrast images with dark *C. elegans* and a bright background. However, changes in illumination or media transparency conditions can produce non-uniform images, which are currently alleviated by image processing techniques. Besides, these machines should avoid *C. elegans* exposure to light as much as possible because light stresses worms, and can even affect their lifespan, mainly when using (1) long exposure times, (2) high intensities or (3) wavelengths that come close to ultraviolet. However, if short exposure of worms to light is required for visual monitoring, then light can also be used as a movement stimulus. In this paper, an active backlight method is analysed. The proposed method consists of controlling the light intensities and wavelengths of an illumination dots matrix with PID regulators. These

regulators adapt illumination to some changing conditions. The experimental results shows that this method simplifies the image segmentation problem because it is able to automatically compensate not only changes in media transparency throughout assay days, but also changes in ambient conditions, such as smooth condensation on the lid and light derivatives of the illumination source during its lifetime. In addition, the strategic application of wavelengths could be adapted for the requirements of each assay. For instance, a specific control strategy has been proposed to minimise stress to worms and trying to stimulate *C. elegans* movement in lifespan assays.

Introduction

The tiny nematode worm *Caenorhabditis elegans* (*C. elegans*) offers us a window into biology because they allow researchers to track in vivo biological events [1], [2]. The ease with which *C. elegans* can be grown, manipulated and observed has driven research to new areas.

Different in vivo assays can be run in which *C. elegans* models are used to analyse their phenotypes, through which toxicity factors can be inferred to certain compounds, such as therapeutic factors to some neurodegenerative diseases, alterations in ageing, etc. As part of this wide variety of assays, two models interest us, Lifespan and Healhspan, for which the motility phenotype is the most widely observed. The Lifespan model [3]–[10] measures the survival percentage of samples submitted to different conditions to infer which factors alter life expectancy. Survival is determined by worm movement existence (life) or its lack of movement after poking (death). In the particular case of the lifespan assay with *C. elegans*, it is known that maximum life is about 3 weeks, and lasts a few weeks more for some strains, which make experiments shorter than for other animals. Healthspan [11]–[13] studies the nematode life quality by observing animal motility features. Reduced movement or its lack of coordination can be due to causes such as ageing, neurodegenerative diseases, intoxication, muscle problems, etc. These assays need about 100 specimens per condition, which entails a huge workload for researchers to

handle them, count them and measure their features. In addition, some of these tasks have to be done daily, which means arduous work. This is why a need arises to automate these assays. Apart from saving researcher time, automated technology also promises objectivity, constant monitoring and new measures of worm features.

There are a number of researcher groups worldwide that are developing new technologies to automate *C. elegans* monitoring tasks. Each technology uses a different methodology, but the common subject is to detect worm movement by imaging at the mesoscale level when monitoring standard Petri plates completely [14]–[17].

Full automation of lifespan and healthspan experiments is a challenging problem because the images captured during assays can present spatial and temporal variability. Spatial variability in an image can be due to different *Escherichia coli* or tested compound concentrations, contaminated areas, lint from the outside on caps (which can adopt quite similar shapes to worms), light refractions on Petri walls, etc. Despite worms' short lifespans, temporal variability remains for various reasons: biological changes (worms feeding, worms defecation, worm tracks, *E. coli* growth, contamination, etc.), changes in temperature (agar evaporation, internal condensations on lids, etc.) and derivatives from devices (illumination derivatives, differences in Petri plate location on different days, sensor sensitivity changes, etc.). The present study pays attention to the *C. elegans* segmentation problem on standard Petri plates, which are due mainly to: (1) medium changes; (2) internal condensations on lids; (3) illumination source derivatives. These variations in lighting conditions could affect the image quality in some areas, and could imply losing some information that might not be recovered with conventional segmentation algorithms.

In the last few years, several software techniques have been used to correct these uneven lighting errors in assays run with *C. elegans* for capturing images and subsequently processing them. Usually a threshold is tuned manually during the assay. However, automatic adaptive methods are used by, for example, [18]–[20], and adaptive Gaussian is

also employed [21], as is Otsu's method [22], [23], which is a clustering-based image and a method based on contrast [24]. There are also graph methods [25], [26] or background modelling [27]. Another technique is edge [28], [29], which detects image gradient magnitude. Filling object areas is usual for improving the segmented image by using dilate and erode methods [30], [31] or filling operations [31].

From our point of view, instead of solving this problem manually or via software, it is better to solve it by hardware with an intelligent illumination system that is able to adapt illumination to changing conditions. This solution must be robust for some changing conditions by simplifying the image segmentation problem. Nevertheless, as far as we know, none of the state-of-the-art monitoring systems has actively controlled its light.

Besides, it has been demonstrated that all visible light wavelengths are lethal for transparent *C. elegans*, especially when applying (1) long exposure times, (2) high intensities and/or (3) wavelengths that come close to ultraviolet [32]. However, this mortality becomes insignificant if light intensity is reduced to units less than $\mu W/mm^2$ and the exposure time is cut to a few seconds per day. Exposure of worms to light leads to withdrawal responses [33], [34], mainly if blue light is applied. WorMotel [35] used a non-controlled red light to detect movement and emitted a blue flash as a stimulus to force movement behaviour in lifespan assays, instead of using illumination with on/off control, which affects the whole plate. In our view, it could be very interesting to control light intensities, exposure times and wavelengths in small zones of the plate as and when desired.

In this paper, an active backlight method is proposed for lifespan and healthspan machines that work with transparent Petri plates and media as it allows precise automatic illumination control. We analyse a control technique based on active backlight capable of regulating dot-to-dot intensity light and its wavelength (Red, Green, Blue). The proposed method consists of controlling the light intensities and wavelengths of a matrix of illumination dots with PID regulators. These regulators obtain

feedback from captured images to adapt illumination to changing conditions. The control references are the desired image intensities. These references are set to the lowest intensity values to allow robust segmentation for minimising worms stress. In addition, a new control action strategy is proposed to take advantage of the wavelength control to stimulate *C. elegans* in an attempt to improve lifespan results.

Materials and methods

Materials

Different illumination techniques can be applied to monitor behaviours of the worms cultured on standard Petri plates. These techniques are defined by the location in relation to the illumination device, the inspected plate and the camera. A backlight configuration consists of placing a camera in front of the illumination system and the inspected plate in between. In our case, the inspected subjects are *C. elegans* cultured on a 55-mm Petri dish with NGM (Figure 1.1A).

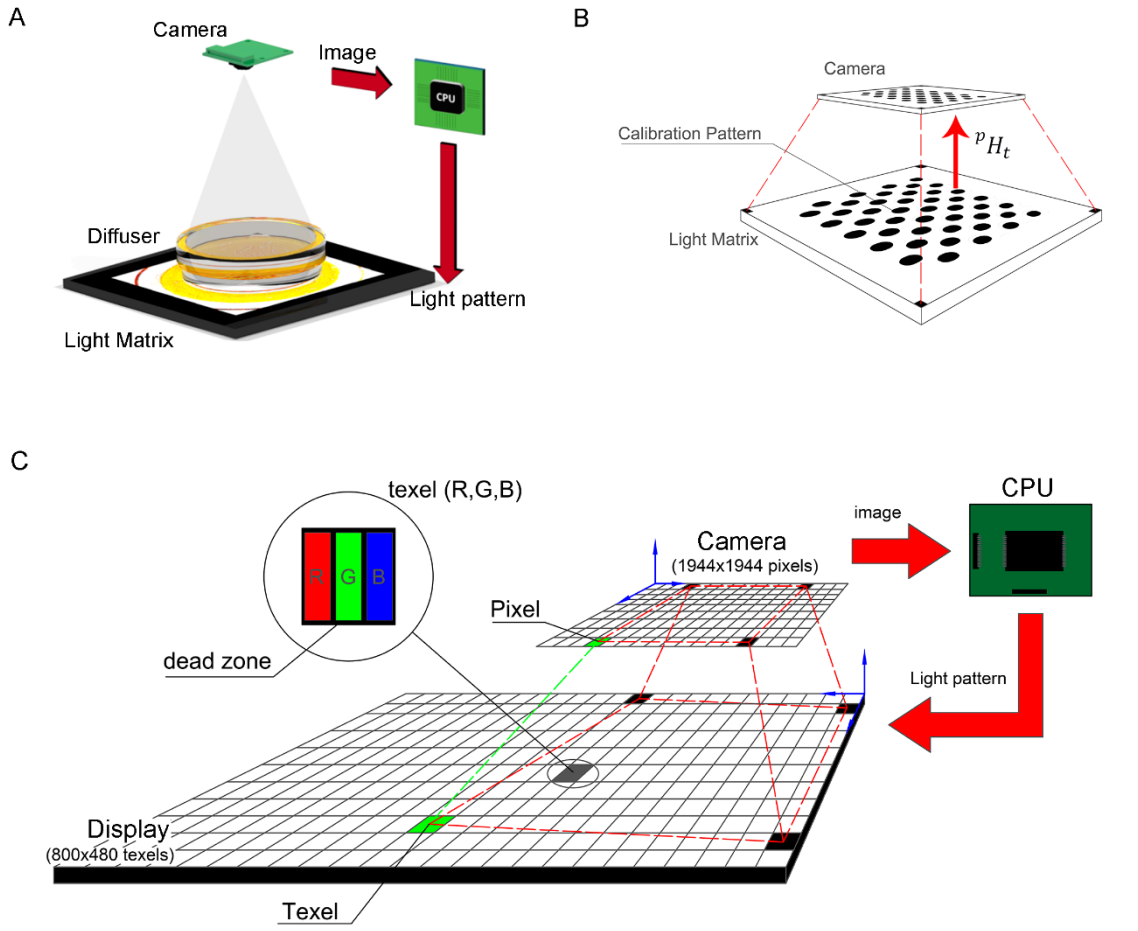

Figure 1.1. Physical Configuration. A: Control scheme. B: Control action going from black, red, orange, yellow to white, from the minimum level (zero) to the maximum level (255R+255G+255B = 765).

A matrix of light dots is required to develop a spatial control, with which intensity and wavelength can be controlled dot-by-dot. Each dot is composed of some subdots of different wavelengths. In our case, these subdots are red, green and blue (R, G, B). There are dead zones between these dots where no light could be emitted, which produces a dark reticular structure on captured images. To avoid this problem, we propose using a diffuser, which is placed on top of the light matrix. On the diffuser, we place the Petri dish in such a way that the light emitted by the dots crosses the transparent Petri dish and media towards the camera that captures high-contrast images with dark *C. elegans* and a bright background. The camera, besides being used to capture images for

monitoring purposes, also serves as the control loop feedback sensor to allow the lighting of each dot to be regulated.

Moreover, in order to control lighting, it is necessary to isolate the system from the environment to reduce ambient light disturbances. Consequently, the system is enclosed in a box, which is not depicted in Figure 1.1A. In addition, the interior of this box is covered with black material to avoid internal reflections.

We have developed a low-cost system as a proof-of-concept. However, this system can be made using other materials and components. Our system is composed of the 7" Raspberry Pi Display with 800x480 texels as the light matrix, a glass diffuser, 55-mm Petri dishes, a Raspberry V1.0 camera (Pi camera) and a Raspberry Pi 3 processor.

Lighting and camera configuration

The first step for system configuration (Figure 1.1A) is to obtain the camera working distance to the dish (77.5mm) in order to observe the whole dish in an image of 1944x1944 pixels, which is determining from the smallest camera angle of view (21º) and then by focusing the lens for that distance to make the image as sharp as possible.

The display can emit three different wavelengths (R, G, B) from each dot or texel (Figure 1.1C). However, the camera does not distinguish among these wavelengths because it is configured as a grey camera. Therefore from the camera's point of view, the three wavelength intensities are integrated into a pixel as grey intensity. We seek an operation point in which lighting should be as dim as possible to minimise stress for worms.

In order to avoid a chaotic system in control, the automatic camera settings are disabled. We tune two configuration parameters (integration time and brightness). The integration time must be quite high to improve image quality in a low illuminated scenario. Brightness is irrelevant for image quality because it also affects noise. To obtain optimal parameters, we place a Petri dish with *C. elegans* and look for integration time values, which make the maximum contrast and sharpness between worms and the background for the given illumination. When finding the best

integration time for that light, the same search is performed for different illumination intensities.

After numerous tests, we verified that the optimum operating point was given by an illumination that came close to orange (R=255, G=190, B=0), an integration time of 100 ms and a brightness of 25, which gave the background image with an intensity level of 48 and the worm intensity near the 0 level.

Calibration

Camera calibration is a mature procedure [36]. Several camera calibration techniques exist, but the present paper focuses on the calibration method based on a bi-dimensional pattern. In this work, the open source software library OpenCV is used. It offers three types of calibration patterns: symmetric, asymmetric and checkboard. Some studies, such as [37], have established that patterns of circles are less sensitive to blurring than a calibration checkerboard. We use an asymmetric pattern of circles (Figure 1.1B) to calibrate the projection matrix ${}^{p}H_{t}$ (Equation (1.1)). In our case, this projection is a homography, a 3x3 matrix. This transformation defines the mapping between texels (points defined in relation to the coordinate system of the illumination system) and pixels (points defined in relation to the camera's coordinate system).

$$y_k = {}^{p}H_{t} \cdot t\text{exel} \qquad (1.1)$$

The OpenCV calibration tool runs an automatic circle recognition procedure. Circles recognition is based on the well-known OpenCV BLOB (binary large object) detection method. This consists of calculating the connected blob centroids with sub-pixel precision. The blob detection method also allows the filtration of returned blobs by colour, area, circularity, etc. The default values of these filter parameters are tuned to extract dark circular blobs. In general, OpenCV calibration can be run without having to adjust these default parameters, but the default values in our specific research had to be adjusted to detect circles.

Controller

Research works to regulate the amount of illumination at a constant level have been previously performed [38], [39]. These works demonstrate that a simple model for each zone can be used to control lighting by a PID regulator. In our case, the dynamics and non-linearities were negligible.

The control references (*ref*) were established to an intensity level of 48 because it is the calculated optimum operation set point. Therefore, the controller was designed around a nominal light amount of 58% (255, 190, 0).

The output (y_k) was measured by the intensity value of the image pixel (Equation (1.2)), where k is the index of each sampling time (T_{sa}=0.11s). To avoid the transformation product matrix calculation for each texel in every iteration, a lookup table was used.

$$y_k = Image_k\left({}^{p}H_t \cdot texel\right) \qquad (1.2)$$

The controller was estabilised when the null control error was reached (e_k=0), which meant that the intensity output reached the reference level (y_k=*ref*). In order to achieve this goal, a PID control action (u_k) was implemented for each texel (Figure 1.2A). A PID controller (Equations (1.3) and (1.4)) had three parameters: k_p (proportional constant), k_i (integral constant) and k_d (derivative constant). In our case, the k_d constant was set at 0 to obtain a proportional and integral regulator. Our application required a moderate settling time (T_{se}<15s). Therefore to simplify our controller, we proposed k_i=k_p (Equation (1.5)) by obtaining a regulator of one degree of freedom. In our case, proportional constant k_p was tuned experimentally to become the maximum positive value, which gave a stable output response (k_p=0.9).

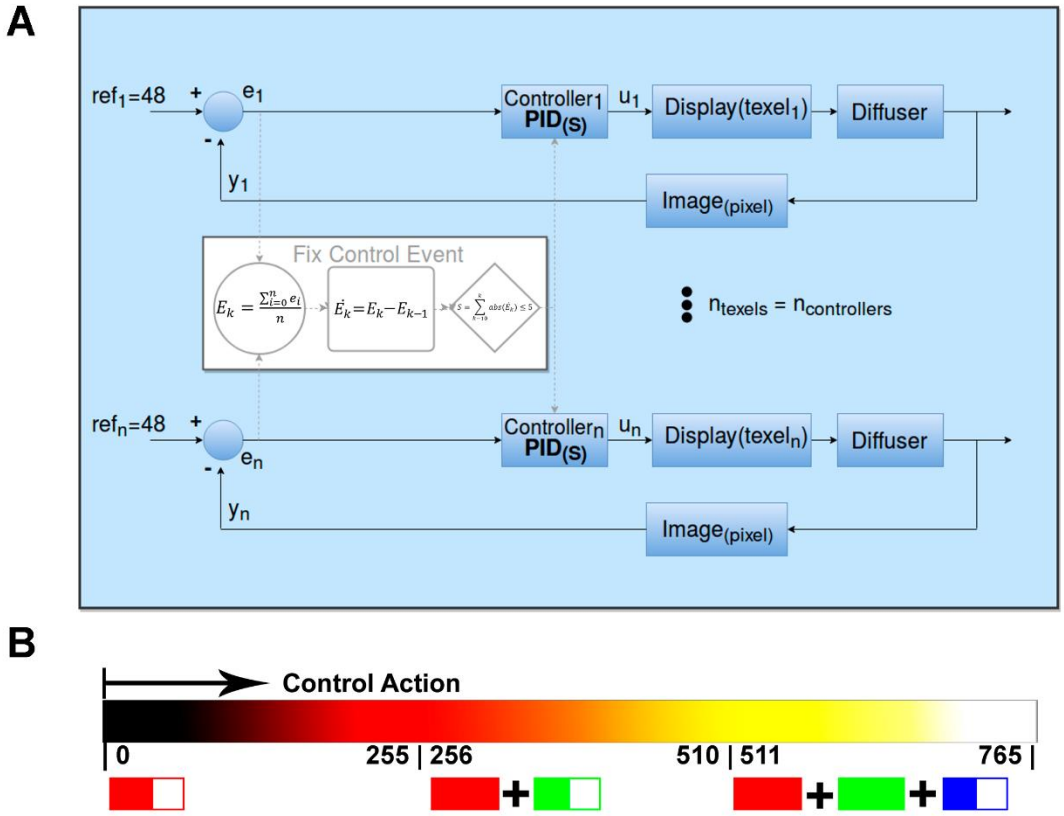

Figure 1.2. Control principle. A: Control scheme. B: Control action going from black, red, orange, yellow to white, from the minimum level (zero) to the maximum level (255R+255G+255B = 765).

At each sampling time *k* and for each texel, one controller reads the corresponding output intensity level (y_k) from the captured image and applies the control action (u_k), which depended on the previous control errors, to close the loop.

$$e_k = (ref - y_k) \tag{1.3}$$

$$u_k = k_p e_k + k_i \cdot \sum_{j=0}^{j=k-1} e_j + k_d \cdot (e_k - e_{k-1}) \tag{1.4}$$

$$\boldsymbol{let}\ \ k_i = k_p\ \ \boldsymbol{then}\ \ u_k = k_p e_k + u_{k-1} \tag{1.5}$$

A control action (u_k) was proposed as the integration of the three wavelength intensities after taking into account a strategic order. This control strategy started when using only red intensity until saturation took place at the 255 level. It continued by adding green intensity and finally blue intensity when green was saturated (Figure 1.2B). The control action increased progressively from black, red, orange, yellow to white. It should be noted that control strategy used blue light as the last option to reach the reference. If this control strategy was not interesting for a specific assay, it could be easily changed to apply only red light, white light, or others.

Fixing the control action strategy

There are a number of control loop iterations after which a stable output was achieved. In our case, the control loop was run until the control error was estabilised at a low value. The control action was fixed when a low control error was detected (fixed control event). This event was defined by $S \leq 5$ (Equation (1.8)), where E_k (Equation (1.6)), is the average total error per image at each sampling time k; n is the texels number of the lighting pattern; $\dot{E}_k$ (Equation (1.7)) is the differential of E_k. This event was detected when the integral of the last 10 instants of the $\dot{E}_k$ came close to zero ($S \leq 5$).

$$E_k = \frac{\sum_{i=0}^{n} e_i}{n} \quad (1.6)$$

$$\dot{E}_k = E_k - E_{k-1} \quad (1.7)$$

$$S = \sum_{k=10}^{k} abs(\dot{E}_k) \leq 5 \quad (1.8)$$

Experiments and results

The homography mapped each texel with the central pixel of its projected area on the image. The reprojection error (RE) was used to measure the calibration quality assessment. RE was defined as the geometric error corresponding to the average image distance, measured in pixels, between a texel point, and its projection according to the calibration

model, and its corresponding measured counterpart. The retroprojection errors obtained at different calibrations fell within the 2.50 ± 0.06 pixels interval. According to these calibrated homographies, a texel projected approximately on an area of 6x5 pixels on the image when no diffuser was used, as seen in Figure 1.3A. The intensity on the image caused by texel was maximum in the projected area centre, which is the integration of the three emitted RGB wavelengths (Figure 1.3B). There were control dead zones between texels, which is why a dark reticular structure is observed in the image (Figure 1.3A).

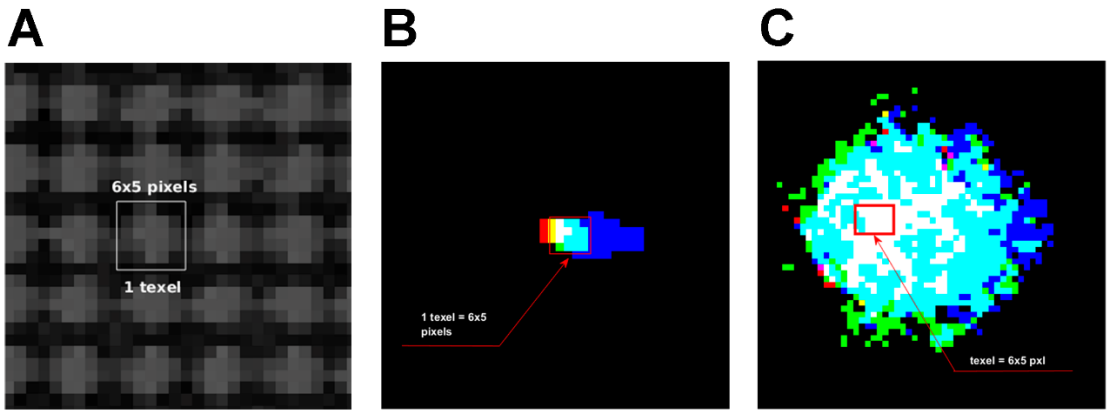

Figure 1.3. Textel projection on image. A: Greyscale image of white illuminated texels with no diffuser. The white box is the image of one texel acquired by the camera. Both images (B and C) show non-zero wavelength intensity values instead of intensities values. B: Image of the each RGB channel of one texel with no diffuser. C: Image of one texel with a diffuser.

There were different reasons for the calibration errors, which we observed one due to physical imperfections, such as small curvatures on the display surface, which caused light refractive dispersion (smaller red dispersion, green and a bigger blue one). As seen in Figure 1.4A, in area 1 the RGB projections match the same pixels, which means that we can act in the desired place. However, RGB have a small offset between the different wavelengths of one pixel or two in area 2.

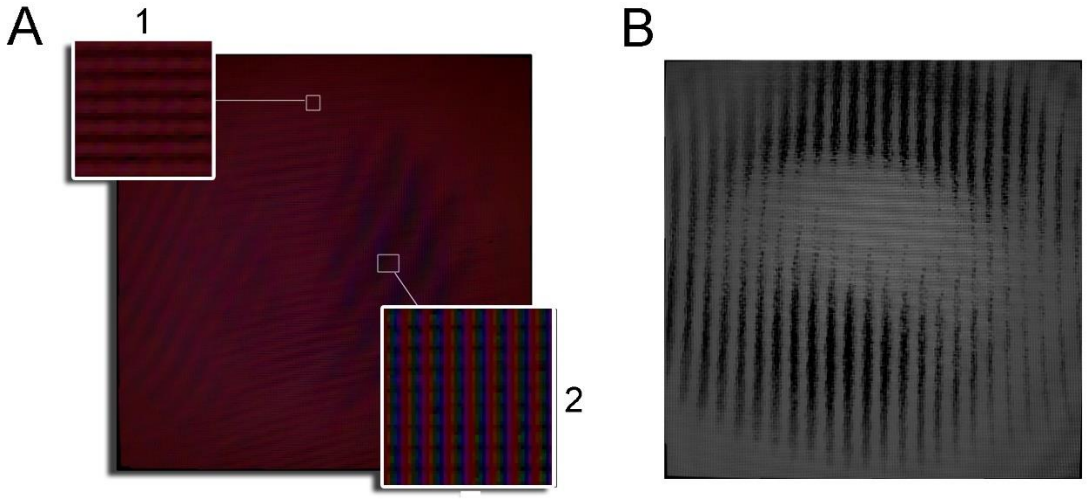

Figure 1.4. Texel colour dispersion. A: Three images were taken with no diffuser, one with each displayed texel illuminated in red, another with all the texels displayed in green and another one, all blue. All these captures was merged in this image at three layers, RGB. Thus we can see for each image pixel how much of each wavelength is affected individually (pseudo-colour image). B: Image captured after eight control loop iterations with no diffuser

Instability

The calibration errors of ${}^{p}H_{t}$ could produce output instabilities. As stated, calibration errors were over 2 pixels, of which can occur in certain areas, which might move mapped pixels to dead zones (non-sensed dark zones). These calibration errors can cause an erroneous control by increasing the control action to the maximum, but without the mapped pixel detecting any change. Instead this control action can alter the measure in a pixel corresponding to a nearby texel, which could generate instabilities in the control (Figure 1.4B).

To avoid this problem, a diffuser was added to the display, which made the light diffuse obtaining bigger projected texels images (Figure 1.3C). Therefore, illumination with no dead zones was achieved and neighbouring pixels had a similar lighting level, which minimised the effects of calibration errors.

Fixing the control action

The effectiveness of the fixing control action strategy was analysed with no Petri dish. Thus the control light pattern had no occlusion therefore it allowed each pixel on the image to reach the reference level (48). In these

experiments, the control action on the display was applied continually over approximately 38*s* to compare the control error evolution of the pattern light applied at each time instant *k*. After a number of iterations k_m of the control loop, a stable control error was achieved henceforth. The period between the k_0 and k_m control iteration is defined as transient period. After k_m iterations, the control lighting pattern tended to achieve a composition with maximum (white) and minimum (black) values (Figure 1.5B), although this provokes no change on the output image. This output image is maintained at the reference properly (a uniform grey image of 48 level) after k_m. Hence, once the control error was estabilised, the control action was fixed (Figure 1.5A) henceforth. Figure 1.5C shows an experiment in which fixed control event is reached at k_m equals 45 iterations. Thus when ($S \leq 5$) was detected, the control action was fixed. Figure 1.5A shows the fixed control lighting pattern at k_m equals 45 iterations. After performing different compensation processes, the time required to fix the control action to fall within the 6.16 ± 1.68*s* interval was estimated.

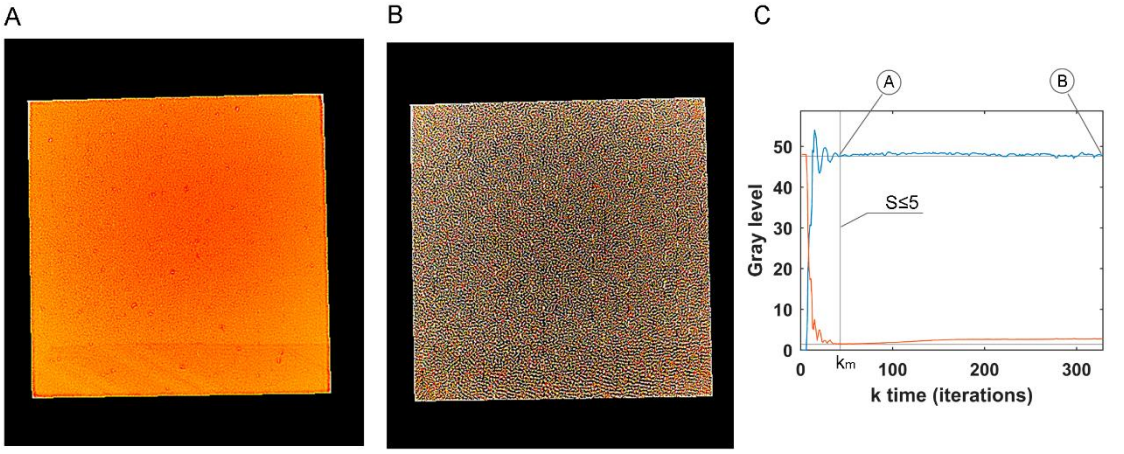

Figure 1.5. Stop control. (A) and (B) are the light patterns used as the control signal at different *k* instants when the error came close to zero, but (A) is the first one to reach it, and (B) is 283 iterations later. (C) Shows the output (blue) which is the grey level mean of image and control error to get reference.

Spatial variability

Some experiments were performed to analyse the quality of the images acquired with compensated at the 48 reference level and the uncontrolled standard white light. Several plates with NGM were tested by illuminating under the stated conditions. The images with background pixels at a grey level circa the 48 intensity level were expected when applying the light control to the system.

When applying the proposed illumination control strategy (Figure 1.6B, E), the captured images achieved nearly uniform illumination and improved image quality (Figure 1.6A, D). According to Figure 1.6F, when applying the illumination control, most of the background image pixels were around the 48 intensity level with worm pixels around the 0 level, as shown in the blue line profiles (Figure 1.6G,H). Figure 1.6C shows an image plate that underwent some kind of spatial intensity variations. When applying the control action (Figure 1.6E), these spatial variations were compensated (Figure 1.6D). The camera was configured at a low gain level and, therefore, images are dark. For this reason, images Figure 1.6C and Figure 1.6D are seen to be normalised to simply improve their graph visualisation. The line profile on this contaminated plate (Figure 1.6H) could reach the reference in almost the whole area, but not all the contamination can be compensated. Some kind of opaque contamination was noted, which produced the low intensity level spots shown in Figure 1.6H.

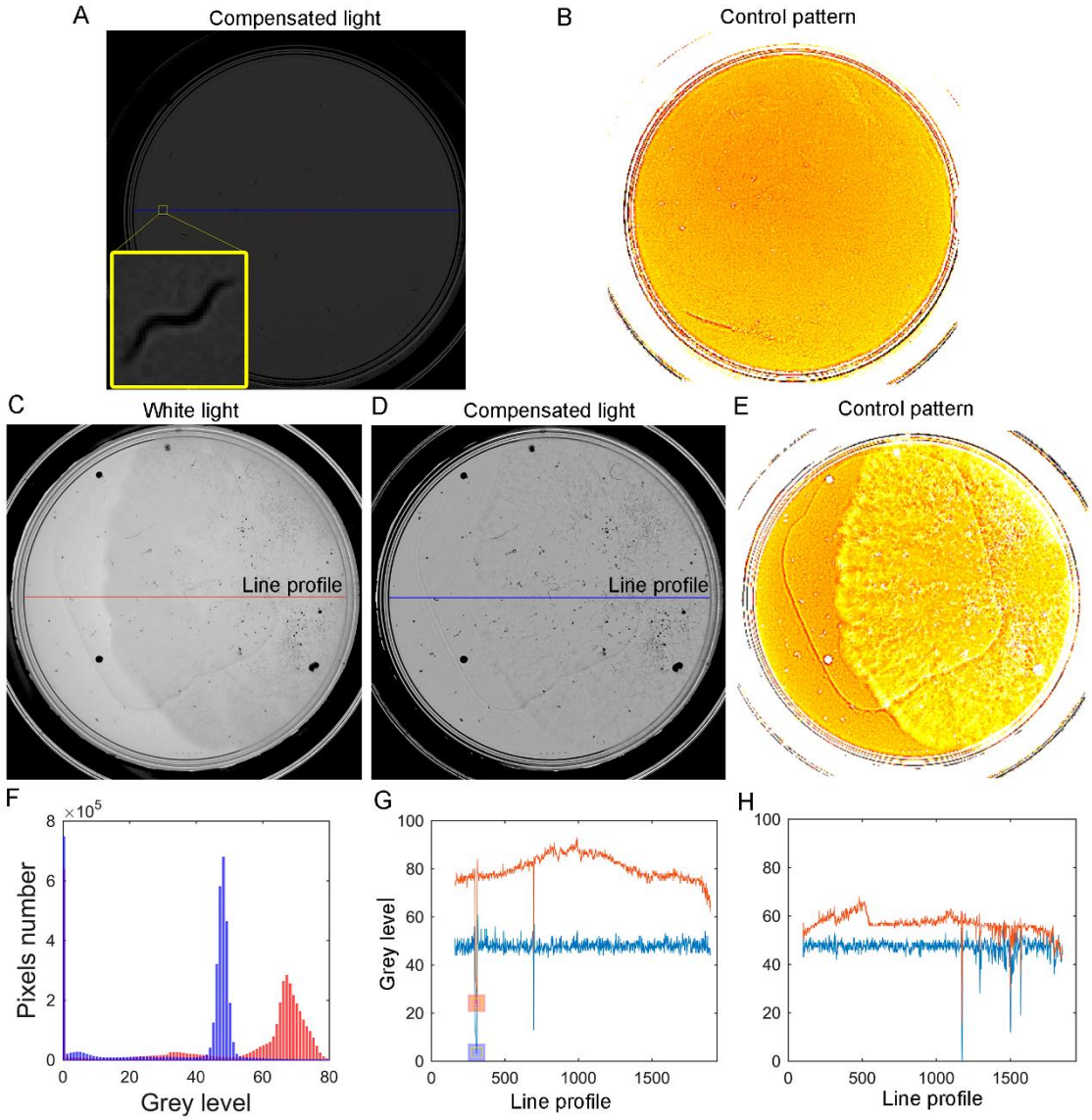

Figure 1.6. Spatial variability under white light. A: Captured image with compensated illumination. B: Control pattern applied to the captured image. C: Normalised image with white backlight. D: Normalised image with compensated light. E: Control pattern applied to the captured image (C). F: Comparison of the image histograms: the red one without applying any control and the blue one after applying the control. G: Comparison of profile lines, the red one without applying the control to (A) and the blue one after applying the control (A). The blue and red squares are the grey levels caused by a worm. H: Comparison of profile lines (C) and (D).

Other experiments compared the first uncontrolled pattern light, used as the starting point in the active control loop, with the final compensated pattern light. The first pattern light was an orange pattern, which

produced a constant grey image of the reference intensities (at level 48) with an ideal transparent medium.

It is well-known that the zones near the wall require greater light intensities than the plate centre. This effect is seen in Figure 1.7D. Therefore, if we used uncontrolled standard light, we would need to overlight the plate centre to properly illuminate the wall zones. However by using active light, we applied only the light required in each zone (Figure 1.7A). This generally reduces the light applied in the centre of the plate. It is stressed that active light would apply exactly the amount of light required to reach the reference. Images of worms can be more easily segmented using lower intensity light when applying the active control (Figure 1.7B) than uncontrolled light (Figure 1.7E).

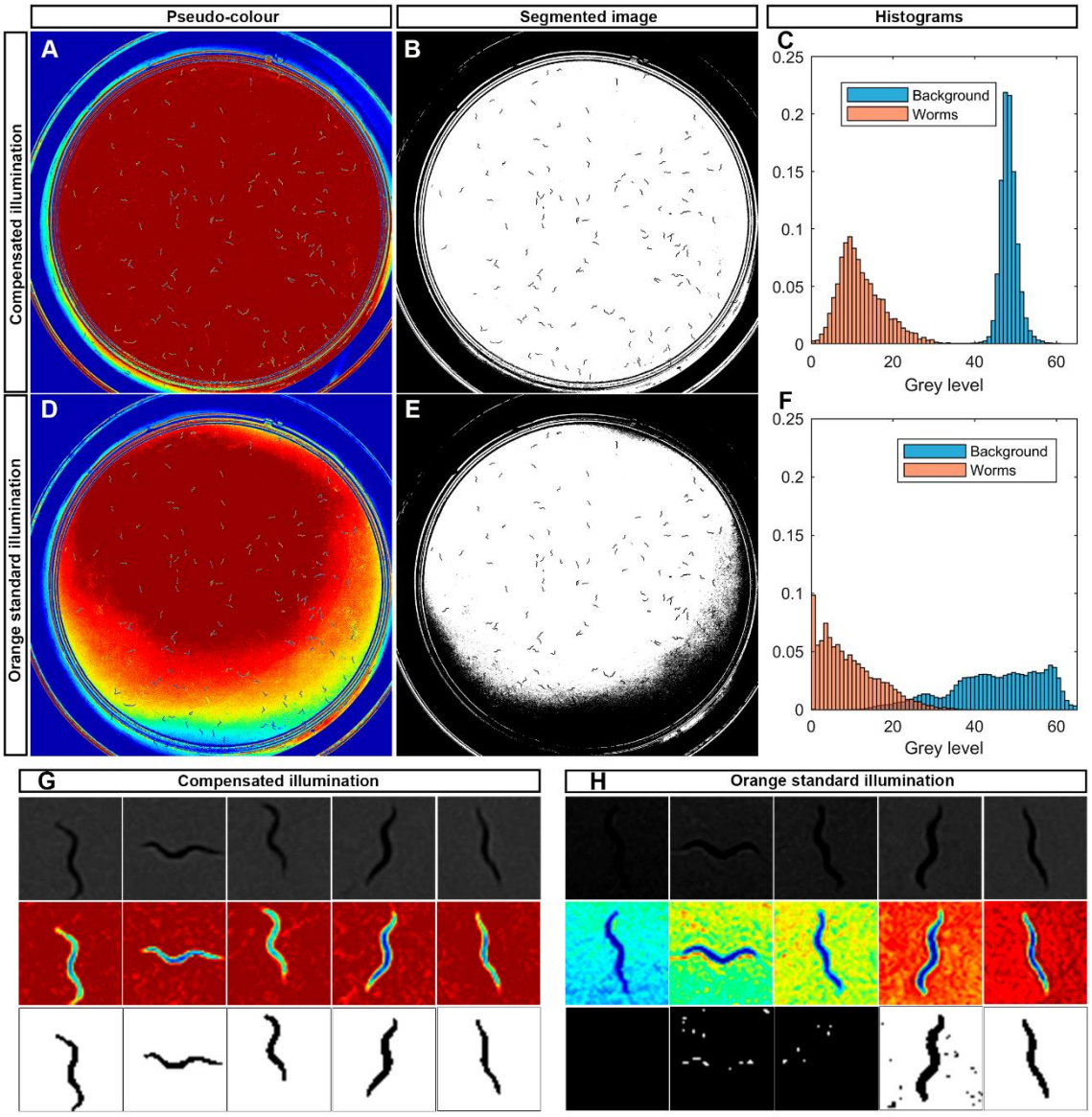

Figure 1.7. Spatial variability under orange light. A: Captured image pseudo-colour with compensated illumination. B: Segmented image of (A) by a threshold method. C: Histogram of grey level of background (blue) and worms (red) from (A). D: Captured image pseudo-colour with orange standard illumination. E: Segmented image of (D) by a threshold method. F: Histogram of grey level of background (blue) and worms (red) from (D). G: Worm image examples from (A) in pseudo-colour, grey scale and segmented. H: Worm image examples from (D) in grey scale, pseudo-colour and segmented.

In order to quantify image quality improvement, Fisher index was used [40], *F* (Equation (1.9)), which is a method that computes the importance of a feature (in our case the intensity levels) for segmentation in two

classes (positive o negative). The respective score $F_{(j)}$ of feature j is given by:

$$F_{(j)} = \left| \frac{\mu_j^{\pm} \mu_j^{-}}{\left(\sigma_j^{+}\right)^2 + \left(\sigma_j^{-}\right)^2} \right| \quad (1.9)$$

where $\mu_j^{+}\left(\mu_j^{-}\right)$ is the mean value for the j_{th} feature in the positive (negative) class and $\sigma_j^{+}\left(\sigma_j^{-}\right)$ is the respective standard deviation.

We compared the mean and deviation between background intensities (histogram blue bars) and worms intensities (histogram red bars), for the uncontrolled standard light (Figure 1.7F) with the compensated light (Figure 1.7C). The compensated images show a higher Fisher index (0.8636 ± 0.1427) than the non-compensated images (0.2049 ± 0.0267). This is why the compensated images provide a better contrast in the zones near the wall and have, at the same time, a narrower variance than the non-compensated images. Figure 1.7G shows some examples of worms in several areas as the background is hold constantly by compensation, while the background of these same worms in the same areas has a wide variability for non-compensated illumination (Figure 1.7H). More examples can be found in Supplementary Figure S1.

Temporal variability

Temporal variations were studied in three experiments (Figure 1.8), which correspond to the three effects that may occur: illumination derivatives due to display fluctuations, media light characteristics which define that media have more or less opacity; condensation on lids, which causes occlusions.

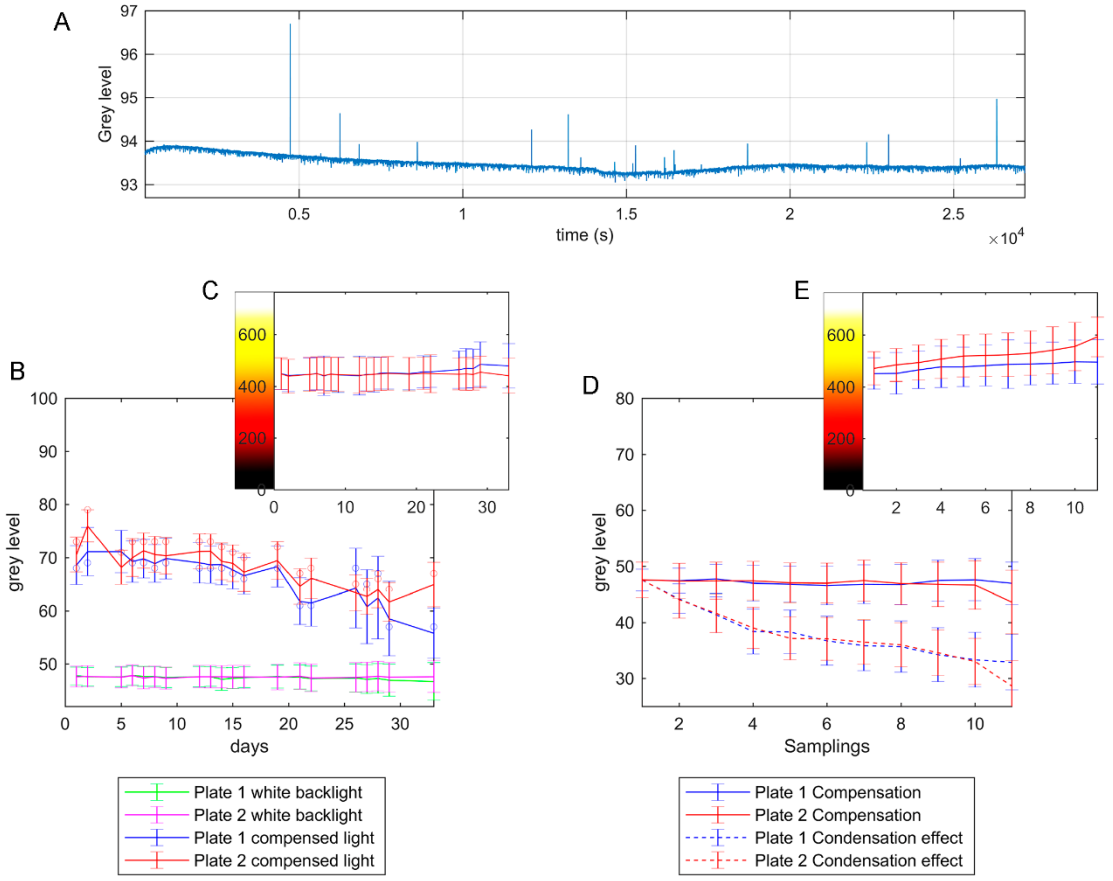

Figure 1.8. Temporal variability graphics. A: The average grey level of the image produced by a white backlight with time (about 30,000s). B: The mean grey levels and deviations of two plates for the white backlight and for the compensated light. C: The mean control signals and deviations applied for compensating images: (B) every day. D: The mean grey levels and deviations of two plates with condensation slowly increasing for the new backlight compensation every time that the mean image grey level error dropped below -3, and for the compensated light at the beginning (this lasted approximately 2h). E: The mean control signals and deviations applied for compensating the images in (D) during each new compensation event.

An experiment to show that the source illumination derivatives were performed. In this case, light intensities were captured over a long time (7.5h). The camera and illumination source noise produced variation in intensities with time. Figure 1.8A shows there was a mean variation by noise with time at less than the ±0.25 grey level. However, there were also illumination derivatives of some peaks that were higher than noise (circa the Δ2 grey level) only for an instant. Display frequency was 60Hz and the

camera was 8Hz. Thus the camera integration time was longer than the display refresh time and, therefore, the refresh action was not significant.

Another experiment was conducted to evaluate the effectiveness of the active illumination control strategy to compensate for medium variability. This experiment consisted of monitoring two Petri plates with solid medium (NGM) and *E. coli* strain OP50 for 33 days. Images were taken once a day (except for weekends) to observe the medium behaviour evolution with the non-compensated white backlight and the compensated backlight. All the media had different light transmittance characteristics, which presented temporal changes throughout the assays days. Figure 1.8B shows two media behaviours for 33 days, and an image grey level over time with a white backlight, from which the media's increase opacity was deduced. When the control was applied, this variability was corrected by keeping the image mean value close to 48 every day, and its standard deviation at the ±2 grey level for the first 3 weeks. When no control was applied, the mean image grey level could vary from 70 grey levels to 55. Finally, in order to evaluate our active illumination control method over condensation, two Petri plates were monitored at an ambient room temperature of approximately 25°C for circa 2 hours. This time was necessary for condensation to occur. Plates were stored in an incubator at 20°C so that the rise in temperature in the room-warmed plates and condensation would be slowly evoked. At the zero time, and before any condensation was observed, a series of control actions was applied until the control error was estabilised. Then the last control action of this series was fixed and saved. Afterward, the error increased over time because condensation slowly appeared and made darker images. When this error was -3 intensity levels, we repeated the previous steps. A new series of control actions was applied until the error once again estabilised, and so on. Every time, and immediately before a new control action was fixed and saved, the control action of the first series was applied only to take one image. This series of images allowed to measure errors in relation to the first lighting compensation throughout the experiment. The control (Figure 1.8E) was also able to compensate for some soft condensation (Figure 1.8D). Condensation brought about a

decrease of up to 18 grey levels in the mean, which could also be compensated.

Discussion

First of all, it was important to analyse all the lighting factors that could affect image quality. Sometimes achieving a pure backlight illumination is difficult. We used a box to isolate the system from outside ambient lighting, but part of the light generated by our backlight bounced off on the box walls, with which a small ambient light component inherently appeared. Thus in order to reduce it, it was necessary to cover the interior with materials that were as little reflective as possible. It was proved that by covering the interior with black EVA rubber, ambient light reduced, which increased the contrast between worms and the background. This was verified by analysing the grey levels of worms, which went from 13 low levels to low ones of 0.

At the plate level, different reflections and refractions appeared on the standard Petri plate walls. Reflections could produce a mirror effect on the wall to show that reflected worms were near the walls. This was why our camera was configured at low sensitivity in an attempt to avoid these mirror effects. Regarding refractions, some light beams that passed through the Petri walls did not arrive at the camera, which produced dark circles near the walls (Figure 1.6). These areas were about 6% of the inspected area, which means that it was unlikely that a worm would be found in that areas because an *E. coli* lawn was strategically placed in the middle of the plate. Moreover, special segmentation software solutions can be applied for these areas.

Homography calibration was performed once at the setting up time with no Petri plate. So when the plate was inserted into the system, it provoked small refractions that increased the calibration errors. This error type could produce small intensity waves on the image when errors are too high. An alternative procedure would be to calibrate homography for each plate. However, the experiments showed that one calibration at the starting time with no plate was robust enough.

From the control point of view, there was a number of iterations *k* of the control loop, after which a stable lighting pattern was applied. This lighting pattern achieved a composition of maximum (white) and minimum (black) values (Figure 1.5B). However, to allow an effective wavelengths control strategy, the control action was fixed earlier when the control error was low (Figure 1.5A). We defined a detection event strategy to fix the control action, but other strategies can be used.

The strategic order (R, G, B) upon the control action was chosen after considering that the wavelengths near the ultraviolet are more detrimental for *C. elegans*' survival. Therefore, blue light proved more detrimental than green light, and green light was more detrimental than red light [32]. Given this strategy, most of the plate was illuminated with light that was close to orange (255, 190, 0), as seen in Figure 1.8C, D. The maximum control action, white light (255, 255, 255), was applied automatically, but only to opaque zones (Petri walls and strong contamination) and worms. As it was not possible to detect worms in opaque zones, applying blue light to these zones is a very interesting strategy because worms tend to avoid blue-illuminated zones [33]. In addition, applying blue light to worms stimulates their movement, which could improve lifespan results. In our case, the maximum intensity level of the blue light was applied to worms because the monitoring process lasted only few seconds. Depending on the application, other control strategies can also be implemented by applying light as desired.

To avoid control instabilities due to calibration errors, stable PIDs regulators were introduced and a diffuser was added to the display. Another solution without a diffuser would be to measure output (y_k) as the average of 30 pixels, which was related to the same texel. However, if we used a diffuser, we would only have to take the central pixel, and in such a way that the computational load of all these means calculations would be avoided. When using a diffuser, a new problem could arise due to the texel lighting affecting not only the pixels associated with it in calibration, but also those associated with neighbouring texels. Hence it became a coupled system by conferring interactions in the control. In

order to control these interactions (Figure 1.3C), a controller with a small k_p was designed. If a faster settling time is required, these interactions can be modelled to apply advanced controllers.

The experimental results show that this method is able to compensate for automatically different illumination changes. This changes involve media transparency on all the assay days, whose mean image grey level can vary from 70 to 55 (Figure 1.8B); changes in ambient conditions, such as smooth condensation on lids, whose mean image grey level can vary by 18 grey levels (Figure 1.8D); light derivatives of the illumination source during its lifetime. Therefore, the proposed control technique simplifies the worms segmentation problem by reaching near uniform illumination throughout the image. This might both increase the quality in all areas (by reducing information loss) and obtain constant illumination in the whole area (by allowing fixed threshold image segmentation).

To a greater or lesser extent, uneven lighting is quite a common problem when monitoring *C. elegans* and other organisms, such as *Saccharomyces cerevisiae*, *zebrafish larvae* and *Drosophila larvae* cultured in Petri plates systems. The new proposed method compensates for some spatial and temporal changes, and makes segmentation easier and more efficient. This method can not only be used in lifespan or healthspan assays, but it should also serve a broad range of applications in optogenetics.

Future research could improve system accuracy by calculating three different homographies, one for each wavelength (R, G, B), which would reduce calibration errors. In addition, this system could be implemented with other lighting matrices with other wavelengths and intensities. Finally, other regulators like predictive control could also be implemented.

PAPER 2

Improving lifespan automation for Caenorhabditis elegans by using image processing and a post-processing adaptive data filter

Joan Carles Puchalt[1], Antonio-José Sánchez-Salmerón[1]*, Eugenio Ivorra[1], Salvador Genovés Martínez[2], Roberto Martínez[2] and Patricia Martorell Guerola[2]

[1] Universitat Politecnica de Valencia, Instituto de Automatica e Informatica Industrial, Valencia, Spain

[2] Cell Biology Laboratory/ADM Nutrition/Biopolis SL/Archer Daniels Midland, Paterna, Valencia, Spain

Puchalt, J.C., Sánchez-Salmerón, AJ., Ivorra, E. *et al.* Improving lifespan automation for *Caenorhabditis elegans* by using image processing and a post-processing adaptive data filter. *Sci Rep* **10,** 8729 (2020). https://doi.org/10.1038/s41598-020-65619-4

Abstract

Automated lifespan determination for *C. elegans* cultured in standard Petri dishes is challenging. Problems include occlusions of Petri dish edges, aggregation of worms, and accumulation of dirt (dust spots on lids) during assays, etc. This work presents a protocol for a lifespan assay, with two image-processing pipelines applied to different plate zones, and a new data post-processing method to solve the aforementioned problems. Specifically, certain steps in the culture protocol were taken to alleviate aggregation, occlusions, contamination, and condensation problems. This method is based on an active illumination system and facilitates automated image sequence analysis, does not need human threshold adjustments, and simplifies the techniques required to extract lifespan curves. In addition, two image-processing pipelines, applied to different plate zones, were employed for automated lifespan determination. The first image-processing pipeline was applied to a wall zone and used only pixel level information because worm size or shape features were unavailable in this zone. However, the second image-processing pipeline, applied to the plate centre, fused information at worm and pixel levels.

Simple death event detection was used to automatically obtain lifespan curves from the image sequences that were captured once daily throughout the assay. Finally, a new post-processing method was applied to the extracted lifespan curves to filter errors. The experimental results showed that the errors in automated counting of live worms followed the Gaussian distribution with a mean of 2.91% and a standard deviation of ±12.73% per Petri plate. Post-processing reduced this error to 0.54 ± 8.18% per plate. The automated survival curve incurred an error of 4.62 ± 2.01%, while the post-process method reduced the lifespan curve error to approximately 2.24 ± 0.55%.

Introduction

Caenorhabditis elegans (*C. elegans*) is a widely used animal model in biological research due to certain advantageous features for investigation[1], [2]. *C. elegans* is small, which allows it to be stored, handled and fed very efficiently. It is transparent, which also makes it easy to observe.

Certain types of behaviour demonstrated by these nematodes may increase our understanding of other more complex animals. Consequently, assays are designed to analyse different issues such as the study of compound toxicity, neurodegenerative diseases, ageing alterations, etc. For ageing assays, the lifespan model is employed [3]–[7], [9], [10], which counts live animals of the same age over their lifetime. These are separated into populations, each of which undergoes a differentiating condition that may alter the life expectancy of a given population. Worm movement indicates life whereas death is defined by a lack of motion after stimulation with a platinum wire. *C. elegans* lifespan is close to 3 weeks, and some strains may live a few weeks longer. Statistical assays, like lifespan, need circa 100 specimens per condition, which greatly increases the number of worms and hinders the technician's task. Therefore, there is a need to automate such assays to save researchers' time and to provide objectivity.

There are different methods to automate *C. elegans* inspection tasks. The most widespread method is to measure worm movement by acquiring images while fully monitoring standard Petri dishes [15]–[17], [41].

Lifespan automation is challenging because a host of problems can arise. The image processing software must be designed to avoid different causes of false-negatives (or undetected live worms) and false-positives (or wrongly detected live worms). False-negatives can be due to worm aggregation problems or to occluded plate zones (e.g. zones near plate walls, or non-transparent zones due to contamination or condensation problems). False-positives can be due to progeny, worm decomposition or dirt contamination problems.

Research groups have developed different culture protocols to avoid progeny and to alleviate worm aggregation, plate contamination and condensation problems. Active lighting techniques[42] can also alleviate plate contamination and condensation issues. However, these protocols and methods have failed to fully eradicate these problems, and thus image-processing software must deal with all these complications.

Reviews[18]–[21], [23]–[31] show that many image-processing software tools have been developed to monitor different types of *C. elegans* behaviour. These tracker tools work differently to our proposed method. They extract certain predefined worm features (speed, body bends, etc.) from the image sequences captured by an image acquisition system. Consequently, they require complex algorithms and/or human assistance and supervision to achieve good results. By contrast, our method extracts lifespan curves by using simple techniques that involve no human threshold adjustments or supervision.

For lifespan assays, we found the two following automated tools in the literature: the Lifespan Machine[16] and WorMotel[35].

On the one hand, WorMotel uses a robot-arm system to transport specific multi-well plates from a buffer cassette into an inspection zone and returns these plates to the buffer cassette after capturing an image sequence. Several image sequences can be captured daily by the same

acquisition system for different assays. WorMotel avoids the worm aggregation problem because each well contains only one worm. Death event detection is based on a simple movement detection algorithm with image-processing differentiation. This method does not require a tracking algorithm because there is only one worm per well. On the other hand, Lifespan Machine is based on many scanners located inside incubators, which can run only one assay per scanner. In these machines, standard Petri plates are used and each plate can contain several worms. These plates are not moved during the assay, which is run to capture image sequences. In this case, each worm's movements can be tracked before death because worms hardly move at the end of their lives.

This paper presents a different image-processing software system, based on an intelligent illumination system that is able to work in both the aforementioned image acquisition scenarios. In this case, the worm tracking problem is solved by using mechanical fixtures and image alignment techniques to correct any placing inaccuracies between the image sequences captured at several time points. We consider our method to be flexible as it can work in many different acquisition scenarios and is easily adaptable to other assays (e.g., healthspan or memory assays). For this reason it has a high frame acquisition to analyse young worm's tracks (e.g. healthspan) and can compare these tracks among days (lifespan).

The shared objective of all these tools is to base death event detection on the last movement detected for a tracked worm. However, false-positives can be detected due to the worm decomposition process, dirt contamination or image alignment errors. False-negatives may also be detected due to worm aggregation and occluded zones.

Lifespan curves are monotonically decreasing functions. Therefore, a lifespan-counting error can be detected when the current live-worm count is higher than a previous count. In this paper, a post-processing adaptive data filter is proposed to correct all the detected lifespan counting errors by taking into account error incidence probabilities to improve lifespan determination results. This technique has been evaluated for lifespan (the

most complex assay due to its long experimental duration) by taking images with controlled lighting based on active vision, which alleviates some errors by improving image quality[42].

The main goal of this work is to demonstrate that a simple method is feasible to obtain lifespan curves by using simple movement detection and filter algorithms when images are captured by an active illumination system. The results demonstrate that lifespan curves were automatically extracted using a specific lifespan assay protocol and two image-processing pipelines applied to different plate zones. Finally, our experiments demonstrated that the new adaptive data post-processing method reduced the initial alive count errors from approximately 4.62 ± 2.01% to 2.24 ± 0.55% per lifespan curve.

Methods

C. elegans *strains and culture conditions*

C. elegans strains N2, Bristol (wild-type) and CB1370, *daf-2 (e1370)* were obtained from the Caenorhabditis Genetics Center at the University of Minnesota. All strains were maintained at 20°C on nematode growth medium (NGM) seeded with strain OP50 of *Escherichia coli* as a standard diet.

A specific lifespan assay protocol

Lifespan assays were performed with wild-type strain N2 or *daf-2* (insulin receptor). The age- synchronised worms were obtained by hatching the eggs from gravid worms in NGM plates of 55 mm diameter, and incubating at 20°C until reaching the young adult stage. FUdR (0.2 mM) was used to prevent reproduction which impacts animal lifespans[8], and fungizone (1 $\mu g/mL$) was added to prevent fungal contamination. The plates with fungal contamination were censored, following standard methods[43].

The following specific culture protocol items were established to alleviate worm aggregation, contamination, plate wall occlusions, and condensation problems:

C. elegans strains (N2 strain and *daf-2*) were used, which do not display aggregation behaviour[44], [45]. In order to lower worm aggregation probability, only 10 to 15 worms were cultured in each Petri plate. In this scenario, the aggregation probability was very low, and decreased with each assay day because the number of live worms decreased.

Petri plates were closed with a lid and an anti-fungal agent (fungizone) was added to reduce contamination. The *E. coli* OP50 lawn was seeded in the middle of the plate as worms tend to stay on the lawn, thus avoiding occluded wall zones. On each assay day, a human operator removed a small set of plates from the incubator and placed each one or more inside one image acquisition systems to capture and save an image sequence per plate. An image sequence consisted of 30 images acquired at 1 fps. Therefore, the time that Petri plates were outside the incubator was quite short, thus, avoiding condensation problems. Room temperature was maintained close to 20°C to prevent condensation, which is produced by temperature changes. If condensation was detected, it was manually eliminated by the human operator before the image acquisition process commenced.

Lighting system method

Different lighting techniques can be applied to monitor worms cultured on standard Petri plates. These techniques are defined by location in relation to the lighting device, the inspected plate and the camera. A backlight configuration consists of placing a camera in front of the lighting system and the inspected plate in between. In this case, both Petri plates and media must be transparent. Backlight illumination obtains high-contrast images with dark *C. elegans* and a bright background.

Active Backlight illumination [42] was used by the image acquisition system to alleviate contamination, plate wall occlusion and condensation problems. It controls grey levels in images by keeping the background and worm grey levels within the same range of values. As demonstrated in [42], active Backlight illumination is more robust in the presence of contamination and condensation problems than standard backlight illumination systems. The compensated images show a higher Fisher index

(0.8636 ± 0.1427) than the non-compensated images (0.2049 ± 0.0267). It is important to remark that the proposed method is based on this active illumination system, which reduces the variability of the captured images. This smart acquisition system facilities automated image sequence analysis, does not need human threshold adjustments and simplifies the techniques required to extract lifespan curves.

Image acquisition method

The image acquisition method was replicated exactly from the Active Backlight illumination referred to in the previous point [42], which consists of an RGB Raspberry Pi camera v1.3, a 7'' Raspberry Pi display and a Raspberry Pi 3 as a processor. The element configuration (Figure 2.1) places the camera above, display as illumination system below with the Petri dish placed between them. The camera sensor is OmniVision OV5647, which has a resolution of 2592 × 1944 pixels, a pixel size of 1.4 × 1.4 μm, a view field of 53.50° × 41.41° and the original lens with optical size 1/4'' and 2.9 of focal ratio. The distance between camera and object (Petri plate) was sufficient to enable a complete picture of the Petri plate (about 77 mm), and the camera lens was focused at this distance. The 7'' display has an 800 × 480 resolution at 60 fps, 24-bit RGB colour. Image sequences were taken to be processed to detect live worms, 30 seconds of 1944 × 1944@1 Hz, which means 30-image sequences. One image sequence per plate was taken daily and images were processed. Plates were placed in a vision system. Then the image sequence was taken and replaced with the next plate for inspection.

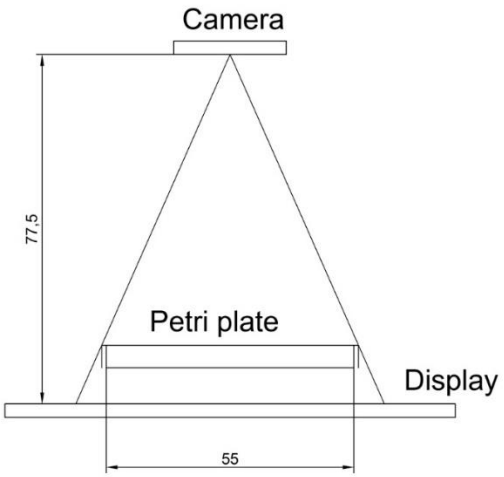

Figure 2.1. System physical configuration. Camera is above, backlight below with Petri dishes placed between them. Units are in mm.

The acquisition system is open-hardware. The guidelines to build this system and the assembly description can be found in previous work [42].

Different image-processing pipelines applied to two plate zones

Death event detection (Figure 2.2 a,c) was defined when a worm did not move during a 24-hour period. This means that no movement was detected between the image sequence captured on one day and the image sequence captured the day before. Motion can be detected in an image sequence (composed of 30 continuous images, captured for 30 seconds) or between image sequences captured on different days. This simple criterion allows lifespan curves to be recalculated every day during the assay.

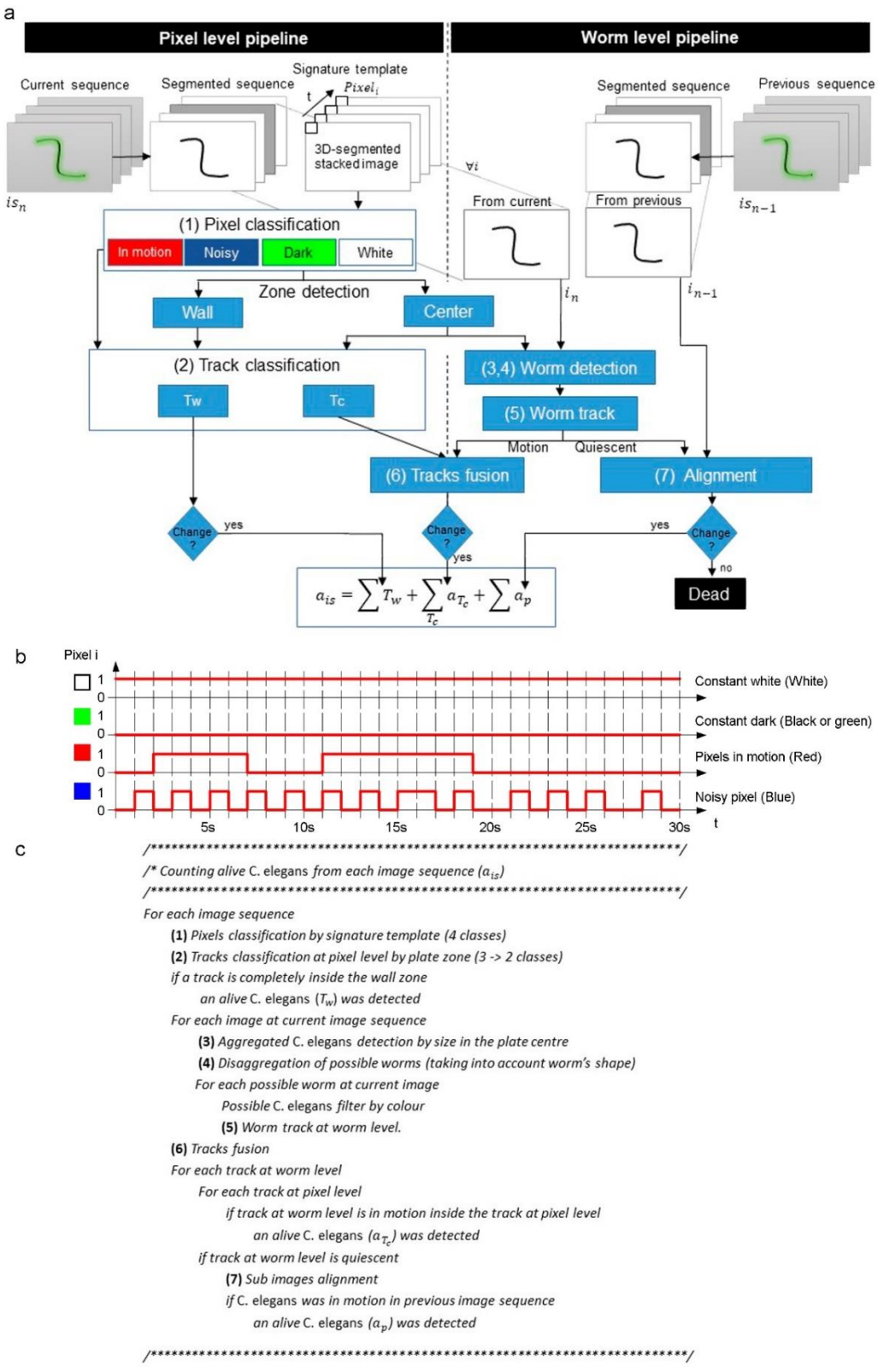

Figure 2.2. Image-processing pipelines. (a) Algorithm flowchart. (b) Pixel level. Signature template examples for the four possible cases. (c) Pseudo-code algorithm.

The proposed techniques were applied at two different levels (Figure 2.2 a). On the one hand, techniques at the pixel level used one-pixel features. At this level, the proposed method used temporal signatures (Figure 2.2 b). The temporal signature of one pixel consisted of the concatenation of all the segmented grey values of that particular pixel in the temporal sequence. On the other hand, techniques employed at the worm level used the features of a set of connected pixels belonging to a worm in one image (blob features).

Regarding worm detection complexity, plates presented two different zones due to their very distinct illumination conditions. While the plate centre presented a homogeneous illumination zone, the wall zone presented dark rings and many noisy pixels. In our case, the active illumination system created some well-illuminated white rings in the wall zone, where worms in motion were detected by simple techniques at the pixel level. Tracks at the pixel level were detected in the whole plate. However, throughout the 30-image sequence, the worms were tracked only in the central zone. Therefore, redundant information about the tracks at these two levels was found in the central zone. This allows tracks to be fused, in order to avoid inconsistencies and count how many tracks were moving at the worm level at the same time inside each track at the pixel level.

Given light refraction on walls, our captured images presented some dark and narrow rings (Figure 2.3) in the wall zone. Therefore, only a motion analysis at the pixel level was possible in this zone. An image-processing pipeline based on a simple movement-detection algorithm at the pixel level was applied near the wall zone. However in the centre of the plate, a motion analysis at pixel level was fused with the motion analysis at worm level.

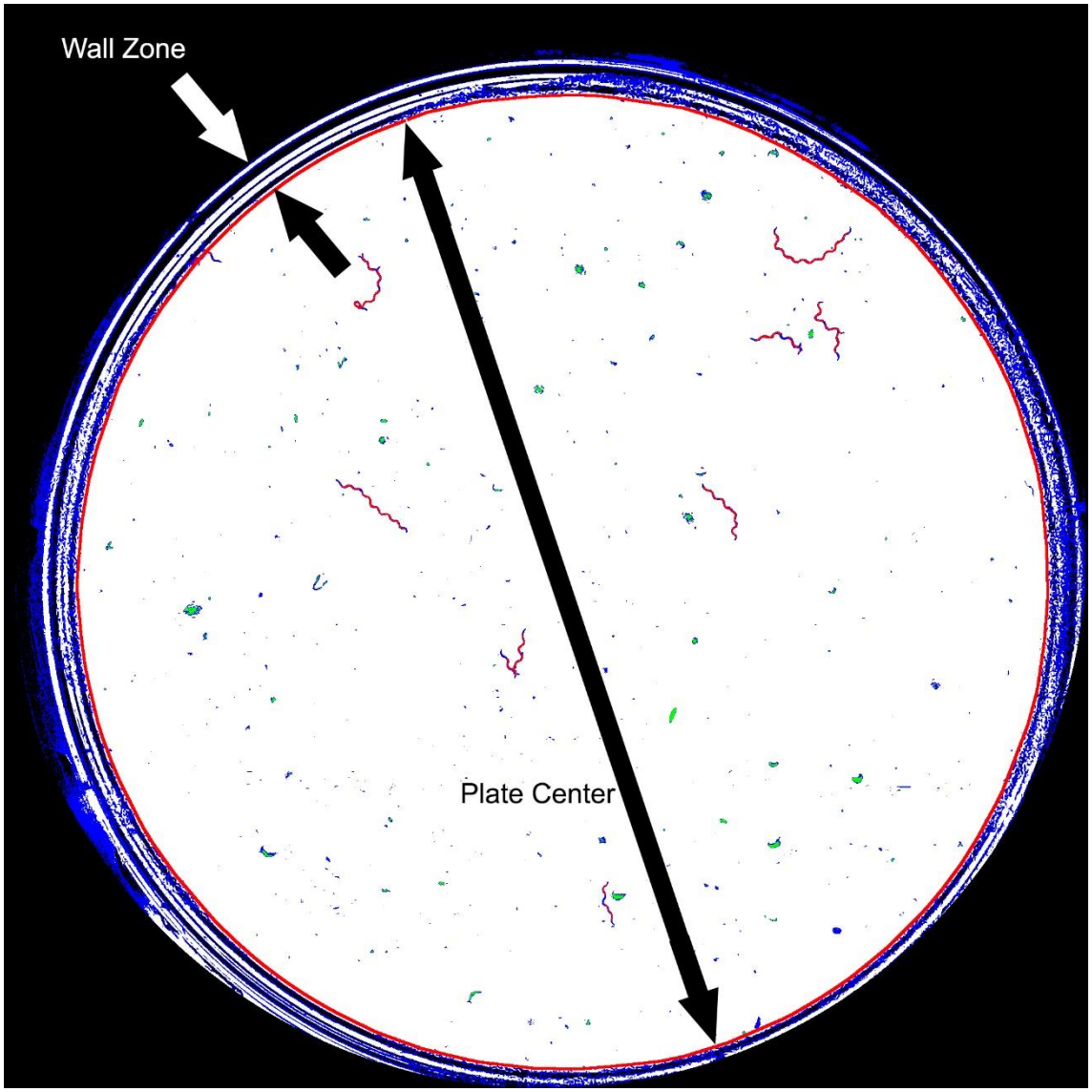

Figure 2.3. Classification at pixel level. The red circumference marks the edge between the two plate zones.

The first step consisted of classifying pixels by their signature templates (Figure 2.2 b). This step involved pixel segmentation per image by taking a fixed 33 grey intensity threshold and avoiding any manual threshold adjustment. This fixed threshold segmentation procedure was possible because the background pixels were controlled as being close to grey level 48 by an active lighting system [42]. Afterwards, the 30-segmented images were stacked in one 30-channel image. Each pixel in the stacked image was classified as a 'constant dark' pixel (black or green), a 'constant white' pixel (white), a 'noisy pixel' (blue) or a 'pixel in motion' (red), depending

on the temporal signature (Figure 2.2 b). The temporal signature of a pixel was composed of its 30 stacked values. If all the values were black, this pixel was classified as 'constant dark'. If all the values were white, it was classified as 'constant white'. 'Noisy pixels' and 'pixels in motion' presented different patterns switching between black and white. Specifically, 'noisy pixels' presented a higher frequency of changes than pixels in motion.

Afterwards, the central plate zone was detected automatically by selecting the white blob with the maximum area. The contour of this blob was the edge between the plate centre and the wall zone. Constant dark pixels were black-coded in the wall zone and green-coded in the plate centre. The result of these steps is shown in Figure 2.3.

The second step consisted of classifying movements following plate zone criteria (Figure 2.4). In this step, the red pixels in the wall zone were dilated to a radius of 40 pixels through the black and blue pixels. The purpose of this dilation was to connect the pixels in motion going through the black rings (cast by wall shadows and reflections) present in the wall zone. Next connected components labelling was applied by considering red, green and blue pixels to be equivalent colours in the plate centre and only red pixels in the wall zone. These steps resulted in tracks at the pixel level (Figure 2.4a). They all had some pixels in motion, which means that at least one live worm was moving in each track. Finally, these tracks were classified into three classes (Figure 2.4b) depending on whether they were completely inside the wall zone (depicted in red), completely in the plate centre (depicted in green) or in between (depicted in yellow). The tracks completely inside the wall zone were denoted T_w and those in between or completely in the plate centre were denoted T_c.

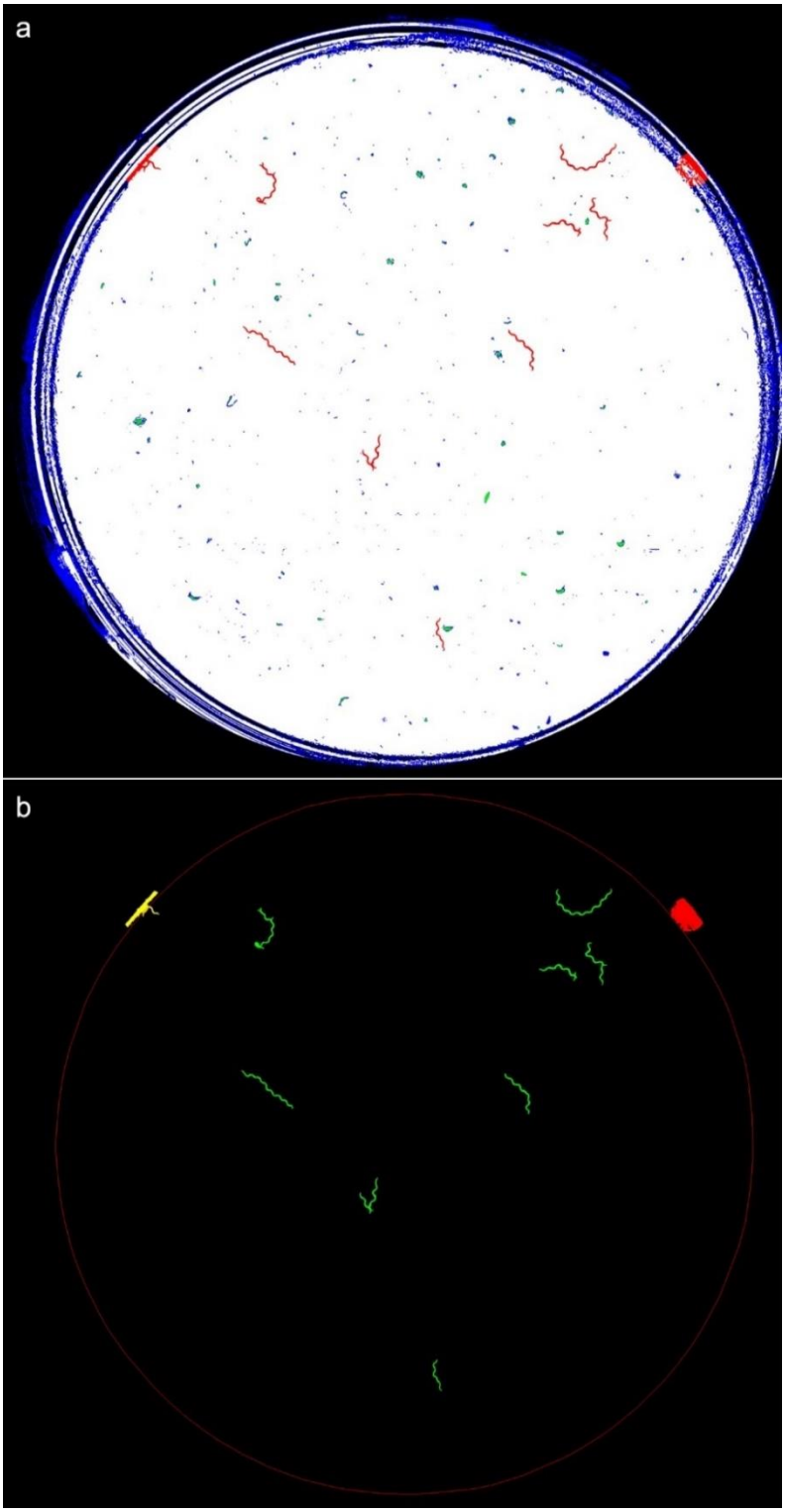

Figure 2.4. Detection of movement and classification. (a) Blobs representing detected tracks (marked in red). (b) The contours of the classified tracks at pixel level.

The image-processing pipeline in the wall zone was completed in this step. In this case, each movement fully detected in the wall zone was counted as one live worm because motions were detected at the pixel level. In this zone, some false-negatives could occur due to occlusion in the black (darkened by wall shadows) and blue (noisy zone) rings. In the plate centre however, the pipeline was developed as far as the worm level for each image.

The third step started by performing connected components labelling (dark blobs) for each segmented image after taking into account only the plate centre (Figure 2.5). These blobs (marked in red and magenta; discarded worms) represented possible aggregates formed by *C. elegans* and dirt contamination (marked in blue). They were filtered according to size by allowing sizes only from 20 pixels (the smallest detected worm area) to 240 pixels (the biggest detected area of two aggregated worms). In our case, some false-negatives could occur due to the aggregation of more than two worms during image sequencing.

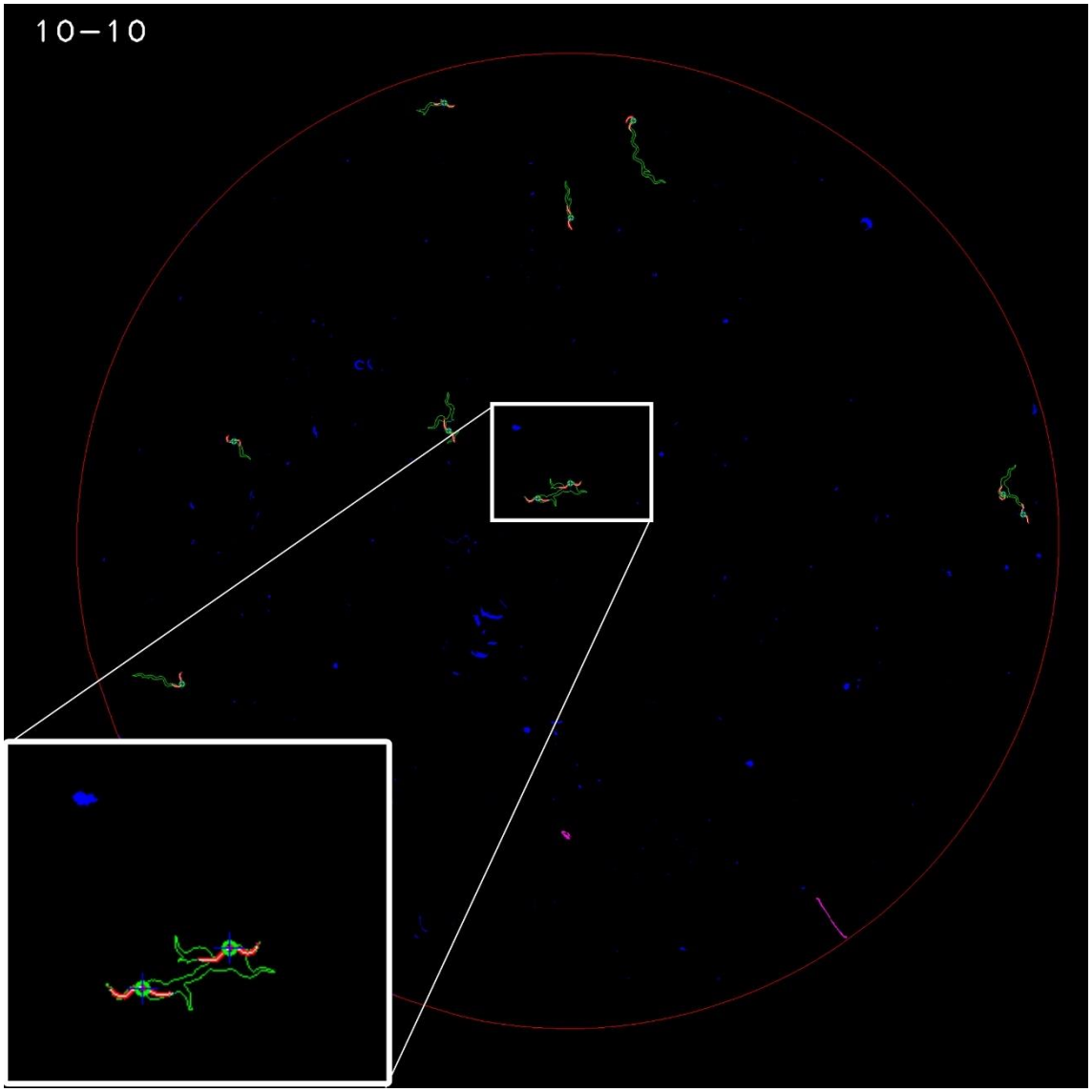

Figure 2.5. An example of a segmented image. The red, blue and magenta blobs represent the segmented results.

The fourth step involved the disaggregation of two possible aggregated worms (Figure 2.6a). This step started by extracting all the end-points (green points) and crosses (blue points) of each blob skeleton (white) (Figure 2.6b). An optimisation algorithm was applied to extract all the possible disaggregated worms by considering shape features (length and width). A possible worm (p_w) was considered a series of end-points and/or crosses connected by continuous skeleton edges. A set of possible worms (s) was a partition of continuous skeleton edges (possible worms (Figure 2.6c)). The cost of a possible worm ($\mathrm{D}(p_w)$) was the Euclidean distance

between the measured length and the width features of a possible worm with its theoretical values. The cost of a set (I_s) (Equation (2.1)) was the mean cost of all the costs of possible worms (n). After thoroughly exploring all the possible sets (s), the final selected set of disaggregated worms was the set with the minimum cost (Equation (2.2)).

$$I_s = \frac{\sum D(p_w)}{n} \quad (2.1)$$

$$\arg\min I_s \quad (2.2)$$

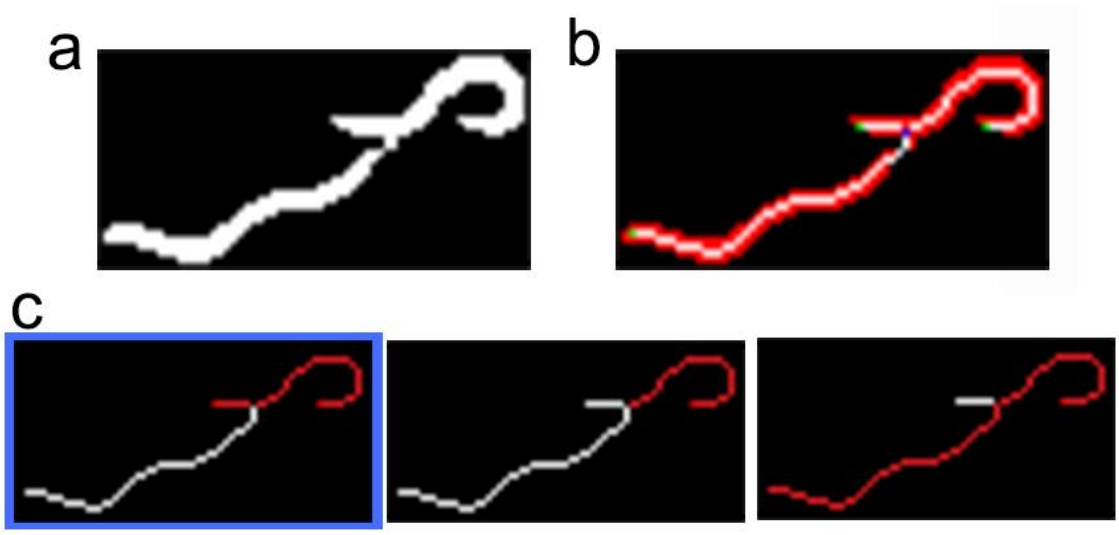

Figure 2.6. An example of two aggregated worms. (a) Segmented subimage. (b) Three skeleton edges (white), two end-points (green) and one cross (blue). (c) Searching space: three possible solutions (the Is cost is lower in the first case, marked in blue).

Then each possible disaggregated worm was filtered by colour features. Worm intensities were expected to be lower than the grey level 20. A detected worm was a blob that fulfilled the aforementioned shape and intensity features.

After detecting worms in the current image, the fifth step consisted of tracking worms along the 30-image sequence. Images were captured at 1 fps, which allowed worms to be more easily tracked because of their overlapping location between images. Then each worm-level track was classified as a motion or quiescent track.

The sixth step consisted of fusing the detected tracks at different levels to decide how many live worms were inside each pixel-level track. On the one hand, the pixel-level tracks (see Figure 2.4b) were detected in the whole plate. On the other hand, the worm-level tracks were detected in the plate centre. This redundant information in the plate centre was used to avoid any inconsistency and to count how many worm-level tracks were in motion at the same time inside each pixel-level track. This count was the amount of live worms moving inside each pixel-level track (a_{T_c}).

A live worm was a blob that accomplished the previous shape and intensity features, and its movement was detected in the last 24 h. It was classified as a live worm if motion was detected in either the current image sequence (a_{T_c}) or between the current image sequence and the previous one (a_P). The second option required comparing different image sequences. The seventh step consisted of image alignment techniques to correct any placing inaccuracies between the image sequences captured at different times.

At the end of their lives, worms do not change their location and hardly change their shape, but do move their heads. Therefore, it is easy to track worms at the end of their lives and thus detect death events, when only slight changes in shape can be expected. In this context, if a quiescent worm was detected along the current sequence of images, it was monitored to see if there were changes in the corresponding sub-image taken one day before. If there was no shape change, a high matching score would be expected between both sub images when allowing a small Euclidean transformation between them.

Finally, the live worm count was the sum of all the tracks completely inside the wall zone, all the live worms detected in each track completely or partially in the plate centre, and all the live worms for which motion was detected when comparing image sequences (Equation (2.3)).

$$a_{is} = \sum T_w + \sum_{T_c} a_{T_c} + \sum a_p \qquad (2.3)$$

Post-processing

Lifespan curves are monotonically decreasing functions. Therefore, a lifespan-counting error could be detected when a current live worm count (or in a current image sequence) was higher than a previous count. These errors can occur for two different reasons: (1) because the live worms detected in the current image sequence were aggregated or hidden in previous sequences (previous false-negatives) or (2) because some blobs, which erroneously appeared due to dirt contamination (dust spots on lids), met the live worm criterion in the current sequence (false-positives).

Herein, a new post-processing method is proposed in an attempt to optimally correct these errors. It is noteworthy that corrections were made only if a count error was detected in the automatically extracted lifespan curves. Corrective actions took into account error occurrence probabilities in order to act accordingly.

The initial number of live worms was known because the expert designed the experiment and placed the worms on the plates. Therefore, this initial value per plate can never exceed the lifespan. If it was exceeded for any plate, this plate count was limited to its initial number. Post-processing was applied individually to each Petri plate so that every plate count would be separately corrected from other counts.

In the first half of the lifespan cycle, more potential errors appeared due to hidden worms and aggregation (false-negatives) than to dirt (false-positives), and survival was high. In the second half of the lifespan cycle, this situation was inverted (dirt accumulated and survival dropped). Consequently, the post-process contemplated these two stages (Figure 2.7).

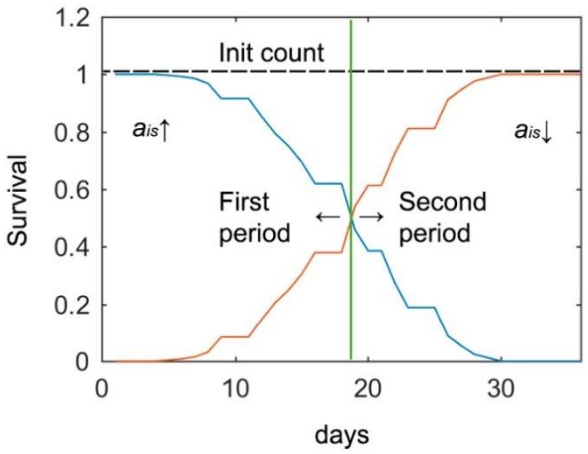

Figure 2.7. Two post-process stages or periods. Blue is the survival curve separated into the first (ais, value is corrected upwardly) and the second (ais, value is corrected downwardly) period by a dividing line on day 18. The red curve is the survival inverse (death curve).

On the plate edge, a shadow was cast by the plate wall, covering about 7% of the plate area in which worms are hidden. Although there was a low probability of the nematode being in that area, this error correction was made by post-processing. This meant that hidden worms were negative errors. Thus during the first cycle period, if a current image detected more worms than the previous day, it was interpreted as worms hiding in the shadow (or worm aggregation), and the previous day's count was corrected by a_{is} being upwardly corrected (Figure 2.7). It is unlikely that worms would remain hidden for more than one day, due to the small size of the shaded area and high mobility of young worms. During the second lifespan period, to reduce errors due to the aforementioned dirty environment, the post-processing strategy changed (positive errors had a higher probability than negative ones), and the currently detected worm count was less likely to be higher than the previous one. Therefore, the current count was the limit of the next day's count (a_{is} is corrected downwardly). With this approach, the error standard deviation was reduced by half.

Source code and lifespan experiment example

The source code is on github with an MIT open source license and the code repository is available (https://github.com/AntonioJoseSanchezSalmeron/lifespandownload).

MATLAB, OpenCV and Java in Windows 10 were used. The code is evaluated with MATLAB R2018b and Java 1.8, and can be downloaded and run by launching MATLAB files (lifespan.m and postprocess.m). There is a lifespan experiment example that can be downloaded from https://active-vision.ai2.upv.es/wp-content/uploads/2020/01/Lifespan18.zipdownload and the processed results https://active-vision.ai2.upv.es/wp-content/uploads/2020/01/Lifespan18_Results.zipdownload.

Validation method

To quantify errors, the lifespan experiment was performed in a standard laboratory without cleanroom facilities. In these experiments, the live worm count was done in duplicate: one automated count and another manual count. The automated count was done using the image-processing techniques described above, while the manual count was done using the captured processed images to check for any automated count errors. Thus the manual curve had to be taken as a reference and the error was measured. Apart from providing to be a good approach, post-processing showed the manual, automated and post-processing curves.

Experiments and results

As previously mentioned, false-negatives and false-positives can occur due to occlusions, aggregation and dirt contamination problems. Some experiments were performed to estimate the probabilities of these errors and to assess the new data post-processing method. Essentially, the lifespan assay was needed for evaluations, whose methods are described above, and it was run four times in four different experiments, three to study variability and one to study robustness to large errors. Each experiment comprised 20 plates (55 mm), each containing 10 nematodes of the N2 strain ($n = 200$). With the lifespan experiments, automated errors and post-processing errors were analysed on the survival curve. For the experiment to study robustness, some errors were forced by displacing plates during data acquisition in order to assess post-processing robustness. First in the lifespan experiments, collision detection was done

to estimate the aggregation probability for several cases (experiments with 10, 30, 60 and 90 worms per plate) to evaluate the most suitable worm count per plate.

Aggregation probability estimation

In the lifespan experiments, worm population density is a widespread problem because clusters make it difficult to detect the exact number of nematodes. Both automated detection and human counts are difficult. The solution to this problem may be as simple as reducing the number of *C. elegans* individuals per plate. As determining an adequate number of worms per plate can be quite subjective, an attempt was made to estimate the aggregation probability depending on worm count. A lifespan assay with four conditions was performed for 30 seconds. Each condition had a worm count per plate that was a unique distinctive factor: 10 worms/plate ($n_1 = 360$), 30 worms/plate ($n_2 = 360$), 60 worms/plate ($n_3 = 360$) and 90 worms/plate ($n_4 = 360$). Collision events were calculated through the 30 images. As Figure 2.8 shows, a 10-worm population caused a reasonable 1% aggregation of two worms, while 30, 60 or 90 individuals increased to 2.6 ± 0.6%, 4.6 ± 1.34% and 6.6 ± 1.26%, respectively. Thus a suitable choice would be 10 (or 15) worms on a 55 mm-diameter plate, which is 0.99 ± 0.24%. Hence we estimated that this percentage was low enough, and the experiments were conducted with this sample number per plate.

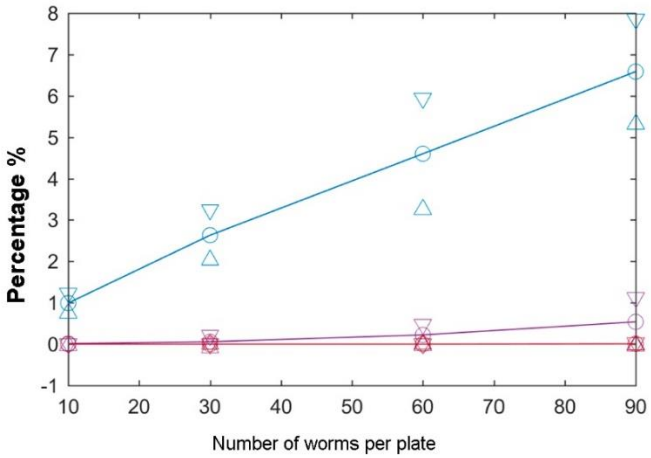

Figure 2.8. Aggregation probabilities. Influence of worm number per plate of 27.5-mm radius, where these curves are the probabilities of aggregation for two (blue line), three (purple line) and four (red line) worms.

False-positive and false-negative analyses per day

The four lifespan experiments were run in a normal laboratory where there were small lint and dust particles. The manual count of the captured images represents our ground truth. Nevertheless, wall shadows hid the worms even from human inspection, although worms were not hidden every day. Therefore, if a manual count was higher on one day than on the previous day, it would be reasonable to assume that worms were hidden in the wall area the day before. So human count regressive correction gave more realistic results, and two different curves (visible and real number of worms) were extracted from the human count, where the difference between these two counts gave the number of hidden worms, from which the probability of this event was calculated. Moreover, counting dirt errors allowed the likelihood of this event to be calculated.

On the first lifespan assay days, the young L4 worms moved faster and covered longer distances than old worms on the last assay days. Both travelled distance and speed decreased with every passing day. This was why the probability of a live worm leaving an occlusion zone lowered with each assay day. However, dirt contamination accumulated with each assay day and, therefore, the probability of finding dirt contamination increased as the assay progressed. It was assumed that errors due to occlusions

(false-negatives) were more probable than dirt contamination errors (false-positives) on the first assay days, and that errors due to dirt contamination (false-positives) were more probable than those due to occlusions (false-negatives) on the last assay days. The experiments confirmed that errors due to occlusions (false-negatives) were more probable than dirt contamination errors (false-positives) on the first assay days. Dirt contamination errors (false-positives) were more probable than those due to occlusions (false-negatives) on the last assay days. As shown in Figure 2.9a, the probability per day of all the hidden events occurring was circa 20% on the first days and the false-positives rate was about 3% during the same period. During the second period, the positive errors increased to 12% and the negative errors dropped to 2%.

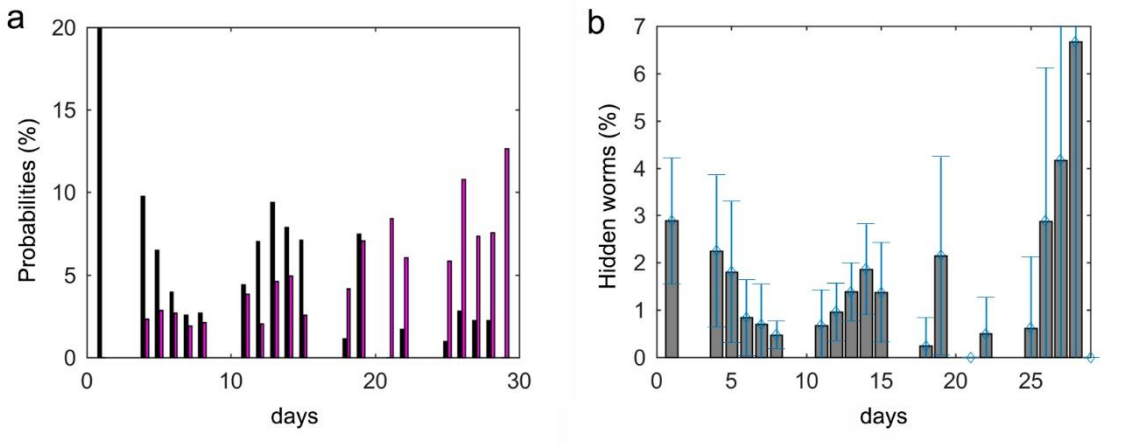

Figure 2.9. FN and FP probabilities per days. (a) Probabilities of false-negatives (black bars) and false-positives (magenta bars) per day. (b) Probability of worms being hidden on each day (they were located in the wall zone).

Some false-negatives could be due to the aggregation of more than two worms during image sequencing. However, the probability of three worms being aggregated for 30 seconds (a complete image sequence) when 10 or 15 worms were cultured in a Petri plate was practically 0% (Figure 2.8).

No detection due to hidden zones

E. coli was sown in the plate centre so, as well-documented, worms will move near this feed zone. If we assumed random movement, 7% of worms would to be found on the plate's edge (wall shadow) because this is the shadow area percentage. Nevertheless, as stated and Figure

2.9b shows, the worm non-detection percentage by the edge zone was less than 3% almost every day. This better detection could be due to two phenomena, (1) worm speed, which facilities their movements to a large space within 30 seconds; (2) the previously stated animal nutritional needs. For the former, we were unable to differentiate between these two reasons for improved detection on the first days when we observed 3% of worms in the hidden zone. However after the mean life period had elapsed and when worms moved more slowly, we observed that the percentage of worms in the edge zone remained below 3%, which indicates that speed was also a reason for improved detection in this zone. On days 27 and 28, the percentage came closer to 7%, possibly because that worms moved quite slowly and *E. coli* may have run out in some plate zones.

Comparing the automated and post-processing results

As stated previously, our ground truth was the corrected manual count lifespan curve, which was compared with the automated and post-processing curves. Figure 2.9 depicts how an optimum day near the mean lifespan can be used to change the post-processing filter strategy. A mean lifespan depends on conditions which may prolong or shorten it, and it usually takes place on day 14 with the N2 strain. A life versus death turning point occurs on this mean lifespan day (Figure 2.7), meaning that there are fewer worms during the second period because some have died. For both these reasons, the period division day was selected as the mean lifespan of N2.

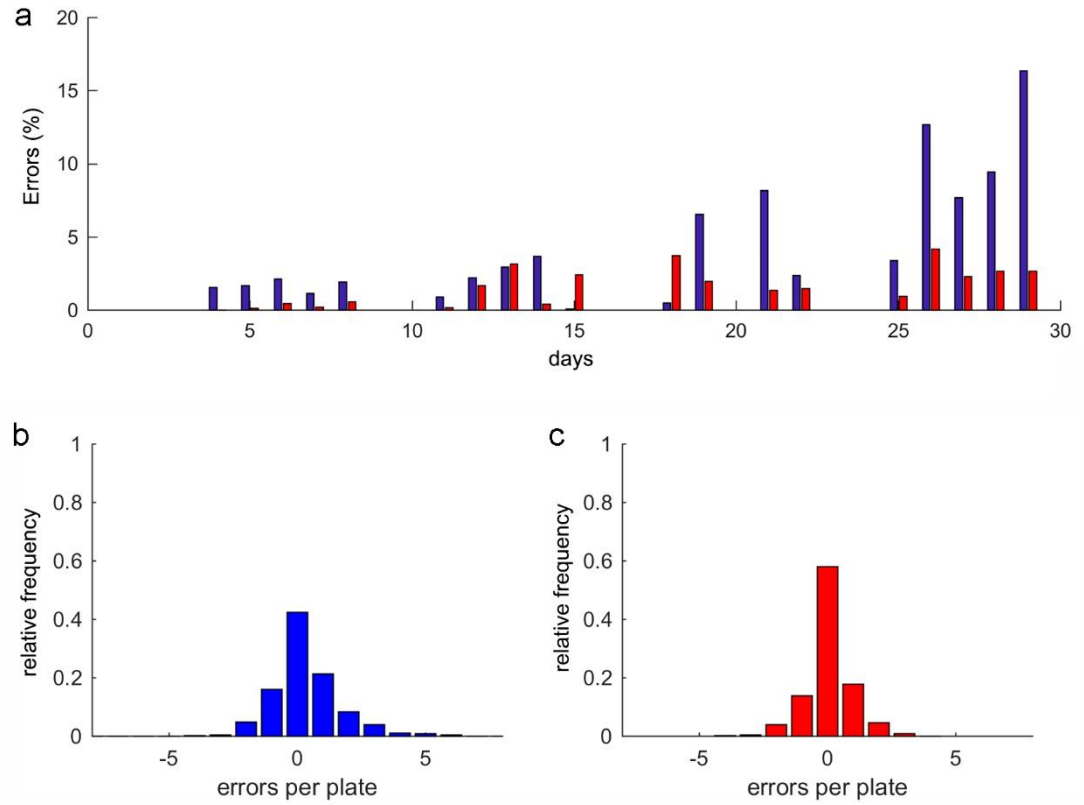

Figure 2.10. Error analysis. The error is E = Automated count – ground truth. Thus negative errors are non-detected worms (false-negative) and positive errors are detected contamination (false-positive). (a) is the absolute error percentage per day of the whole population, and the automated error (blue bars) is compared to the filtered result error by post-processing (red bars). (b) shows the automated error frequency distribution per plate for all three experiments with a positive or negative sign (in individuals), while (c) is the post-processing error frequency distribution.

To assess this method, three lifespan experiments were conducted with the N2 strain, where each one composed 20 plates with circa 10 worms per plate. Experiments were performed following the methods described in this manuscript. The results are shown in Figure 2.11a. These results indicated that an automated measurement had a typical error of 4.62 ± 2.01%. These values included errors due to contamination and dirt, which could vary according to room conditions. For all three experiments, post-processing always gave improved results by reducing the global error from 4.62 ± 2.01% to 2.24 ± 0.55%, and by the diminishing error spikes that spontaneously appeared at any time (Figure 2.10c). Thus the post-process reduced not only the mean error, but also variability (Figure 2.10a). This effect was observed more clearly in plates (Figure 2.10b)

where the automated error followed a Gaussian distribution of a mean of 0.32 individuals, a standard deviation of ±1.4 individuals and a non-error probability of 42%. When post-processing was applied, the mean error decreased to 0.06 individuals, the standard deviation to 0.9 individuals, but the non-error probability increased to 60% (Figure 2.10c). This variability per plate according to standard deviation narrowed because high abnormalities of four or six errors were filtered. In order to check robustness, errors were produced on purpose by randomly forcing plate displacement during some captures, which gave false-positive errors (Figure 2.11b). In this case, the automated error increased from 4.62% to 8.02%, but the post-processing algorithm was able to correct errors and reduced it to 1.8% error.

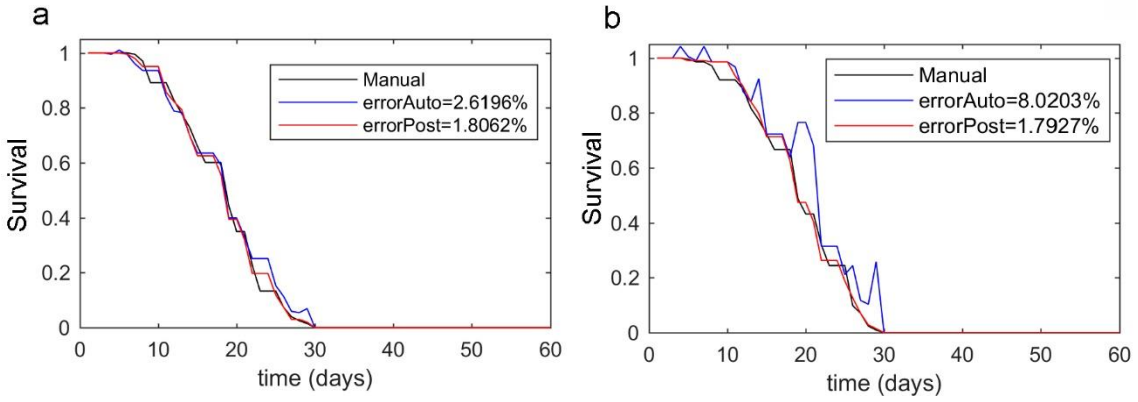

Figure 2.11. Lifespan curves. The lifespan curves measured manually (black line) and automatically (blue line), and the curve post-processing based on automated filtering (red line). (a) is a typical lifespan of the N2 strain. (b) is the N2 strain lifespan, but with some forced errors.

Another lifespan experiment was conducted following the same methods, but with n = 152 individuals and the *daf-2* strain with a longer lifespan, up to 60 days[46], [47]. This number of days is considerably longer than that of the N2 lifespan, thus facilitating dirt accumulation. Therefore, it was of interest to study the *daf-2* strain lifespan applying this method. This longer life expectancy gave a distinct mean lifespan. Thus the daily life and death probabilities changed as regards both conditions and strains. As expected, the optimum selected day was also the mean lifespan (42), and the results revealed that this approach was correct. As Figure 2.12 shows, errors higher than the N2 lifespan curves appeared, which was to be expected

because contamination was higher. Nevertheless, the automated error was 8.54% and post-processing correction lowered this error to 3.43%.

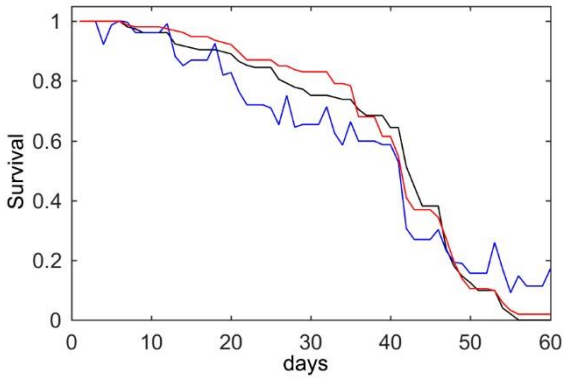

Figure 2.12. The daf-2 survival curve. The black line is the manual count, the blue line is the automated count and the red line results from applying the post-processing method.

Discussion

The methods described herein were evaluated for the controlled illumination based on active vision, which maximized image quality and simplified image processing. These methods are also flexible as they can be applied to different acquisition scenarios, such as lifespan, healthspan, memory assays, etc. Furthermore, it is possible to conduct several experiments in parallel in the same device because plates can be replaced while data are being processed. Other methods, like Lifespan Machine, have the advantage of high throughput (but it cannot analyse other characteristics like healthspan) or WorMotel (which keeps worms isolated). The proposed method can be run in parallel with manual capture of image sequences, as in “Lifespan machine”, or even automated capture as in “WorMotel”.

A post-processing filter took into account the probability of errors occurring on different days by applying various error correction strategies to minimise final count errors. The optimal corrective action considered that all the errors on the first assay days were false-negatives and all the errors on the last days were false-positives. The results indicated that it was more advantageous to correct errors on the first assay days by taking them all to be false-negatives because their incidence probability was

higher than for false-positives, and it would be more useful to correct errors on the last assay days by considering them all to be false-positives. This filter was applied independently of each plate.

The experimental results showed that the automated counting errors of live worms followed a Gaussian distribution, with a mean of 0.32 individuals (almost 0.0) and a standard deviation of ±1.4 individuals per Petri plate. Post-processing reduced this error to 0.06 ± 0.9% individuals per plate. The automated survival curve gave an error of 4.62 ± 2.01%, while the post-processing method reduced it to approximately 2.24 ± 0.55% of the curve error. Outliers were alleviated by this method which, hence, provided more robustness to plate displacements and dirty environments, and helped to ease typical occlusion problems due to aggregation, hiding, contamination or condensation. As the graphs reveal, the error average per plate came close to zero, hence: the larger the sample, the fewer errors on the lifespan curve. Thus by reducing errors with post-processing, the sample size is smaller for a given error, which implies shorter experimentation and analysis times, and cheaper costs in relation to plates, animals, storage, etc.

In order to reduce the negative errors caused by occlusions (wall shadows, aggregation, etc.) different tools and methods were developed and used. On the one hand, the motion analysis that worked at pixel level was applied to wall zones to detect live worms despite occluded dark rings. Theoretically, the probability of worms being inside this wall zone was 7%, but the results indicated that this probability was less than 3% because the feed was sown in the plate centre. On the other hand, the probability of three-worm aggregations came close to zero when using 10 to 15 worms on a 27.5 mm-radius plate. When a two-worm aggregation was detected (probability of 1.09%), an optimisation process was applied in an attempt to disaggregate them.

We studied two strains, N2 and *daf-2*, which were those assessed by this method. The results indicated that our post-processing method is a good lifespan determination method for any nematode strain, even for a long lifespan during which dirt and contamination progressively increase. It

may also be suitable to set the mean lifespan as an optimum day to change the correction strategy.

PAPER 3

Small flexible automated system for monitoring Caenorhabditis elegans lifespan based on active vision and image processing techniques

Joan Carles Puchalt[1], Antonio-José Sánchez-Salmerón[1]*, Eugenio Ivorra[1], Silvia Llopis[2], Roberto Martínez[2] and Patricia Martorell Guerola[2]

[1] Universitat Politecnica de Valencia, Instituto de Automatica e Informatica Industrial, Valencia, Spain

[2] Cell Biology Laboratory/ADM Nutrition/Biopolis SL/Archer Daniels Midland, Paterna, Valencia, Spain

Puchalt, J.C., Sánchez-Salmerón, AJ., Ivorra, E. *et al*. Small flexible automated system for monitoring *Caenorhabditis elegans* lifespan based on active vision and image processing techniques. Sci Rep **11**, 12289 (2021). https://doi.org/10.1038/s41598-021-91898-6

Abstract

Traditionally *Caenorhabditis elegans* lifespan assays are performed by manually inspecting nematodes with a dissection microscope, which involves daily counting of live/dead worms cultured in Petri plates for 21–25 days. This manual inspection requires the screening of hundreds of worms to ensure statistical robustness, and is therefore a time-consuming approach. In recent years, various automated artificial vision systems have been reported to increase the throughput, however they usually provide less accurate results than manual assays. The main problems identified when using these vision systems are the false positives and false negatives, which occur due to culture media changes, occluded zones, dirtiness or condensation of the Petri plates. In this work, we developed and described a new *C. elegans* monitoring machine, SiViS, which consists of a flexible and compact platform design to analyse *C. elegans* cultures using the standard Petri plates seeded with *E. coli*. Our system uses an active vision illumination technique and different image-processing pipelines for motion detection, both previously reported, providing a fully

automated image processing pipeline. In addition, this study validated both these methods and the feasibility of the SiViS machine for lifespan experiments by comparing them with manual lifespan assays. Results demonstrated that the automated system yields consistent replicates (p-value log rank test 0.699), and there are no significant differences between automated system assays and traditionally manual assays (p-value 0.637). Finally, although we have focused on the use of SiViS in longevity assays, the system configuration is flexible and can, thus, be adapted to other *C. elegans* studies such as toxicity, mobility and behaviour.

Introduction

C. elegans has been successfully used as a biological model for a wide range of studies related with development, longevity and diseases. In particular, lifespan assays in *C. elegans* has become one of the most widespread research trial models.

In biological terms, *C. elegans* has a lifespan of approximately 3 weeks and it is sensitive to environmental conditions, such as light and temperature. Thus, phototaxis [2] and thermotaxis [48] stimuli should be considered when performing lifespan assays as they could impact on the nematode's life expectancy in extreme conditions. In *C. elegans*, phototaxis is characterized by a withdrawal response from wavelength light source shorter than blue light [49]. Thus, the lower the wavelength, the greater the nematode's response. Light not only causes a simple escape response, but also causes death when blue-violet and at shorter wavelengths [33]. In the case of thermotaxis, nematodes also exert a withdrawal response to a heat source5. Just slight heat exposure induces hyperthermia, which reduces life expectancy and causes death. Both stimuli cause stress in the nematodes, therefore, protocols are based on storing cultures in temperature-controlled incubators under dark conditions during the assay, exposing them to ambient conditions only in short inspection periods (a few minutes every day) under the dissection microscopes.

Traditionally the *C. elegans* lifespan assay [1], [2], [33], [48]–[50] has been performed manually by expert inspection using a dissection microscope, and counting every day the number of nematodes surviving under specific culture conditions [3]–[7] in standard Petri dishes.

The dead or alive criterion is inferred from *C. elegans* movement, which categorizes the worm as alive if movement is detected, and dead otherwise. However, this is complicated due to animal slowness in accordance with its ageing, which ends when worms fail to move at all during inspections. This is why nematodes are mechanically stimulated by an expert applying pick stimulation to confirm death. This task, which has to be done to each worm successively, is both arduous and laborious.

The difficulty arises when assays require large numbers of nematodes. In this context, there is a need to increase the screening capacity, reduce errors and produce objective results.

Different automated lifespan systems have been described for studying *C. elegans* viability, mobility or fecundity. Most of them capture and process images of *C. elegans* cultured in different constrained scenarios to facilitate detection of the time of death. Some systems use standard Petri dishes, such as Lifespan Machine (LM) and SiViS. On the other hand, there are systems, such as WorMotel, microfluidic devices and others, that use non-standard plates.

The Lifespan Machine (LM), is an example of a medium-scale-plate image-capture device for macro-inspection (8μm), and is based on the simultaneous capture of 16 standard Petri plates per scanner [16]. Although it is based on automated detection, this device only allows a small number of frames to be monitored per minute due to the slow image scanning process. Besides, a large number of plates in an assay will require many scanners, which may make the conditions heterogeneous, for the same measurement. In addition, the plates cannot be exchanged, and remain fixed in the equipment until the end of the experiment, thus preventing the devices from being used in parallel for other assays. In order to increase flexibility, our device has managed to take enough

images to track the *C. elegans* paths. This feature also enables it to perform other kinds of assays (such as dispersion, healthspan, etc.). In addition, it allows the Petri plates to be changed during the experiments, as well as measuring plates under the same conditions.

Another example of a lifespan-assay machine is the WorMotel [35]. This machine automates the plate-changing process, allowing for large-scale screening under the same conditions by using a robot handling system, which transports plates from buffers to inspection zones. However, it uses non-standard plates, where each well contains only one *C. elegans* to simplify death detection. It should be pointed out that worm behaviour might be modified due to isolation in a small space [51], and this set up does not allow long-trajectory analysis. By contrast, in our system, worms are inspected in standard Petri plates measuring 55 mm in diameter, holding 10-15 individuals and thus permitting more complex social behaviour [52], [53].

Further examples of inspection equipment are based on microfluidics with techniques such as micropillars [54]–[56], which consist of keeping the nematodes between micropillars. The advantage is that fluid can be replaced by keeping the worm in position; however, it is subject to mechanical stress. These machines use non-standard plates and are therefore often difficult to adopt by traditional laboratories, where standard Petri dishes have been used for many years.

There is also open-source software to process image sequences, either to detect the nematodes or even to extract subtler characteristics that may provide other types of information. These include trackers that observe an individual worm [28], multi-trackers that follow the progress of several individuals [15] and microscopy devices that extract micro-features from a worm [57]. There are also several tools for animal detection and phenotype identification. Phenotypes for motility [15], [19], [23], [29], [58], longevity [14], [59] or fecundity [21], among others.

The goal of our study was to validate the methodologies and a new automated system for *C. elegans* longevity studies. Our system is

characterized by its compact, flexible, scalable and used-friendly design. This newly described method for *C. elegans* lifespan assays is based on the integration of different computer vision techniques, such as active vision [42] and adaptive motion detection techniques [60], which we evaluated together. The active vision method improves image quality and minimises the light intensity emitted by the lighting system illuminating the worms. The other method, motion detection, also implements a post-processing adaptive data filter; this method improves worm detection. All in all, this system enables the automation of *C. elegans* lifespan assays using computer vision techniques in a scenario similar to the manual assays. The new method described herein draws on the traditional manual *C. elegans* lifespan inspection method, but incorporates fully automated image processing methods. This paper begins by describing the SiViS machine and methods, which include building a prototype, and the computer vision techniques employed. Secondly, we report lifespan assays performed to compare the automated SiViS results with manual expert's results for validation proposes. Finally, we draw conclusions and suggest future studies.

Materials and methods

To test the proposed automated method, a SiViS prototype has been designed, developed and validated. Thus, several methods are explained in the next subsections: (1) the SiViS and software GUI designed and (2) the light control, image processing and lifespan validation employed.

Compact mechanical design

SiViS has two closed compartments: one for the inspection area (Figure 3.1 a, b) and the other for electronics. The closed inspection compartment attenuates the environmental conditions of lighting and temperature, to minimise them and thus reduce their direct effect on nematode life expectancy. There is a door for easy introduction and replacement of Petri plates. Forced ventilation ensures that the inspection area stays at room temperature (Supplementary Figure S1) to prevent condensation and hyperthermia, and a sensor registers the temperature and inserts it as

metadata in each image. The inspection area has a slot where the pallet (Figure 3.1c) is fitted.

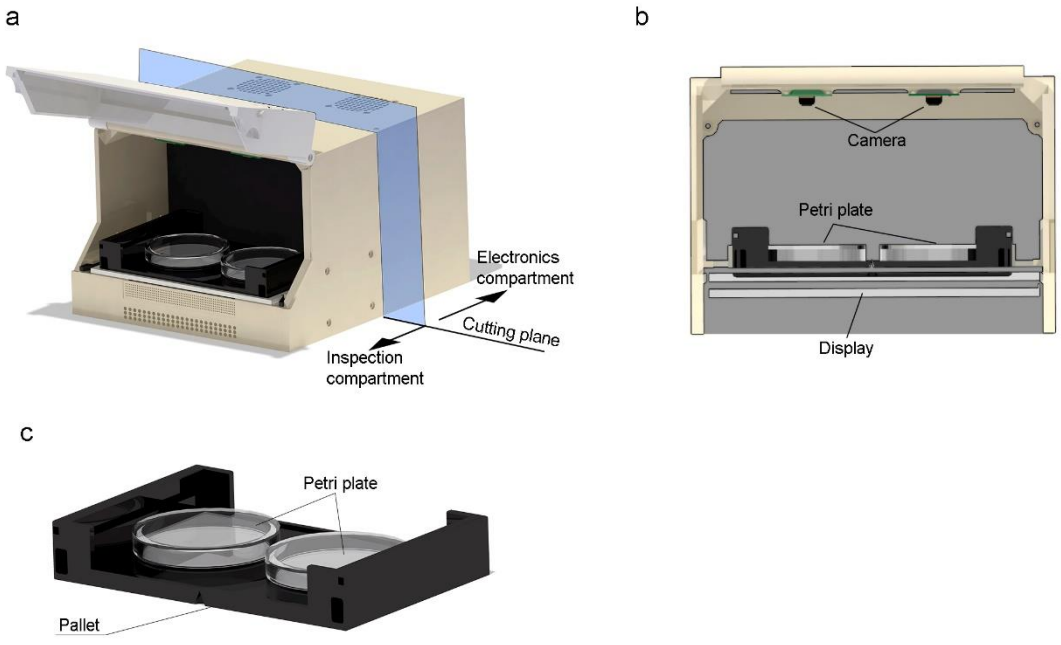

Figure 3.1. Prototype of the SiViS device. The image was obtained with SOLIDWORKS 2020 SP3.0. (a) SiViS with the open door, showing the pallet inside the inspection area. The electronic compartment, at the back, is closed and therefore hidden from view. (b) Section showing the inspection area and the distribution of the components. (c) Pallet with two slots for the Petri plates.

The Petri-plates fit into the pallet (Figure 3.1c) facilitating storage, as well as improving their handling and correct placement in the inspection area. The design was conceived to include two slots for two Petri plates. The pallet is rectangular (140×90 mm), with two circular holes inside measuring 54 mm in diameter, into which the two 55mm-diameter Petri plates are slotted. It is rigid with just a small amount of flexible material for the circular plate-slots, allowing the necessary deformation for the plates to slot in. The pallet has two grooves by which it can be fitted into the device frame, thus restricting potential shifting and rotation. The pallet rests on the lighting system diffuser. All of these features avoid displacement and ensure that the plate is always in a similar position, in order to improve repeatability.

The vision system in the inspection compartment is configured in a traditional backlight way, with the lighting system below, Petri plate above, and camera overhead (Figure 3.1b). This device has two 5MP cameras to inspect each Petri plate, thus enabling the parallel inspection of two Petri plates of 55 mm diameter.

Prototype construction, components and assembly

The mechanical components were produced by 3D printing, with the fused filament fabrication (FFF) method. Materials employed were polylactic acid or polylactide (PLA), which melt at between 150 and 160°C. There is an elastic piece to forcibly fit the plate onto the pallet, this material is Filaflex, and was fabricated in the same process.

Electronic components: 7" Raspberry Pi display of 800×480 pixels size, 155×86 mm visible area and 16.7 million colours, Raspberry Pi v3, Raspberry Pi NoIR Camera v1, Multiplexor for Raspberry Pi Camera. The components and the guidelines to build this system and the assembly description can be found in the repository https://github.com/JCPuchalt/SiViS.

Lighting control

To help automate image segmentation we used the method described in a previous work [42], which is based on keeping the image pixel level at a reference value as shown in Figure 3.2b, by regulating light intensity dot to dot from the lighting system. This system uses the display as a lighting system (actuator) onto which a different projection pattern is drawn at each sampling time. The camera also functions as a sensor, feeding-back the signal and adjusting the control action to obtain a constant reference throughout the entire image. This method enhances worm definition and improves image visibility despite certain kinds of dirtiness and condensation.

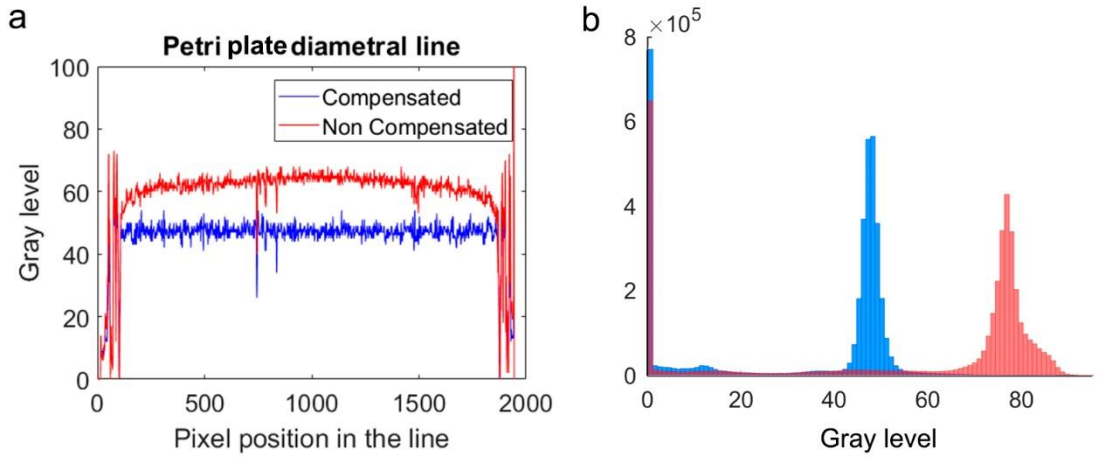

Figure 3.2. Light control results. The image was obtained with MATLAB R2020b. (a) Two images were taken of the same plate, one image was not compensated (red) while the other was compensated (blue). For comparison, the grey pixel level is shown in diametral line (profile line) to the Petri plate of each image. The diametral line measurements correspond to the intensity line profile. Compensated image tends to reference level (48). (b) The compensated image histogram shows the background level approximates the reference level (48).

A proportional controller (PID) was designed to cancel out errors in few iterations. Errors are the differences between references and measurements. The references are the desired intensity levels in the images. The measurements are the intensity levels in the captured images. The control actions, calculated by the regulator, are the light intensities of the light points. An automated calibration process was performed to obtain the homography relation between pixels and points of light.

Caenorhabditis elegans are sensitive to blue light [32], [35], so an important aspect of this system is that we can select the amount of blue, green and red that the nematode is subjected to, and thus control the levels of light stress imposed. To regulate light intensity, we used the strategy of increasing the RGB components of each pixel by first increasing the red component progressively. When red reaches saturation, green is added progressively to the saturated red (255), after green becomes saturated too, the same is done with blue component. The parameters were configured so that the blue component was not required for control action compensation, however in the opaque zones the blue component was required to try to compensate. These dark areas are the plate ends, since the plate walls generate shadows (Figure 3.2a).

Flexible image processing techniques

These techniques [42] are based on nematode *motion detection* and *post-process* filter. During this assay, several *C. elegans* were cultured in standard Petri plates, which were transported daily from the incubator to the inspection zone.

The active lighting system allows a fixed threshold segmentation algorithm to automatically extract dark blobs in all images captured with SiViS. After some image processing steps, a blob filter is applied. This filter is based on features of shape, color and movement. Finally, live worms are detected based on movement features extracted from different days.

As previously stated, the pallet was designed to improve repeatability for plate replacement, and software [42] was employed to compare nematode position on different days. This software estimates the translation and rotation of nematodes and transforms this data to match blobs between images.

Motion detection techniques

Nematode movement slows down with ageing, so this is an important feature to observe when tracking worms. Likewise, data on maximum velocity must be established. After observing 10 plates and taking into account numerous studies [13], [15], [28], worm speed was estimated at between 0.2 mm/s and 0.5 mm/s, which represents 50% of its size per second. Thus, taking an image per second ensures overlap of the nematode in each consecutive image, which makes tracking easier and more accurate. Regarding *nematode motion*, at least a sequence of In images per plate (In=30) were taken every day at 1 fps. The image resolution achieved was 30μm/pixel, which provides enough information for behavioural analysis, and also captures the entire plate. Movement integration was extracted from this sequence (Supplementary Figure S2). This motion information can be observed in this sequence when worms are young; however when they age their movement has to be compared with the sequence taken on the previous day. If nematode position does not change from one day to the next, then the worm is dead.

Lifespan automation is challenging because a host of problems can arise. The image processing software must be designed to avoid different causes of false-negatives (or undetected live worms) and false-positives (or wrongly detected live worms). False-negatives can be due to worm aggregation problems or to occluded plate zones (e.g. zones near plate walls, or non-transparent zones due to dirt or condensation problems). False-positives can be due mainly to dirt problems.

Post-process filter technique

Lifespan curves are monotonically decreasing functions. Therefore, a lifespan-counting error could be detected when a current live worm count was higher than a previous count. These errors can occur for two different reasons: (1) because the live worms detected in the current image sequence were aggregated or hidden in previous sequences (previous false-negatives) or (2) because some blobs, which erroneously appeared due to dirt (dust spots on lids), met the live worm criterion in the current sequence (false-positives).

A post-processing method is proposed in an attempt to optimally correct these errors. It is noteworthy that corrections were made only if a count error was detected in the automatically extracted lifespan curves. Corrective actions took into account error occurrence probabilities in order to act accordingly.

In the first stage (half of the lifespan cycle), more potential errors appeared due to hidden worms and aggregation (false-negatives) than to dirt (false-positives), and survival was high (Supplementary Figure S2). In the second stage (half of the lifespan cycle), this situation was inverted (dirt accumulated and survival dropped). Consequently, the post-process contemplated these two stages. In the first stage, if an error was detected the previous count (Supplementary Figure S3) is corrected upwardly and in the second stage actual count is corrected downwardly.

This post-process method corrects the errors detected taking into account the different probabilities of occurrence of the errors in two different

phases separated by a threshold. This threshold can be defined as the meanlife of the strain used in the assay.

User-friendly software

In order to manage the daily image-capture tasks, two software applications were created on a server (desktop PC) (Figure 3.3). One is the CaptureCE software, which enables the user to design experiments easily in a graphical interface, automatically programming image-acquisition tasks in a user-friendly way. Thus, the user only has to click on a button to take the images, and see them in real-time; consequently, if contamination is shown, the contaminated plates can be censored. The images are sent from SiViS to server via Ethernet. The other software is the ProcessorCE (Figure 3.3 b), which enables image processing and survival-curve creation by clicking on a button, as easily as with CaptureCE (Figure 3.3 a).

The use of this device is simple. Petri plates are fitted into pallets, which are stored inside an incubator. Pallets are later removed from the incubator and fitted into the SiViS slot. Once pallet images have been taken, the pallet in the SiViS slot is exchanged for another one for inspection, and so on. Pallets are numbered, in order to follow a sequential procedure, whose sequence matches the programmed sequence of tasks automatically created by the CaptureCE software. Hence, the user follows the procedure, which noticeably reduces human errors in this process.

a

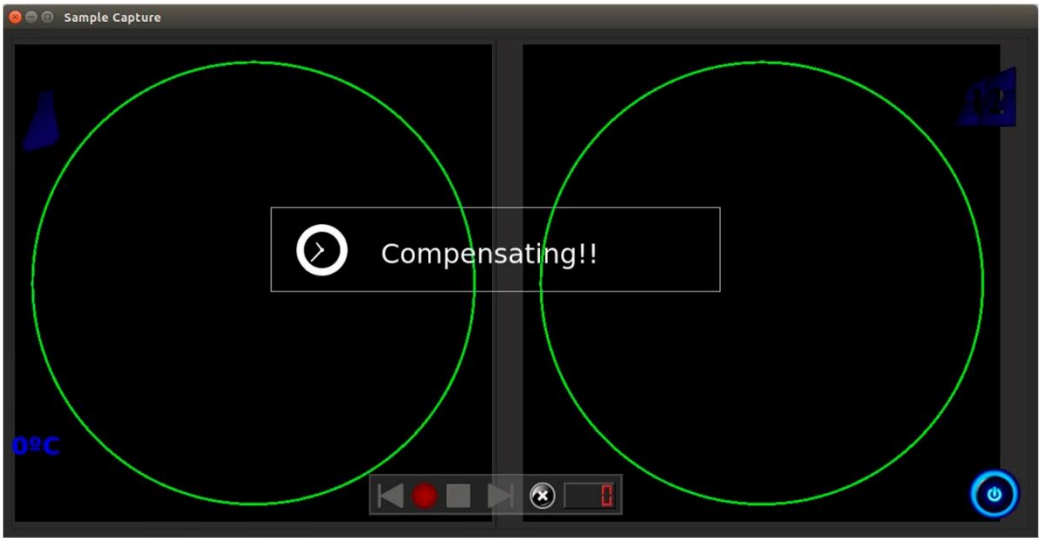

b

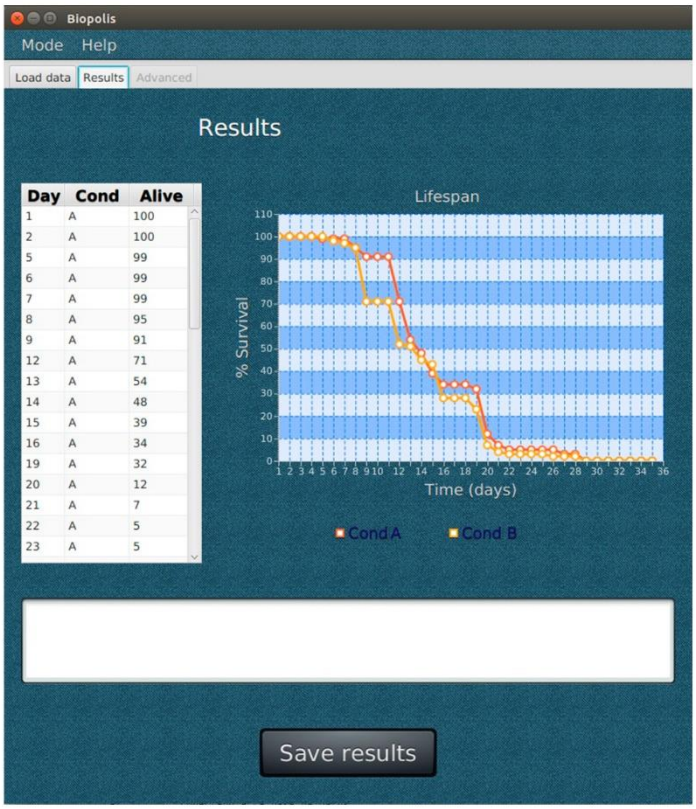

Figure 3.3. Graphic user interfaces. (a) CaptureCE interface is like a video player which shows the two pallet plates in real time. Experiments are created and the experiment to be captured is selected. (b) ProcessorCE interface is used to select captured experiments to be processed and provide the corresponding survival results.

Lifespan validation

***Caenorhabditis elegans* strains and culture conditions**

Caenorhabditis elegans strains N2, Bristol (wild-type); CF1038, *daf-16 (mu86)* and CB1370, *daf-2 (e1370)* were obtained from the *Caenorhabditis* Genetics Center at the University of Minnesota. All strains were maintained at 20°C on nematode growth medium (NGM) seeded with *Escherichia coli* strain OP50, as standard diet.

Lifespan assays

Lifespan assays were performed with the wild-type strain N2 or the corresponding mutant strains deficient in *daf-16* (CF1038 (*daf-16, mu86*)) and *daf-2* (CB1370, *daf-2 (e1370)*. Age-synchronized worms were obtained by hatching the eggs from gravid worms in NGM plates and incubating them at 20°C until the young adult stage was reached. FUdR (0.2 mM) was used to prevent reproduction [8], [10], and fungizone (1μg/mL) was added to prevent fungal contaminations. The drug metformin was added to NGM at a dose of 50 mM. Young adult worms (10-15 per plate) were used for the first day of lifespan experiments. Viability was scored daily (except weekends) with the automated SiViS device until 100% of nematodes were dead. In parallel, manual experiments were performed. In these experiments, nematodes were scored under a dissection microscope and considered as dead if they failed to respond on being prodded with a platinum wire. At least, two independent assays were carried out in each test.

Statistical analysis

Statistical significance among lifespan curves was estimated by log rank test using GraphPad Prism v. 4 statistical software. This test was used to analyse reproducibility on *C. elegans* N2 lifespan curves obtained in the automated SiViS system. Furthermore, correlation between manual and automated experiments was evaluated by comparing lifespan curves in N2 strains and the mutant strains in *daf-2* and *daf-16*, exhibiting extended or shortened lifespan.

Results and experiments

SiViS integrates different techniques, which might lead to some unexpected behaviour. In order to assess the correct functioning of the system, several experiments were performed. Thus, lifespan curves data from different trials were used to asses various features, such as repeatability and correlation between manual and automated count. The correlation was performed for wild-type strain N2 strain and for mutants CF1038, *daf-16 (mu86)* (short-lived strain) and CB1370, *daf-2 (e1370)* (long-lived strain). In addition, the anti-diabetic drug metformin, which has been reported to increase *C. elegans* lifespan, was included in the validation study [11], [24], [61].

Automated system provides repeatable results

Lifespan measures, in particular, are well known to exhibit substantial run-to-run variability in *C. elegans*, due to stochastic events [62].

In order to determine the repeatability of the method for counting live nematodes in the automated device, we obtained different lifespan curves from six independent experiments (Table 3.2) with wild-type nematodes in standard growth conditions (NGM plates). Results, shown in Figure 3.4, indicate low levels of deviation among the different curves measured in the device. We obtained overlapping curves, showing little variation in median lifespan (p-value log rank test: 0.699). Therefore, we can conclude that the automated system produces consistent replicates (Table 3.1). This further demonstrates the high degree of homogeneity and repeatability offered by this system.

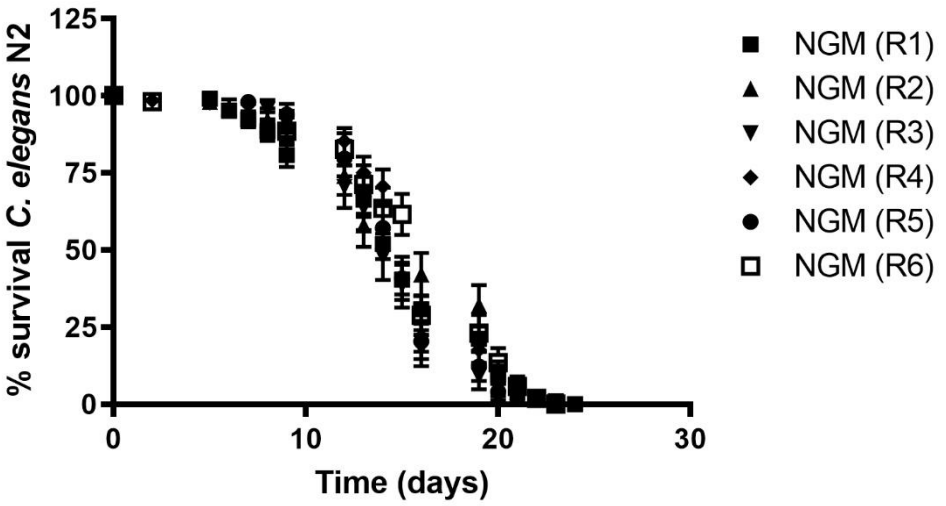

Figure 3.4. N2 survival curves. The graph was obtained with GraphPad Prism v. 4. Lifespan curves of C. elegans N2 obtained from independent experiments with the automated system, in standard conditions (NGM). Curve comparison was estimated by Log RanK T-test (p value: 0.699). A comparison among replicates is indicated in Table 3.1.

NGM replicates	Sample size	Nr. plates
R1	104	8
R2	50	4
R3	44	4
R4	68	6
R5	49	4
R6	52	4

Table 3.1. Sample size and number of plates are indicated for each independent assay with wild-type *C. elegans* strain N2 in standard growth conditions (NGM plates).

	P value				
NGM replicates	**R2**	**R3**	**R4**	**R5**	**R6**
R1	0.4796 (ns)	0.6951 (ns)	0.3124 (ns)	0.5324 (ns)	0.37775 (ns)
R2	–	0.2043 (ns)	0.8660 (ns)	0.1210 (ns)	0.9928 (ns)
R3	–	–	0.1750 (ns)	0.9821 (ns)	0.3029 (ns)
R4	–	–	–	0.668 (ns)	0.9621 (ns)
R5	–	–	–	–	0.1296 (ns)

Table 3.2. p-values estimated in the comparison among replicates of NGM. A Log Rank t-test was applied. *ns*: without significant differences

Lifespan curves of wild-type C. elegans obtained in the automated device correlate with manual assays

A critical test of the automated system developed is to verify that nematode lifespan measured by this device is similar to that for animals reared under conventional agar-plate-based conditions. To do so, we performed parallel studies of animals maintained in NGM plates, and recorded live worm-counts by machine and using specialized technicians.

Survival curves obtained for *C. elegans* N2 by the automated system were statistically similar to those obtained by manual worm-count assays. As shown in Figure 3.5, very similar results were obtained for both approaches, without significant differences between both curves (p-value: 0.637).

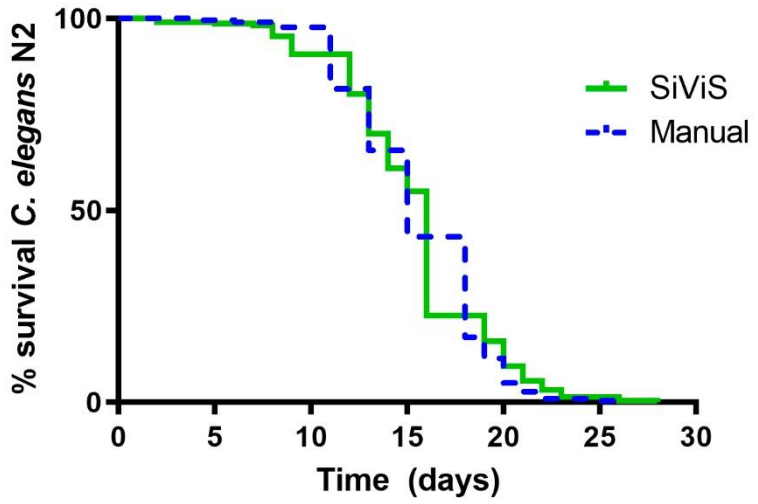

Figure 3.5. Manual-automated comparison for N2. The graph was obtained with GraphPad Prism v. 4. Comparison of lifespan curves obtained by the automated system and by a manual assay for *C. elegans* wild-type strain N2. Data from four independent experiments (n=200/condition; 16 plates/condition). To compare curves a Log Rank T-test was applied (p value: 0.637). Mean lifespan of 16 days (for automated system) and 15 days (for manual assay). Maximum lifespan of 26 days (automated and manual assays).

Validation in C. elegans mutant strains

The IIS pathway is the best-characterized longevity pathway in *C. elegans*. Reduced signalling through this pathway leads to the activation of FOXO-family transcription factor *daf-16* [63], [64] and results in robust lifespan

extension. Reduction-of-function mutations or RNAi knockdown of several components of this pathway, including the genes encoding the insulin-like receptor *daf-2* or the PI3-kinase *age-1* [46], have been reported to enhance longevity.

Accordingly, our next step was to analyse whether mutations known to modify lifespan also produced the expected phenotypes in our automated system. Lifespan curves from mutant strains for CF1038, *daf-16 (mu86)* and the long-lived CB1370, *daf-2 (e1370)* were obtained both with SIVIS and manual assays.

As shown in Figure 3.6, the mutant strain for *daf-16* exhibited a significantly shortened lifespan compared with the wild-type strain N2 ($P<0.0001$), both for manual and automated results (Figure 3.6 a, b). Thus, a mean lifespan of 13 days (for N2) and 12 days (for CF1038) was obtained in the assays scored in SIVIS, and 14 days (for N2) and 12 days (for CF1038) in the manual assays. These results indicate that the automated system significantly detects a shortened lifespan in the case of CF1038, *daf-16 (mu86)*, as reported in the literature. Furthermore, the comparison between the manual and automated systems for each strain clearly shows very similar survival curves (Figure 3.6 c, d).

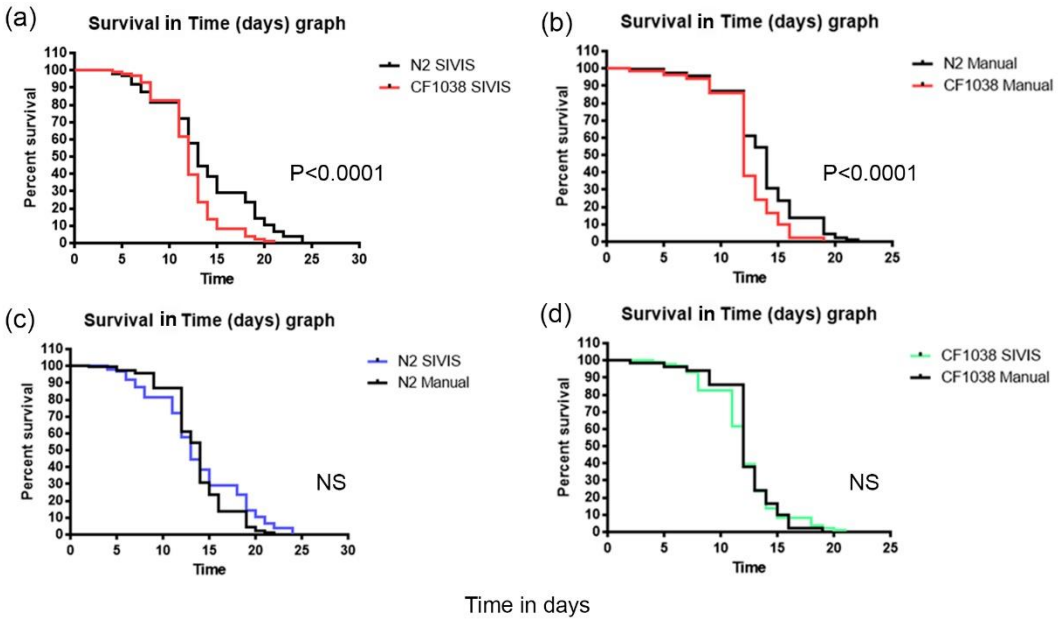

Figure 3.6. Lifespan of short-lived strain CF1038, *daf-16 (mu86)*. The graph was obtained with GraphPad Prism v. 4. (a) and (b) show the comparison between survival curves for CF1038 and the wild-type strain N2 in assays performed in SIVIS and manually, respectively. (c) and (d) show the comparison between the manual and automated system SIVIS for each strain. Data from three independent assays for automated assays (*n*=300 and 24 plates/condition) and two for manual assays (n=200 and 16 plates/condition).

This correlation was also observed for the long-lived strain *daf-2*, but it was necessary to modify the threshold of the post-process filter method (stated in the Flexible image processing techniques subsection). For the common lifespan strains the threshold was about the meanlife (14th day), nevertheless for this longer lifespan strain the threshold should be later (Supplementary Figure S4). As shown in Figure 3.7, curves without this correction differed from the manual assay, while a post-process correction of algorithms enabled a correct survival measurement for lifespan in the long-lived strain CB1370 (*daf-2*).

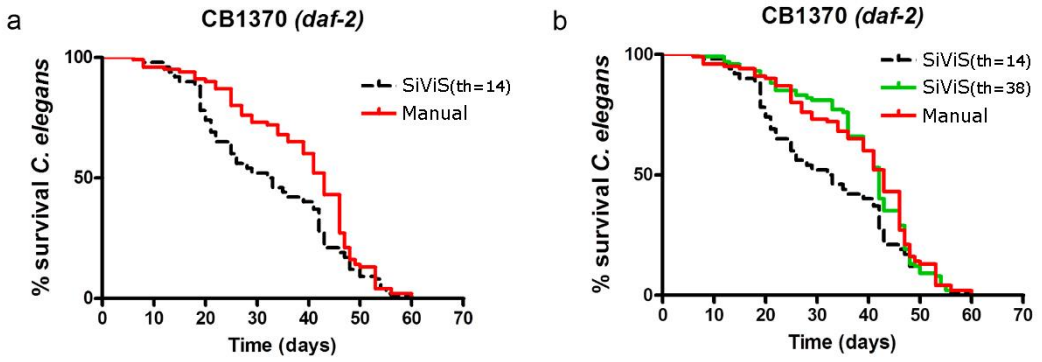

Figure 3.7. Manual and post-process lifespan comparison of *daf-2* mutant strain. The graph was obtained with GraphPad Prism v. 4. (a) Curves obtained in SIVIS differed significantly using the standard correction algorithms with the threshold (*th*) set in 14 (*th*=14). (b) Post process of correction algorithms set in *th*=38 enabled correct survival measurement of lifespan in long-lived strains like CB1370 (*daf-2*). Data from two independent assays (*n*=100 and 8 plates/condition).

Validation of metformin

Metformin is a widely used first-line drug for treatment of type 2 diabetes and has been shown to extend lifespan. Recently, it was shown that metformin increases *C. elegans* lifespan via the lysosomal pathway [24], [65].

In this study, metformin was used at 50 mM, as a dose that previously showed positive effects on *C. elegans* longevity [61]. Manual lifespan experiments were performed in parallel with experiments in the automated system. Results indicated that, as previously described, metformin significantly increases *C. elegans* lifespan, both in the manual ($P<0.0001$) and in the automated system ($P<0.0001$) (Figure 3.8). Furthermore, the mean lifespan in the presence of metformin increased 66.6% (manual assay: NGM=Day12, Met=Day20) and 52% (automated assay: NGM=Day12.5, Met=Day19). No significant differences were observed between manual and automated curves for the different feeding conditions (p-value control:0.1820; p-value metformin: 0.469).

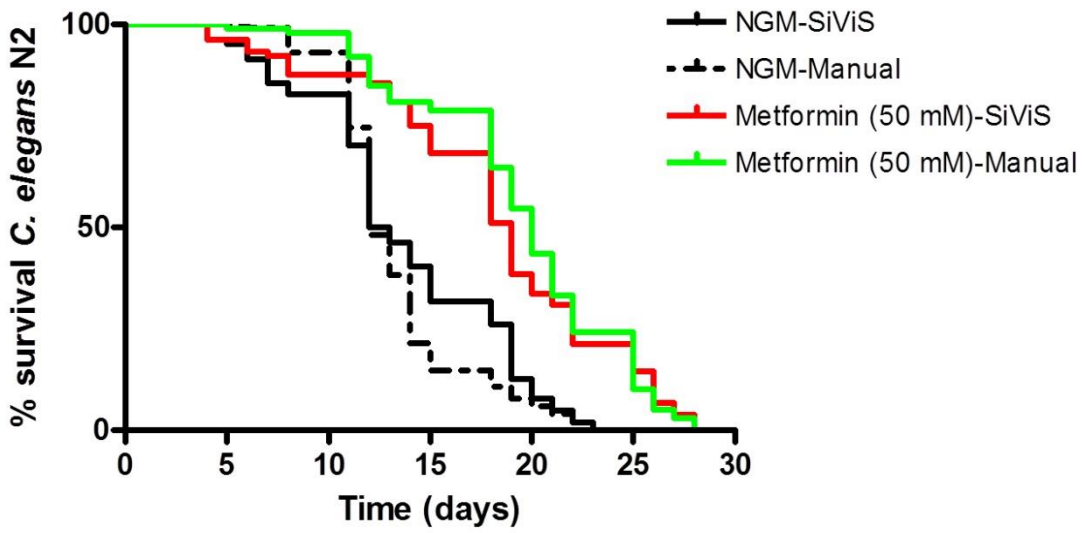

Figure 3.8. Manual-automated comparison for Metformin. The graph was obtained with GraphPad Prism v. 4. Effect of metformin on *C. elegans* lifespan measured in manual lifespan assays and in the automated SIVIS system. Data from two independent assays (*n*=100 and 8 plates/condition).

Conclusions

Here we have presented a new automated method that reproduces the results of the traditional *C. elegans* lifespan method. This automated method frees the expert from the repetitive and arduous work involved in manually counting large nematode populations. It is also a flexible system because, in addition to lifespan assays, it can be used to measure other *C. elegans* phenotypes, such as those related to dispersion, healthspan, memory or food preferences, among others, by simple code modification. Moreover, it is small and use-friendly, enabling more than one experiment to be conducted in parallel on the same device, since the plates can be removed from the inspection area even though the experiment is still underway.

This new method using the SiViS monitor is based on two techniques: i) active vision [42] and ii) flexible motion detection [60]. This live/dead criterion facilitates accurate daily worm-counts, even though the plate is removed and replaced each day. By being able to change the plates, several experiments can be monitored at the same time, which provides

greater productivity and throughput. This also makes it more flexible, so the experimental conditions can be customized. The other technique proposed here relates to active vision, which is an area of computer vision, achieved by adding a control system. Intelligent illumination may highlight the image characteristics of interest, making the light intensity more uniform. This facilitates image segmentation by providing more refined images, which could reduce processing time. Intelligent illumination is a controlled illumination system, which regulates the light intensity and components to which the worm is subjected and, therefore, a lighting pattern can be defined in order to stress the nematode as little as possible, while maintaining optimum image quality.

In this work, a SiViS prototype has been designed, developed and validated for lifespan assays. Results show it is a good approach for lifespan assays in automated worm-count using the methods described herein, without significantly statistical differences between automated and manual counts. Moreover, no significant differences were found between independent measurements, thus its repeatability is good. These conclusions are not only for the N2 strain, but also apply to metformin treatment or to other strains (*daf-2* and *daf-16*), whose lifespans are up to two or three times longer, or shorter. Therefore, the methods are suitable for a variety of lifespan assays.

Considering that SiViS is a satisfactory measuring system, given the above, it has several other advantages. The first relates to the possibility of replacing the Petri plates during the experiment, thus enabling the monitoring of new experiments at any moment. Another advantage is its small size, thus it can be easily scaled up by increasing device number. In addition to this, plate replacement could be automated to achieve a fully autonomous lifespan assay process.

In a future work, we will endeavour to increase sensitivity, which should reduce variance error. If variance error were reduced, sample size might also be reduced, which would save time, number of animals and storage space. In order to achieve this improvement in sensitivity, one solution might be to stimulate worms to make them move, making it easier to

detect them. Several other options exist to create this stimulus, such as phototaxis, chemotaxis or vibrotaxis.

PAPER 4

Reducing Results Variance in Lifespan Machines: An Analysis of the Influence of Vibrotaxis on Wild-Type *Caenorhabditis elegans* for the Death Criterion

Joan Carles Puchalt[1], Pablo E. Layana Castro[1] and Antonio-José Sánchez-Salmerón[1]*

[1] Universitat Politecnica de Valencia, Instituto de Automatica e Informatica Industrial, Valencia, Spain

Puchalt, J.C.; Layana Castro, P.E.; Sánchez-Salmerón, A.-J. Reducing Results Variance in Lifespan Machines: An Analysis of the Influence of Vibrotaxis on Wild-Type *Caenorhabditis elegans* for the Death Criterion. *Sensors* **2020**, *20*, 5981. https://doi.org/10.3390/s20215981

Abstract

Nowadays, various artificial vision-based machines automate the lifespan assays of C. elegans. These automated machines present wider variability in results than manual assays because in the latter worms can be poked one by one to determine whether they are alive or not. Lifespan machines normally use a “dead or alive criterion” based on nematode position or pose changes, without poking worms. However, worms barely move on their last days of life, even though they are still alive. Therefore, a long monitoring period is necessary to observe motility in order to guarantee worms are actually dead, or a stimulus to prompt worm movement is required to reduce the lifespan variability measure. Here, a new automated vibrotaxis-based method for lifespan machines is proposed as a solution to prompt a motion response in all worms cultured on standard Petri plates in order to better distinguish between live and dead individuals. This simple automated method allows the stimulation of all animals through the whole plate at the same time and intensity, increasing the experiment throughput. The experimental results exhibited improved live-worm detection using this method, and most live nematodes (>93%) reacted to the vibration stimulus. This method increased machine sensitivity by decreasing results variance by

approximately one half (from ±1 individual error per plate to ±0.6) and error in lifespan curve was reduced as well (from 2.6% to 1.2%).

Introduction

Lifespan assays in *C. elegans* has become one of the most widespread research trial models [5], [6]. Assay procedure is based on daily nematode survival counts in large populations. Traditionally, this process has been conducted manually by experts, whose ability to discern whether a worm is dead or alive entails several issues, such as [6]. The dead or alive criterion is commonly inferred from *C. elegans* movement, which categorizes the worm as alive if movement is detected, and dead otherwise. However, this is complicated due to animal slowness in accordance with its ageing, which ends when worms fail to move at all during inspections. This is why nematodes are mechanically stimulated by an expert applying pick stimulation to confirm death [66]. This task, which has to be done to each worm successively, is both arduous and laborious. Given the fact that lifespan assays are labour-intensive, repetitive and time-consuming, various devices have been developed for assay automation to improve *C. elegans* assay throughput [16], [21], [57]. These lifespan machines are generally based on computer vision, and they attempt to emulate manual inspection procedures by interpreting sequences of captured images. Despites these advances, lifespan machines must overcome challenges concerning the detection of motility on the last days of worm life because they become very lethargic, requiring *C. elegans* monitoring over long time spans in order to observe any motion. This leads to a series of complications, such as memory for image storage, computational load, inspection times, etc. The issue related to lack of motion in manual inspection has been solved by mechanical stimulation with a platinum wire pick but, to date, lifespan evaluation devices have proved ineffective. There are high-throughput handling mechanisms that can help to stimulate the worms. Automating a platinum wire pick to individually tap each worm is an expensive and complex solution, which is also slow to execute [67]. Other kinds of mechanical stimulation exist [68]–[71], which are non-localised, such as

vibration [72]–[75]. Vibration is able to induce a withdrawal response by stimulating *C. elegans*; namely, vibrotaxis, whereby the worm responds to mechanical vibrations. Tapping causes a mechanical wave that propagates through the medium so, in essence, tapping on a Petri plate is a vibrational source. Mechanical vibration has the advantage of being transmitted through the medium to the whole sample and can, thus, achieve large-scale stimulation, and develop a simpler, more economical vibration system. After an in-depth state-of-the-art study, no reference was found in which vibration stimulation has been used as a method to verify nematode life or death in lifespan machines. It has been employed for other purposes, such as modelling nematode mechanosensory neurons [76], modelling withdrawal response behaviour [68], identifying genes, and worm memory and habituation [77]. Some examples of techniques are available whose implementation involves no kind of vibrator system. MWT [15] resorts to a solenoid tapper to tap plates to study memory and habituation. This machine is also used to observe behaviours like chemotaxis and food preference. To demonstrate that sensory modulation is integrated at many levels [72], a dual cone speaker was utilised. This device allowed the configuration of vibration parameters which, in turn, enabled tests to study behaviour and memory consisting of a sound piezoelectric sheet speaker [75]. Ultrasound devices are employed to reveal the molecular mechanisms of ultrasound neuro-modulation [78]. Besides mechanical stimulation, phototaxis can also be used as a stimulation method. Worm exposure to light induces to withdrawal responses [33], [35], [79]–[81], principally using a blue-light wavelength. Nevertheless, high intensity light is required to stimulate worms, which affects their lifespan and can even kill them [32].

Here, we present a new method based on vibration to stimulate *C. elegans* in Petri plates for lifespan assays, to confirm whether worms are dead or alive. This new method permits the monitoring of nematodes in plates and can be adapted to any automatic inspection device. This method provides more robust detection of worm on their last days of life, during which they hardly move, and reduces lifespan results variance by approximately one half. It is easily automatable and stimulates every

worm at the same time, achieving a very high animal response ratio (>93%). In addition, there is no statistically significant indication that vibration affects the nematode's life expectancy.

Materials and Methods

We used a system composed by a lifespan machine (lighting and vision subsystems) and our proposed vibration subsystem. This system is an improved sensor to calculate lifespan automatically, which enabled us to compare lifespan results with and without vibration conditions. Three experiments were performed to analyse several effects. The vibration timing experiment to study worms' responses (vibrotaxis) to different vibration stimuli. The habituation experiment to analyse the worm inhibition to repetitive stimuli. And Lifespan error experiment to study the improvement in live worm detection by comparing the detection of two different lifespan conditions.

Lifespan Machine

We worked with an automatic lifespan machine [42] and the typical microscope configuration as shown in Figure 4.1 a, where the camera is placed above (Raspberry Pi camera rev 1.3), low-intensity lighting (Raspberry Pi 7" display) is positioned below (backlight), and Petri plates are placed between them (camera is to 77.5 mm from the object). The automatic camera settings are disabled, and the shutterspeed and brightness values are set at 100,000 µs and 25 respectively. It employs one camera to take images of the entire Petri plate (55 mm), it gives about 30 µm/pxl. Nevertheless, there are small dark zones in the wall areas where shadows appear, which represents less than 5%. Consequently, there is a small probability that a worm may be hidden from view. This method is based on active vision, which is used to control light intensity making every image pixel reach a given level of intensity. The reasons for this controlled intensity are: (1) to improve image quality and (2) to stress worms as little as possible due to high light intensity (phototaxis effect). The basic procedure consists in taking an image (Figure 4.1 b) and applying

image transformation to obtain an illumination pattern (Figure 4.1 c), which is drawn on the display. More details are to be found in [42].

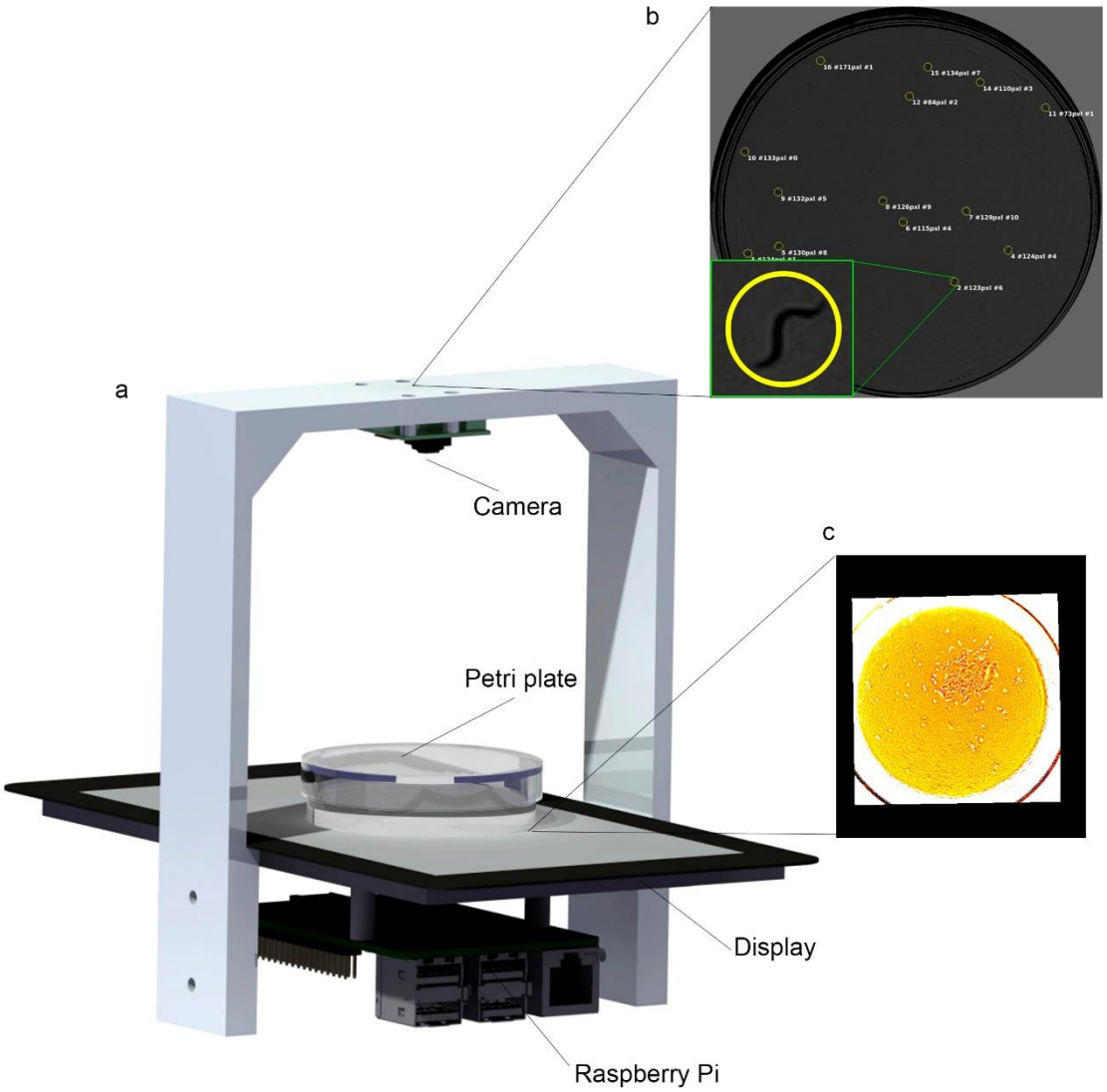

Figure 4.1. Scheme. (a) Lifespan machine used. (b) A Petri plate image, with a zoom of an example worm. (c) Illumination pattern example which is drawn on display.

The experiments run on this machine involve two steps: the first step consists of image sequence acquisition once a day. The second step involves offline processing of image sequences to extract a survival curve for each condition. In this machine, the dead or alive criterion and image processing are defined by the method in [60]. A sequence of 30 images per plate is taken every day at 1 fps. From this sequence information is

extracted about nematode motion detection, when a pixel value changes. This consisted of classifying pixels by their signature templates. This involved pixel segmentation per image by taking a fixed 33 grey intensity threshold and avoiding any manual threshold adjustment. This fixed threshold segmentation procedure was possible because the background pixels were controlled as being close to grey level 48 by an active lighting system. If all the values were black, this pixel was classified as 'constant dark'. If all the values were white, it was classified as 'constant white'. 'Noisy pixels' and 'pixels in motion' presented different patterns switching between black and white. Specifically, 'noisy pixels' presented a higher frequency of changes than pixels in motion. Standard computer vision algorithms, such as tracking and images alignment, allows us to automatically obtain lifespan curves from the image sequences that were captured once daily throughout the assay.

Vibration Mechanism

We have designed and developed a vibration system (Figure 4.2 a) to be installed in the automated lifespan system previously cited [42], and schematically represented in Figure 4.2 c. The vibration method is based on a vibrator motor and, therefore, this simple system can be redesigned and adapted to other lifespan machines. The structure was produced with a 3D printer, composed of both rigid and elastic pieces. The elastic pieces restrain the rigid ones in the equilibrium position, which allows for displacement due to deformation of the elastic part, which returns to the initial position once vibration stops. Figure 4.2 a shows that the rigid component (white coloured material) is the main structure onto which the vibrator motor is fixed (grey actuator on figure), and the elastic support and the Petri plate are thereto attached. The motor provides the source of vibration, transmitted through the rigid structure to the Petri plate. Vibrations (Figure 4.2 b) are produced when the vibrator motor spans an asymmetric mass. Therefore, the mechanical parameters are invariant, except for angular velocity (frequency), which denotes that vibration frequency and intensity are dependent variables because they depend on angular velocity. Therefore in this case, the controllable variables are angular speed and application time. The guidelines to build this system

and the assembly description can be found in this repository (https://github.com/JCPuchalt/vibrotaxis).

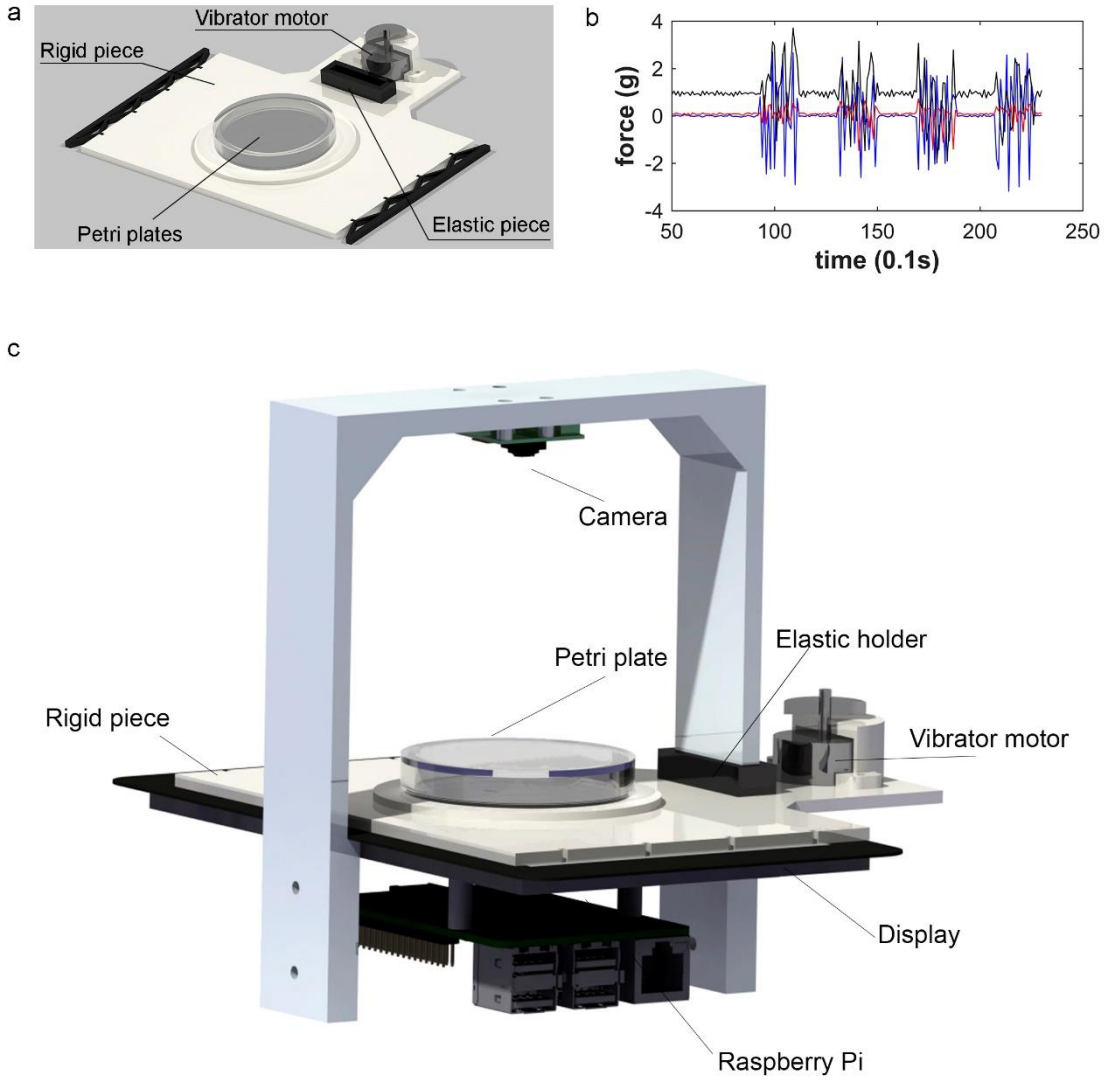

Figure 4.2. Vibrator system. (a) Vibration system parts. (b) In our study, a Petri plate mounted on the rigid component was subjected to vibrations of between 2g and 3g on the X axis and the Z axis, and between 1g and 2g on the Y axis, when the vibrator motor was fed 12 V for 3 s time periods. The measurements were taken by an Inertial Measurement Unit (IMU) GY-521, recording the values shown in (b) (pallet vibration intensity). (c) Assembled altogether: vibration system adapted and the lifespan machine used.

Sample Design

Nematodes were provided by the Cell Biology Laboratory at ADM Nutrition/Biopolis SL/Archer Daniels Midland. They were maintained by

following standard methods [43]. A *C. elegans* wild-type strain culture N2 was prepared and all nematodes were age synchronised and pipetted onto solid NGM in 55 mm Petri plates, and fed *Escherichia. Coli* strain OP50. On the first day of worm adulthood, the plates were stored in an incubator in the dark. Temperature was maintained at 20°C. FUdR (0.2 mM) was added to plates to sterilise worms [82] and to, thus, ensure a constant number of individuals, and fungizone (1 µg/mL) was added to prevent fungal contaminations. FUdR alters lifespan, and therefore a control condition is used with which to compare all conditions. Young adult worms (15 per plate) were used for the first day of lifespan experiments.

Experimental Design

Three experiments were designed. For all the experiments, the vibrator system was mounted on the automated lifespan machine [42]. These components were fitted inside an incubator to maintain Petri plate temperature constant, and to prevent external light from reaching them. For all the experiments, the data on the contaminated dishes were censored. For the vibration assays, the prototype rested on four silicone supports so that no vibration was transmitted to neighbouring devices. These vibration conditions were subjected to vibration for *t* s, followed by a sequence of images that was saved for 30s. These conditions were named *V* with subscript *d* (the day they started undergoing vibration) and subscript *t* (vibration duration in seconds). Every vibration condition has two plates, each one with 15 worms (*n*=30). The conditions with no stimulus were also captured for 30 s, and their nomenclature was *NV* (No Vibration).

Methodology before and after the Vibration Conditions

The $V_{conditions}$ of experiments 1 and 2 were based on worm movement comparison made between, before and after vibration, in addition to its reaction and detection. Thus, it was necessary to acquire images of two consecutive sequences (Figure 4.3). The first sequence consisted of 30 images at 1 fps, which was before vibration when natural worm behaviour could be recorded. As soon as the first sequence finished, vibration was

applied, followed by a second sequence (also 30 images) when worm response to vibration was analysed.

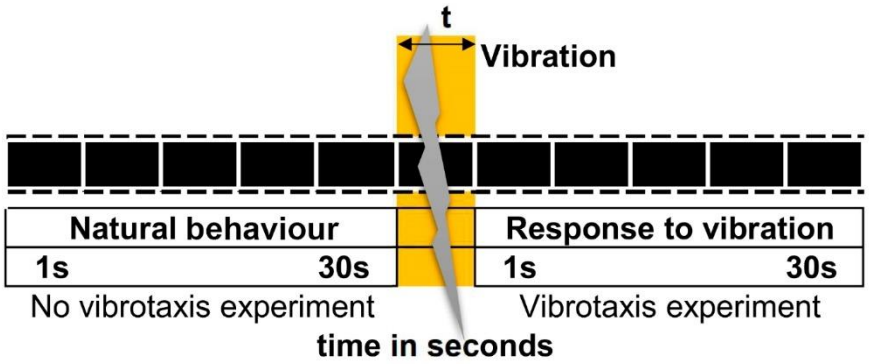

Figure 4.3. Before and after the vibration methodology. Image sequences: a continuous image recording at 1 fps for 30s (natural behaviour), followed by vibration applied for *t* s, and finally another 30s sequence when worm reaction was recorded.

Experiment 1: Vibration Timing Experiment

The aim of this experiment was to study worms' responses (vibrotaxis) to different vibration stimuli. Three different vibration timings were applied in this experiment by defining three conditions, $V_{d_9-t_1}$, $V_{d_9-t_5}$ and $V_{d_9-t_{1,3,5}}$, as shown in Figure 4.4. The light blue squares represent zero vibration and the white squares mean no data were collected. The other squares show that a 1s stimulus was applied (yellow squares) to the $V_{d_9-t_1}$ condition. For the red squares, a 5s stimulus was applied to the $V_{d_9-t_5}$ condition. The $V_{d_9-t_{1,3,5}}$ condition was subjected to stimulus lasting 1s (days 9, 12, 13 and 14), 3s (days 15, 16, 17 and 19) and 5s (days 20 and 21). The sample size of the three conditions was about 140 worms per condition with nine plates per condition.

Figure 4.4. Timeline Experiment 1. Vibration timing/response experiment. White squares denote days with no data acquisition, light blue squares were inspected without vibration (t = 0 s), yellow squares show the worms stimulated for 1 s (t = 1 s), dark blue ones for 3 s (t = 3 s) and red ones for 5 s (t = 5 s).

By using the vibration methodology before and after, as shown in Figure 4.3, this experiment enabled comparisons to be made of the amount of movement variation for these conditions, the percentage of worms that responded to vibration (response index to the stimulus) and the number of live worms detected.

Experiment 2: Habituation Experiment

The habituation effect was analysed by changing the number of times that vibration was applied. A 3 s long vibration was applied once daily, starting on a specific day "d" that depended on the condition, and continued until the end of the nematode lifespan (see Figure 4.5). The dark blue squares represent the stimulus application days for each condition depicting before and after the vibration method (Figure 4.3). The light blue squares denote the data acquisition without any vibration in order to avoid the habituation effect. The $V_{d_2-t_3}$ condition obviously achieved the highest levels of stimulation (from day 2 to day 21) while no vibration was applied for the *NV* condition (No Vibration). Each condition consisted of samples with two Petri plates containing approximately 15 worms (*n*=30), except for $V_{d_2-t_3}$ with 10 Petri plates *n*=174 and the *NV* condition with *n*=170.

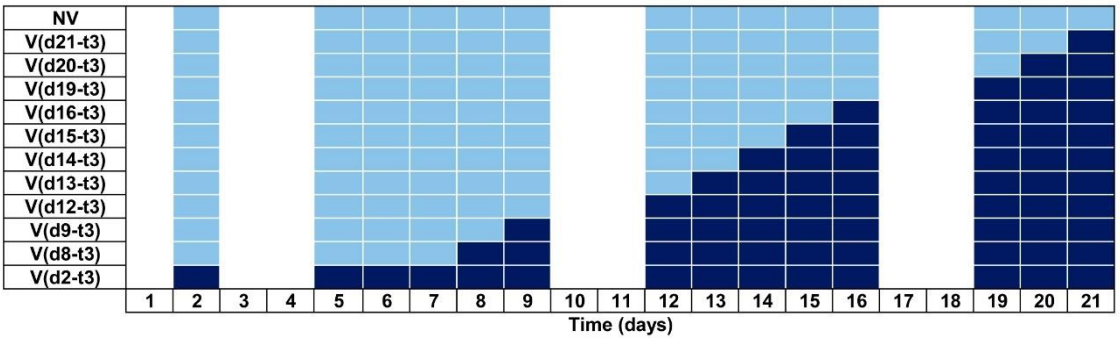

Figure 4.5. Timeline Experiment: Habituation experiment. The white squares are days with no data acquisition, the light blue squares were inspected without vibration (t = 0 s) and the dark blue ones for 3 s (t = 3). It represents the vibration application (dark blue squares) during the lifespan per condition.

Experiment 3: Lifespan Error Experiment

This experiment aimed to study the improvement in live worm detection by comparing the detection of two different lifespan conditions (Figure 4.6).

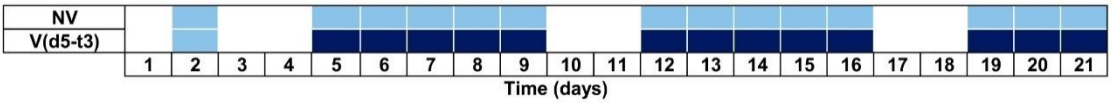

Figure 4.6. Timeline Experiment 3: Lifespan error experiment. White squares denote no data acquisition. Light blue squares depict data acquisition, but no stimulus. Dark blue ones represent data acquisition with a 3 s stimulus.

Condition *NV***,** no vibration was applied, as shown in Figure 4.6 ($NV_{condition}$), whose measures were taken once daily, except at weekends. Two replications were used: n_1=113 and n_2=124. Condition $V_{d_5-t_3}$. This was done by applying vibration t =3s immediately before the 30s image capture ($V_{condition}$), which is the time required for Petri plate inspection. The sample size was n=114 individuals and days with vibration were 5, 6, 7, 8, 9, 12, 13, 14, 15, 16, 19, 20 and 21.

Ground-Truth Data for the Validation Method

For each experiment, the lifespan curves were counted manually by an expert to obtain reference nematode survival values (ground-truth). The followed technique was the same as that for automatic counting (no change in shape and position on the current day and the previous day), but with human supervision by inspecting the machine-captured images. If the number of worms detected was higher on one day than on the previous day, we inferred that worms had remained hidden from view and, therefore, the value was regressively rectified. For experiments 2 and 3, this manual count was done by analysing the captured sequence of 30 images. However for experiment 1, this manual count was obtained by inspecting each plate on three occasions and at three different times by considering the highest of the three values. Therefore, this approximation provides a more accurate value than other experiments because this procedure detects more hidden worms.

Results

Vibrotaxis Analysis

On hypothesizing that vibration-based stimulation could improve lifespan evaluation, it was important to prove whether or not nematodes reacted to vibrotaxis. The no-response ratios corresponded to live worms with no detected movement, as shown in Figure 4.7 for certain conditions taken from experiments 1 (Figure 4.7 b) and 2 (Figure 4.7 a). In experiment 2 (Figure 4.7 a), on day 9 a significant worm percentage (15%) was obtained for the $NV_{condition}$, which began with a lack of movement recorded during the 30 s inspection for signs of ageing. This percentage continued to increase throughout the animals' lifetime to reach 29% no detectable movement. The worms subjected to vibration ($V_{conditions}$, 3s) reacted by moving, mostly throughout their whole life. The no-response rates significantly increased only on the last 2 or 3 days of their lifetime. Thus by applying a 3 s vibration stimulated worm movement with the following results: 99% in week 1, 98% in week 2 and 93% in week 3 (Figure 4.7 a).

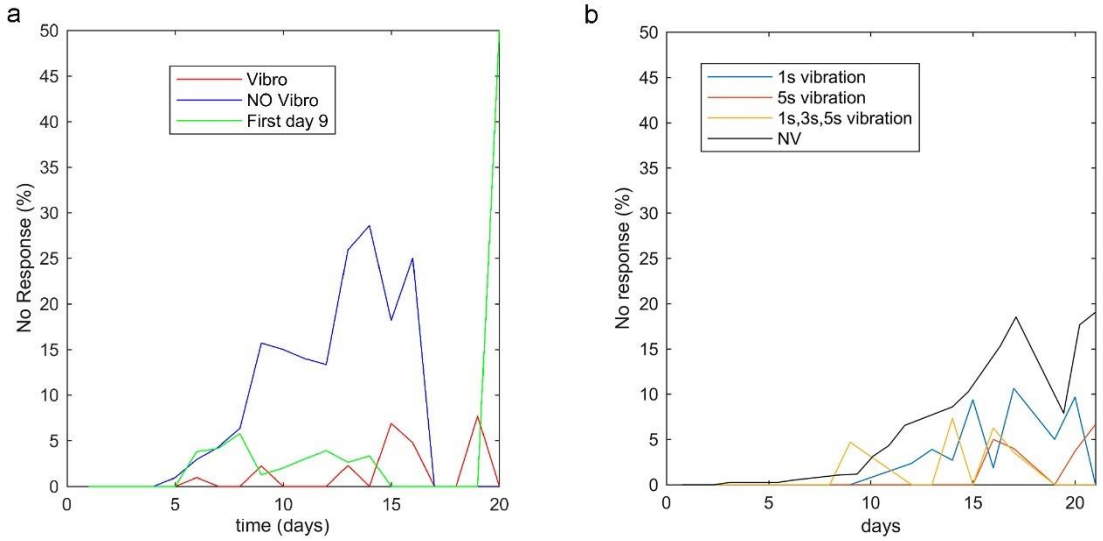

Figure 4.7. No movement detection. (a) In experiment 2 (habituation experiment), few animals were left in the three samples on the last days (2–4), due to nematode death. At such low survival rates, the non-response ratios were variable as of day 18. On day 20 of "first 9 days of the stimulation conditions" (green curve), the non-response ratio was 50% because there were only two worms left. (b) Experiment 1, the blue condition shows the no-response percentage after applying a 1 s vibration, the red condition applied a 5 s vibration, the orange one lasted 1

s [on days 9, 12, 13 and 14], 3 s [days 15, 16, 17 and 19] and 5 s [days 20 and 21], while the grey one denotes the no-vibration condition.

Habituation Analysis

There was a memory and habituation effect, as shown in Figure 4.7 a,b, whereby worms became used to stimulation and, consequently, to respond less to it. Because of habituation, worms displayed less reaction sensitivity (Figure 4.7 a) and less intensity (Figure 4.8 a) and, therefore, the number of nematodes that reacted decreased and those that reacted displayed fewer movements. The mean movement measured 500 $pixels^2$ in 30 s and the maximum was 1200 $pixel^2$ (Figure 4.8 a), the worm width is 3 *pixels*, thus equivalents in linear millimetres were 0.14 *mm/s* and 0.34 *mm/s* respectively, which corresponds to other studies targeting this phenotype [13], [15], [21], [28]. The habituation effect was observed on the last 2 or 3 days of worms' lives (danger awareness vs. ageing) when comparing two groups (Figure 4.7 a): the $NV_{condition}$ had a 71% response (blue curve) and the $V_{condition}$ had a 93% response (red curve). The third group (green curve) was submitted to less stimulation (starting on day 9), which improved its response on the last days with a 100% response between 15 and 19 days for the same vibration time (3 s) versus the condition stimulated from day 2. Due to this finding, it seemed better to seek a strategy whereby vibration was not applied from day 1, but rather from the day on which a significant percentage of live *C. elegans* started to go undetected by movement. The first day could be set between days 5 and 9 for the wild-type strain, whose no-response rates were between 2% and 15%. In addition, changing vibration parameters may alleviate habituation, as indicated by the data taken from experiment 1 (Figure 4.7 b), whose results show that vibrotaxis increased by changing the vibration time every 5 days (from 1 s, 3 s to 5 s). On the days when vibration timing changed (days 15 and 20), the worm response was 100% and the response average increased. In general, high magnitudes of vibration times (5s) also seemed to reduce habituation to the stimulus for a longer time, but adaptation was finally successful (days 20 and 21; see Figure 4.7 b). It is also important not to overstress nematodes. Therefore, we considered it appropriate to choose short vibration times and to reduce application

days. According to previous deductions, and as a starting point for further studies, it seemed reasonable to choose the first day to be somewhere between days 5 and 9 to begin the stimulus and apply a vibration time of at least 3 s.

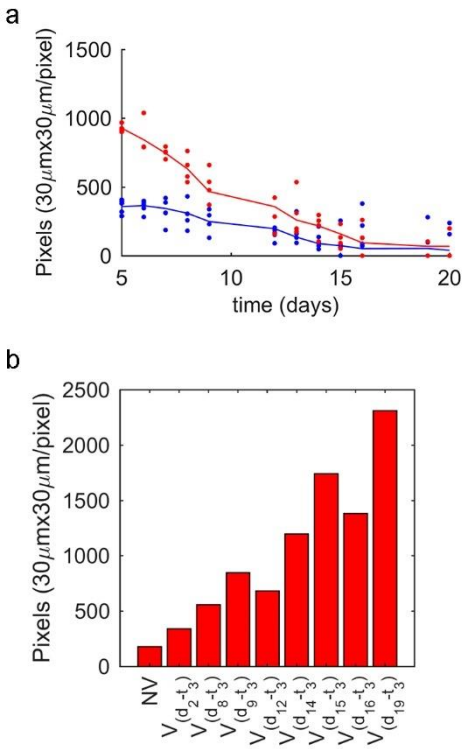

Figure 4.8. Ageing effect. (a) Amount of movement (area in pixels) in time, blue line denotes the $NV_{condition}$ and the red line is $V_{d_2-t_3}$ (vibration started on day 2); (b) This figure shows the same as the previous one, but with details of day 19. Each bar is a condition (left to right) to represent from the lowest stimulus $V_{d_2-t_3}$ to the highest $V_{d_{19}-t_3}$.

We can observe the ageing effect (Figure 4.8 a), and how the amount of movement reduced for conditions *NV* and $V_{d_2-t_3}$ ($V_{d_2-t_3}$ shown after stimulation). In a detailed view (Figure 4.8 b), the stimulation habituation effect can be seen after being analysed. Subsequent to vibration, Figure 4.8 b shows a trend by which worms were stimulated on a greater number of days; these nematodes moved less than those receiving the stimulus for fewer days. A reduction in movement can be problematic because if a nematode does not move enough at a specific image resolution, the software may not be able to detect it during inspection.

Error Variability Analysis

After considering memory, habituation and ageing issues, in order to verify that this new method could improve the no-response ratios of an automated vision machine, we compared the detection error to two factors (stimulation versus no stimulation) with several of the samples taken from experiments 1, 2 and 3. Thus for the $V_{condition}$, in the lifespan error experiment (experiment 3) we attempted to maximize the *C. elegans* vibrotaxis effect by selecting the parameters deduced from the vibration timing experiment (experiment 1) and the habituation experiment (experiment 2), according to which we chose both parameters: (1) a 3 s vibration for stimulation and (2) stimulus applied from day 5. The $NV_{condition}$ of this experiment was performed without vibration. To compare the total error of the lifespan curves for both conditions, we compared them for the same sample size. Thus two replications were studied for this condition. The error per day ($e_{(k)}$) is the difference between manual lifespan curve (*SM*) and the automatic lifespan (*SA*) for a specific day (k) (Equation (4.1)(1.1) of the sum of all Petri plates for one condition. The total error (e_T) (Equation (4.2)) is the mean of all $e_{(k)}$, for those days with data acquisition (N_k).

$$e_{(k)} = \left|\mathrm{SM}_{(k)} - \mathrm{SA}_{(k)}\right| \quad (4.1)$$

$$e_T = \frac{\sum_k^{N_k} e_{(k)}}{N_k} \quad (4.2)$$

Obviously, when a more accurate approach in detection is achieved, the sum of all errors (Equation (4.2)) tends to zero, therefore the error is analysed at Petri-plate level. The error per plate (Equation (4.3)) is the difference between ground truth per plate (X_p) and measured value per plate (x_p). The mean error per plate (Equation (4.4)) is the mean of the error of all plates (N_p) for a certain condition. Finally, the standard deviation of the plates errors for each condition is defined in (Equation (4.5)).

$$e_{P_{(p)}} = x_{(p)} - X_{(p)} \quad (4.3)$$

$$e_P = \frac{\sum_{p=1}^{Np} e_{P(p)}}{Np} \quad (4.4)$$

$$sigma = \sqrt{\frac{\sum_{p=1}^{N_p} e_{P(p)}^2}{Np - 1}} \quad (4.5)$$

The results for this condition gave (Figure 4.9 c,d) n=113 individuals, a total error (e_T) of 2.5%, a mean error per plate (e_P) of −0.17 individuals and a deviation (*sigma*) ±1.05 for replication 1. For replication 2 (Figure 4.9 e,f), sample size was 124 individuals, with a total error of 2.7%, a mean error per plate of 0.04 individuals and deviation ±0.98 individuals were obtained. For both replications (Figure 4.9 a,b), sample size was 237 individuals, with a total error of 2.19%, a mean error per plate of −0.06 individuals and deviation ±1.02. Therefore for the $NV_{condition}$, the standard deviation error per plate was about ±1 individuals. The $V_{condition}$ (Figure 4.9 g,h) had n=114 individuals, a total error of 1.23%, a mean error per plate of 0 individuals and deviation ±0.59 individuals. According to these experimental results, when stimulation lasted 3 s and started on day 5, the total error (e_T) lowered for similar sample sizes of about 120 worms, from approximately 2.5% to 1.2%, with an uncertainty reduction from 1.0 individuals to 0.6 individuals (standard deviation of error per plate, *sigma*). Moreover, we found a statistically significant difference between both variances of error, with p-value ≈ 0. This demonstrated a reduced uncertainty.

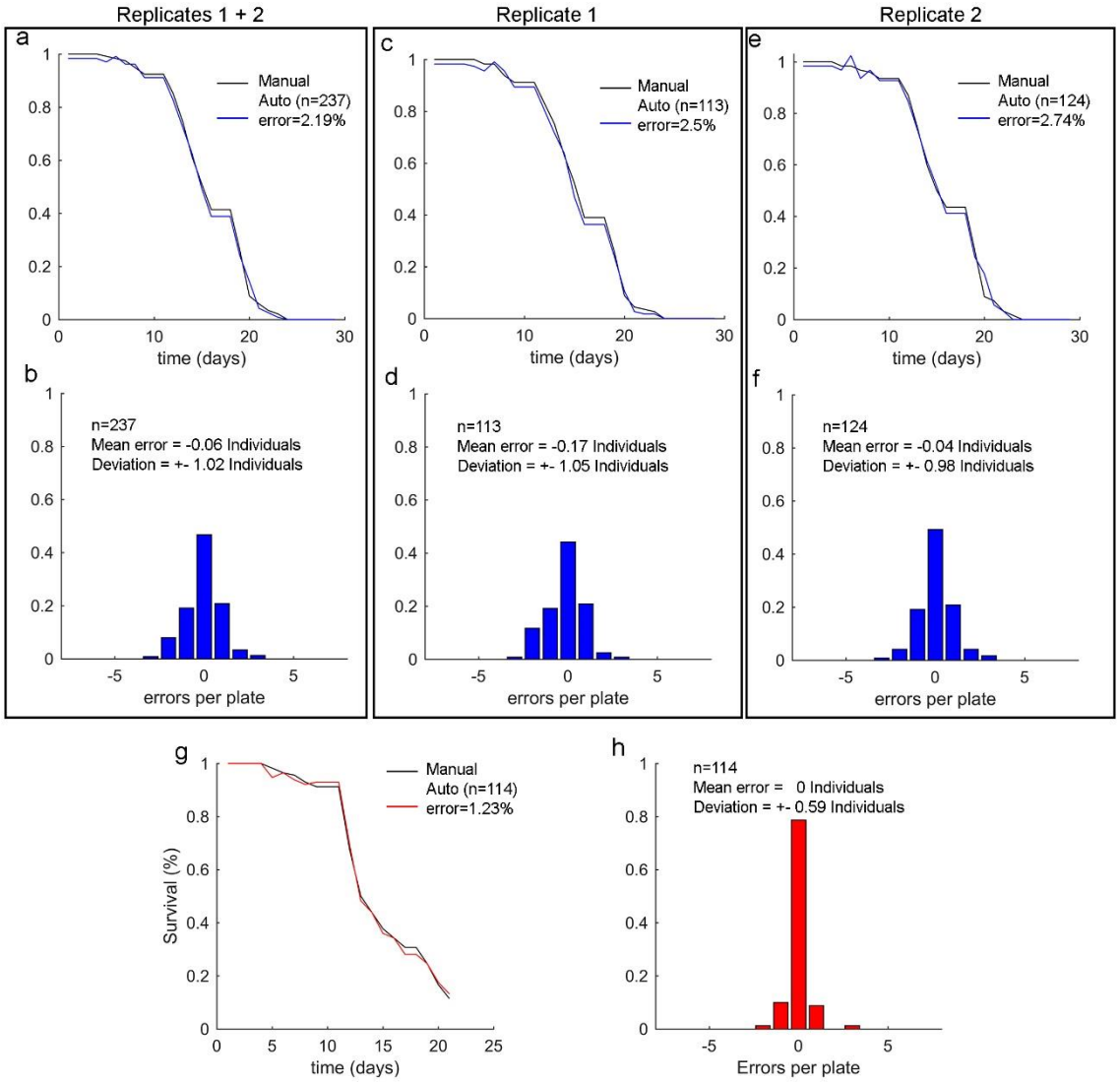

Figure 4.9. Lifespan results of experiment 3. (a–f) belong to the $NV_{condition}$. (a) is the survival curve as a percentage per one for all the replications. (b) is the error distribution per plate for all the replications. (c,d) are replication 1. (e,f) are replication 2. (g,h) belongs to vibration condition $V_{d_5-t_3}$.

As previously mentioned, experiments 1 and 2 were performed to define vibrations *d* and *t*. Nevertheless having several sample groups, for which plates were inspected before and after applying the stimulus, made it possible to study the improvement in the margin of error during detection, although these experiments were not comparable because some conditions had changed. Based on these experiments, it was possible to increase the assay number to develop a better approach, in which an improvement in detection was observed when vibration was

applied. In all cases, fewer errors were detected in the samples subjected to vibrations than the non-stimulated samples, reducing errors by 50% in some cases thanks to the vibrotaxis-associated movement.

For the habituation experiment (experiment 2), only two of the eleven conditions were compared: the least exposed to vibration (*NV*) and the most exposed ($V_{d_2-t_3}$). Both had similar sample sizes, 170 and 174, respectively. The error results (Figure 4.10) showed how the $V_{condition}$ before vibration (Figure 4.10 b) had a ±1.35 deviation per plate, which changed to ±0.85 (Figure 4.10 c) after deviation. When comparing the survival curves (Figure 4.10 a), the total error went from 2.9% to 0.48%. In order to observe possible differences for the NVconditions, Figure 4.10 d shows that the error was 2.35%, which was similar to the $V_{condition}$ before vibration (2.9% error).

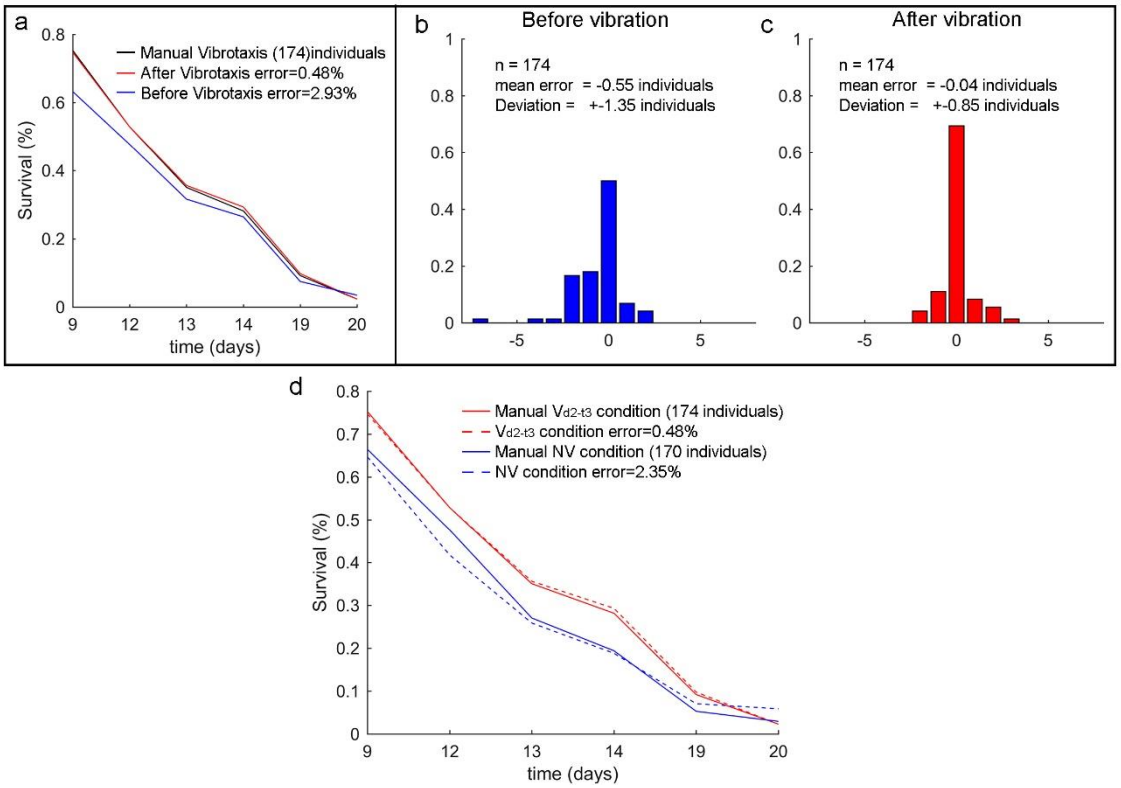

Figure 4.10. The lifespan results of experiment 2. (a) are the survival curves of the $V_{d_2-t_3}$ condition before and after vibration. (b) is the error histogram before vibration, (c) is the error histogram after vibration. (d) is experiment 2 survival curve for two samples: one was subjected to vibration (the previous $V_{d_2-t_3}$ condition) and one was not ($NV_{condition}$). It is possible to compare the errors of both methods.

In experiment 1 (Figure 4.11), manual measurements were taken during three periods; these three measurements gave rise to different results because some worms may have been hidden by wall shadows cast in some areas. We selected the maximum values of these three measurement periods. Hence, in this experiment, the manual curve was more accurate. In this scenario the actual worm number was slightly higher than that detected by a single daily measurement. The reason for this was that the errors in experiment 1 were slightly higher (Figure 4.11). Similarly to the previous assay results, the error also reduced with vibration for the 1 s stimulation, before (Figure 4.11b), with deviation ±1.03 individuals per plate, and after (Figure 4.11c) this value was ±0.75, while the errors in curves were 4.42% and 2.79%, respectively (Figure 4.11a). For the 5 s vibration, the deviation error before the stimulus was ±1.05 (Figure 4.11e), the total error was 6.36% (Figure 4.11d) and after vibration (Figure 4.11f) there were ±0.87 individuals error per plate and a 2.52% total error.

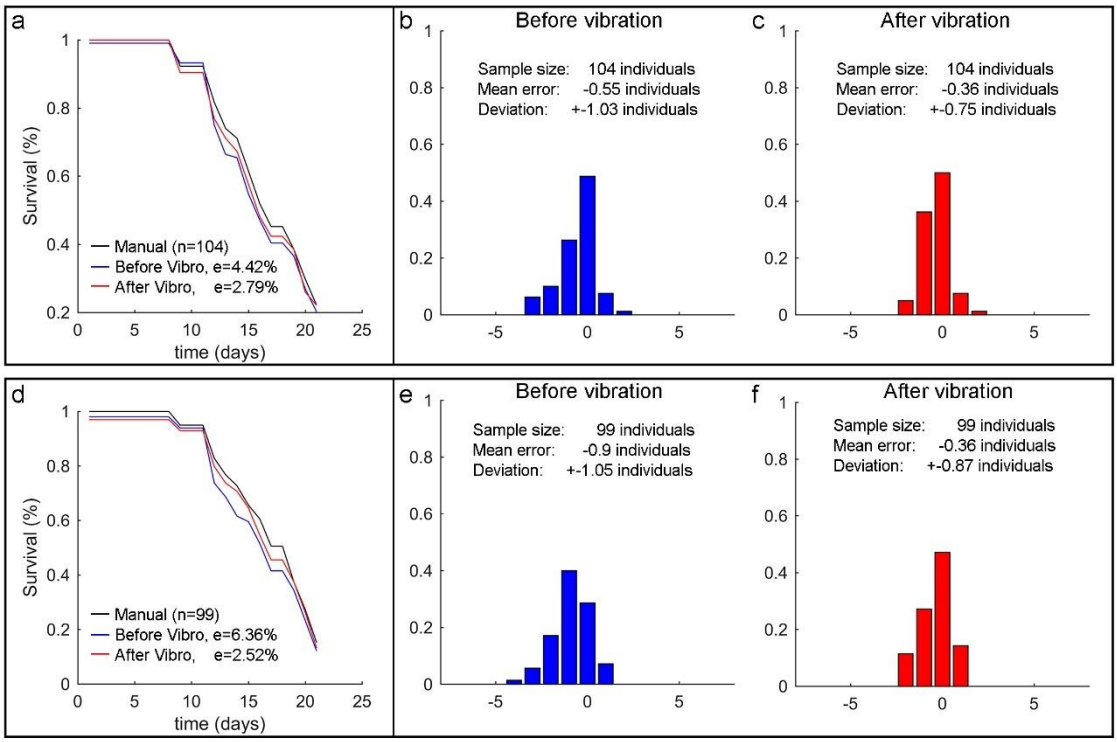

Figure 4.11. Lifespan results of experiment 1. (a–c) are the condition $V_{d_9-t_1}$ sample (subjected to a 1s vibration from day 9). This represents an error before and after vibration. (d–f) are for the condition $V_{d_9-t_5}$ sample (subjected to a 5 s vibration from day 9).

The previous results would seem to indicate that the larger the sample size, the nearer the mean error would move towards zero, although some uncertainty remained. With this method, uncertainty improved by reducing standard deviation. Thus, reducing the total error also diminished the sample size for the same error, and in such a way that costs and times were cut and accuracy increased.

Worm movement began to decrease significantly between days 5 and 9, in fact some individuals even remained motionless during inspection time. Thus, it is logical to start vibrotaxis and its analysis from these days onwards (Figure 4.7 a), because this new method improved the error from these days on. Furthermore, the most interesting range for the survival study was approximately around the mean lifespan time, which was on about day 14 in the wild-strain (N2).

Vibrotaxis Effect on the Lifespan Analysis

Finally, we studied the survival curves between conditions *NV* and $V_{d_2-t_3}$ (extreme cases) of the habituation experiment to verify that vibration did not affect nematode life expectancy. These curves corresponded to the manually recorded ones in experiment 2 (n_{NV}=170 and $n_{V_{d_2-t_3}}$=174), which were used because manual counting was our ground-truth. Through the Log-rank test and the Cox proportional hazards regression model, we observed there were no statistically significant differences between them, with *p*-values of 0.06 and 0.105, respectively, as shown in Figure 4.12, where both conditions are drawn with the Kaplan-Meier estimator. Thus it can be inferred that statistically, vibration did not affect the wild-type strain lifespan. According to the data obtained and the vibration type applied during lifespan, vibrotaxis appeared not to affect the life expectancy of *C. elegans*. Vibration lasted only 3 s each day with an acceleration of about a 4*g* peak. Consequently, applying this new method without altering the results due to the stress applied is a fundamental factor.

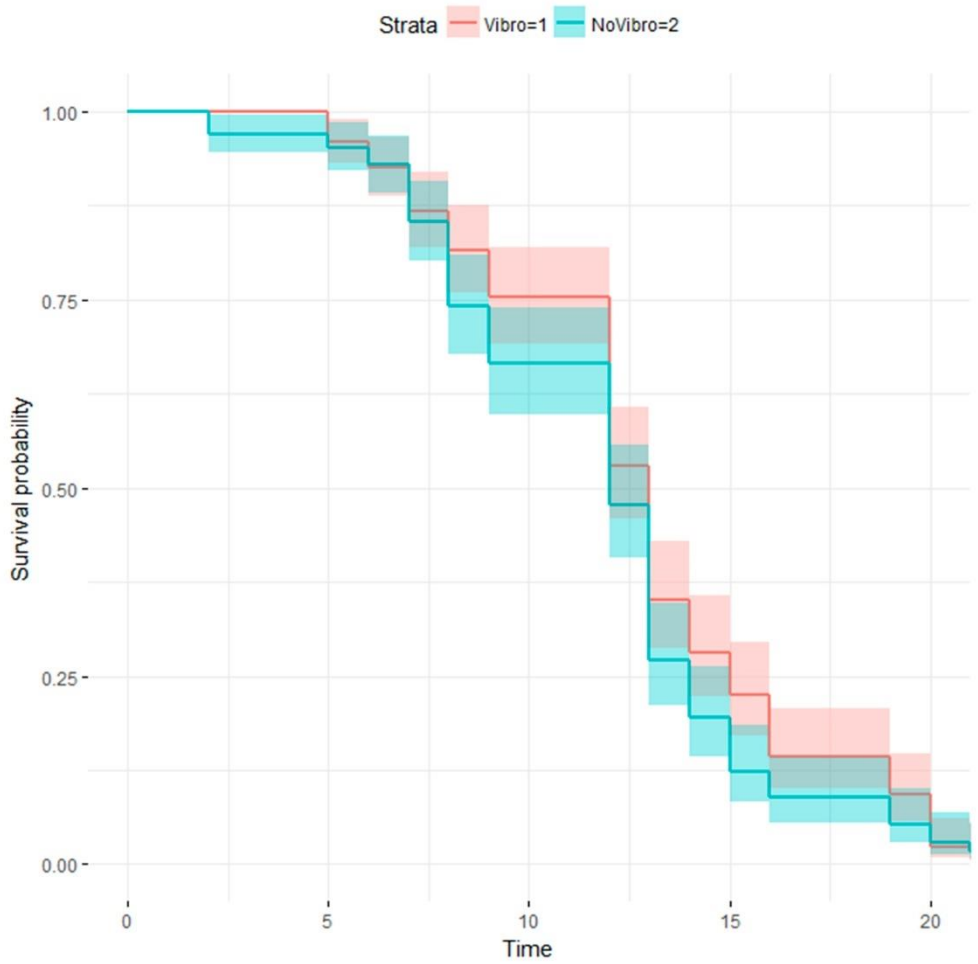

Figure 4.12. Vibrotaxis effect in lifespan. Kaplan-Meier survival curves for *NV* (blue) and $V_{d_2-t_3}$ (red) conditions of experiment 2.

Conclusions

The new method reported here aims to improve live worm detection, which is achieved by worm motion response rates of more than 93% (depending on the case). This fact demonstrates our technique is an effective stimulation method and, in some cases, the sensitivity for lifespan of the automated systems under the same conditions even doubled (from 2.6% to 1.2%), and the error variance per plate reduced by half (from ±1 individual to ±0.6). According to the findings obtained in our experiments, vibration did not statistically alter *C. elegans* life expectancy (wild-type strain).

Therefore, we have designed a new simple automated inspection system which increases throughput over manual methods and improves sensitivity in detection for automated methods. This method avoids manually stimulating worms one by one, which releases the expert from these repetitive tasks. Therefore, it is possible to reduce the sample size for the same error value, which means reducing both time and costs. In addition, worms respond to vibration quickly. Hence sufficient motion leads to more rapid motion detection, which in turn allows for a shorter monitoring period.

In our experiments, we also found that habituation reduced movement. The habituation effect is caused by the worms' ability to remember past non-threatening situations and recognise similar ones, although high vibration makes this habituation more difficult. An overstimulation can be a limitation to improve lifespan results with the proposed method. Consequently stimulation needs to be as infrequent as possible. Hence stimulation should be initiated between day 5 and day 9 throughout the remainder of their lives, a time at which the N2 nematodes began to become lethargic, whereupon attempts were made to stimulate motion.

The improvement afforded by our method also depends on the cleaning and condensation conditions because errors may increase with a critical degree of these factors. However, smooth condensation problems can be alleviated by our technique given both the position change and/or image grey level variation.

If we consider that the observed movement responses caused by vibration in the wild-type strain were significant, the proposed method is highly promising and can be applied to other strains. Furthermore, this method could be applied to the phenotyping of strains by undertaking studies of certain mechanosensory problems, which we will carry out in a forthcoming work.

PAPER 5

Multiview motion tracking based on a cartesian robot to monitor *Caenorhabditis elegans* in standard Petri dishes

Joan Carles Puchalt[1], Jose F. Gonzalez-Rojo[1], Ana Pilar Gómez-Escribano[2], Rafael P. Vázquez-Manrique[2] and Antonio-José Sánchez-Salmerón[1]*

[1] Universitat Politecnica de Valencia, Instituto de Automatica e Informatica Industrial, Valencia, Spain

[2] Laboratory of Molecular, Cellular and Genomic Biomedicine, Instituto de Investigación Sanitaria La Fe, Valencia, Spain and Centro de Investigación Biomédica en Red de Enfermedades Raras (CIBERER), Valencia, Spain

Abstract

Data from manual healthspan assays of the nematode Caenorhabditis elegans can be complex to quantify. The first attempts to quantify motor performance were done manually, using the so-called thrashing or body bends assay. Some laboratories have automated these approaches using methods that help substantially to quantify these characteristic movements in small well plates. Even so, it is sometimes difficult to find differences in motor behaviour between strains, and/or between treated vs untreated worms. For this reason, we present here a new automated method that increases the resolution flexibility, in order to capture more movement details in large standard Petri dishes, in such way that those movements are less restricted. This method is based on a Cartesian robot, which enables high-resolution images capture in standard Petri dishes. Several cameras mounted strategically on the robot and working with different fields of view capture the required *C. elegans* visual information. We have performed a locomotion-based healthspan experiment with several mutant strains, and we have been able to detect statistically significant differences between two strains that show very similar movement patterns.

Introduction

Caenorhabditis elegans is a one-millimetre-long worm that is widely used as a model animal in biology, but also in preclinical assays to test drugs, which may be used later in higher organisms before progressing to regular clinical studies [1]. Some trials consist of treating the worms with drugs, in parallel with the appropriate controls, and then subjecting them to lifespan or healthspan assays [12]. The simplest experiment to quantify is the lifespan [1], [2], which studies the conditions that induce and increase the lifespan of a given organism. Nevertheless, longevity is not the only factor to consider in human health, but also how healthy the individual is for the entire time period. Thus, there are experiments to quantify healthspan which asses the life quality.

Healthspan is generally described as the period in life during which the organism is in good health. In human clinical settings, grip strength, gait analysis and ability to perform daily tasks are often used as criteria to assess good health. In *C. elegans*, several physiological and functional parameters that change with age can be studied, such as lipofuscin accumulation or pharyngeal pumping [83]. Among these, the most powerful predictor of longevity appears to be movement. As in humans, *C. elegans*' ability to move diminishes with aging, as they decline towards a state of frailty where they are only able to move their head, characteristic of the later stages in life.

In *C. elegans*, healthspan can be measured by analysing motility behaviour [84]. Researchers understand the amount of movement, coordination, body bends, reversals, pirouettes, travel distances or orientations can determine if there is neuronal, muscular or sensory damage, as well as animal proactivity. Some of the traditional methods to quantify movement is to check the number of (1) thrashing in a time period [85], or (2) the maximum distance that the worm moves, from a given point, among others. In our case, we are comparing worms suffering from locomotor problems due to neurodegenerative diseases, with healthy worms (N2). Therefore, only a movement parameter (such as thrashing) can be used to assess health [86].

Using manual methods, it is difficult to quantify movement, because it is not easy to visually measure a displacement or a trajectory angular variation. As stated above, quantification of movement enables us to study the conditioning factors altering health, whether these are drug treatments, different food intake or inter-strain genetic differences. These assays can identify harmful conditions (i.e. unhealthy food, drugs, deleterious mutations, etc.), so they can be neutralized. Conversely, they can be promoted, if they are beneficial. Importantly, the differences in behaviour between conditions and/or strains can be very subtle, and the statistical tests are not able to point out these variances. Therefore, it is important to analyse these behaviours in greater detail. In summary, there are several drawbacks in manual experiments that make automated experimentation essential.

Some of the automated systems rely on taking image sequences of the whole Petri plate area [15]–[17], [21], which cannot capture high-resolution images of *C. elegans*. Most of healthspan automated systems require restricted worm movement (e.g. using glue or microchambers) thus allowing high-resolution image capture with a fixed camera. There are systems in which this restriction is performed with medium-sized multiwell plates [87] harbouring a few nematodes. Also, small-sized multiwell plates are used [14], [35], [83], [88] in which just one animal is placed, usually to control individual identity in a healthspan study throughout its lifespan [89]. These small wells are almost worm size, and due to this small restricted area, the movement variations can be captured by a camera at high-resolution. However, under these restrictions, the nematodes cannot perform certain movements, trajectories and interrelations. Another method that has many advantages involves the use of microfluidic chambers to restrict movements, but again carries the same problems [90]–[93]. On the other hand, there are also micro-pillars [54]–[56], [94], which force the worms to pass through predetermined paths, which also alter the trajectories.

Our method, described herein, allows software-processed tracking of all worms, maintaining their individual identity at low-resolution, while

mechanical tracking can be done using another camera with higher resolution. In this way, all worms can be assessed individually at two different resolutions, in a less restricted setting, with longer and more coordinated movements. This allows for social interactions of multiple worms in a less artificial environment. Here, we describe this new method, and we compare automated versus manual assays, in order to assess whether both techniques provide similar results. Our experiments demonstrated significant statistical differences in movement between the wild type standard (N2 Bristol), a strain expressing a long track of CAG triplets (RVM66) and *unc-1* mutants, which show strong incoordination, hence validating this method.

Materials and methods

Before going into more detail, at this point, we give a general description of the method presented in the current manuscript: It is based on a Cartesian robot (Figure 5.1), which moves a carriage on the XY axes. On the Z axis, a head axially moves up and down, this head holds two high-resolution cameras (named microcameras) which have focal length of 102.61 *mm* and 1.09 *µ/pxl* and a laser to locate both microcameras. The carriage has a backlight, a Petri plate support for two plates, a beam splitter and a low-resolution camera (named macrocamera) with focal length of 3.6 and 27.31 *µ/pxl* per plate. In this way, we have two different resolutions at the same time to inspect the same Petri dish. Detailed techniques to achieve this concept are described in the following points.

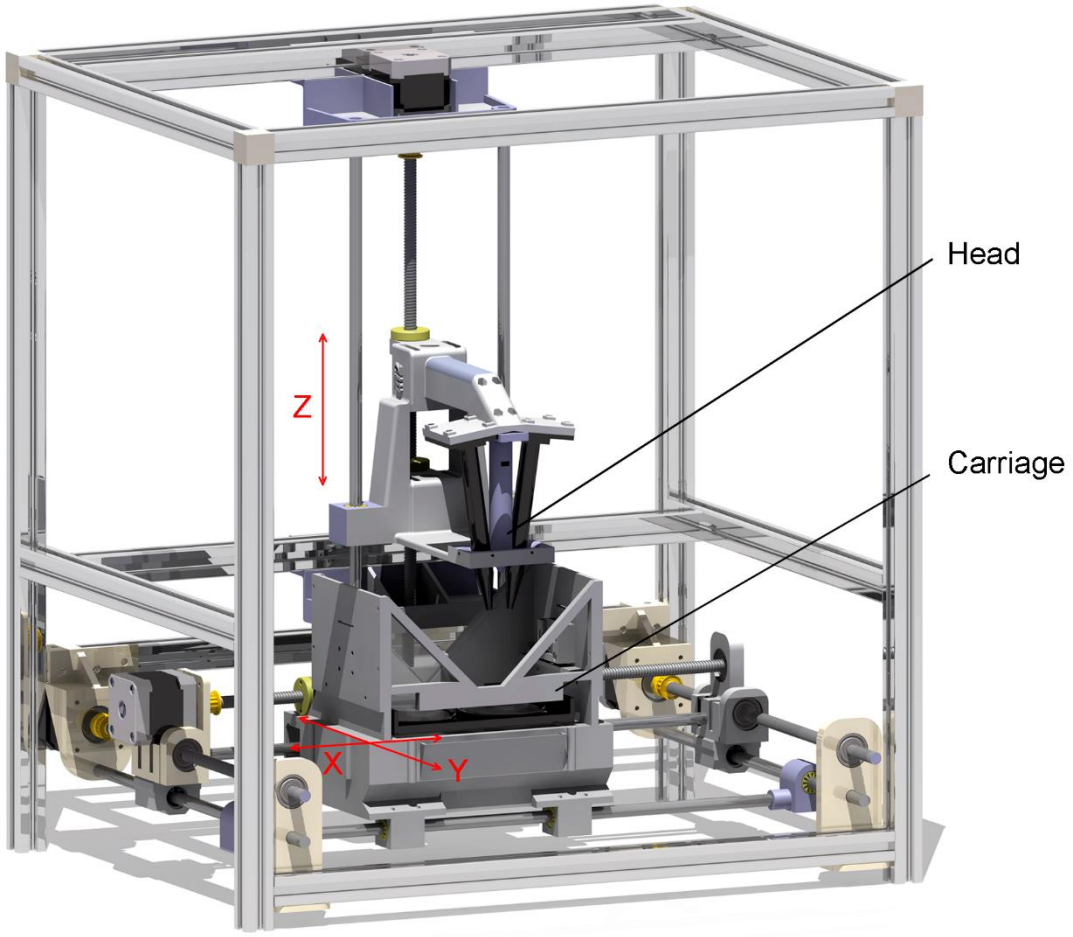

Figure 5.1. Multi-view cartesian robot. This is the general view, showing all components.

The device structure has been assembled with 20x20 *mm* aluminium profiles. The parts have been designed to hold the motors, shafts and PCBs in the structure. These clamping parts, as well as the head and the carriage, have been printed with PLA material in a 3D printer (BCN3D Sigma 3D printer-6). Four Nema 17 stepper motors have been employed, a Teensy 3.6 microcontroller has been used to control them and a DRV8825 to feed each motor. Regarding the image capture, it consists of four Raspberry Pi v.4 with cameras (picam v1.3), configured 2592x1944@3Hz. The lighting system is a 7" 800x480 dot display controlled by one Raspberry Pi. To achieve the light beam reflection/transmission, a 45° and 50T/50R beamsplitter is used, thus the reflected light has a 45° inclination while the transmitted light is not deformed. Finally, the Master is an Intel

Desktop Computer i7-4790 CPU@3.60GHzx8, 7.6 GiB RAM and Intel Haswell Desktop Graphics.

Vision system

The vision system is composed of two microcameras and two macrocameras, which inspect two 55 *mm* diameter Petri plates. Each macrocamera captures an entire plate, while the microcameras magnify a small region of interest where a worm is located.

The carriage

The carriage (Figure 5.2a, b) has the backlight (display), the Petri plate support, the beam splitters and the macrocameras assembled on itself. The lighting is a 7" display, on which a Petri plate support is fixed. Each beamsplitter is placed fulfilling two restrictions, one is it must keep 45°C with respect to the surface of the display and therefore with respect to its illumination. Another restriction is that the beamsplitter must be large enough to reflect and transmit the entire Petri plate image. Each macrocamera is positioned perpendicular to the display and at a position and distance such that the reflected image from the display remains centred and complete in the camera. In other words, the Petri plate image remains fixed with respect to the macrocamera, despite the fact that the carriage moves in X and Y, thereby all the worms in the plate can be tracked in the low-resolution images sequence uninterruptedly. The display is also fixed with respect to the macrocamera, therefore each point drawn on the display can be correlated with a camera pixel, this allows active vision [42].

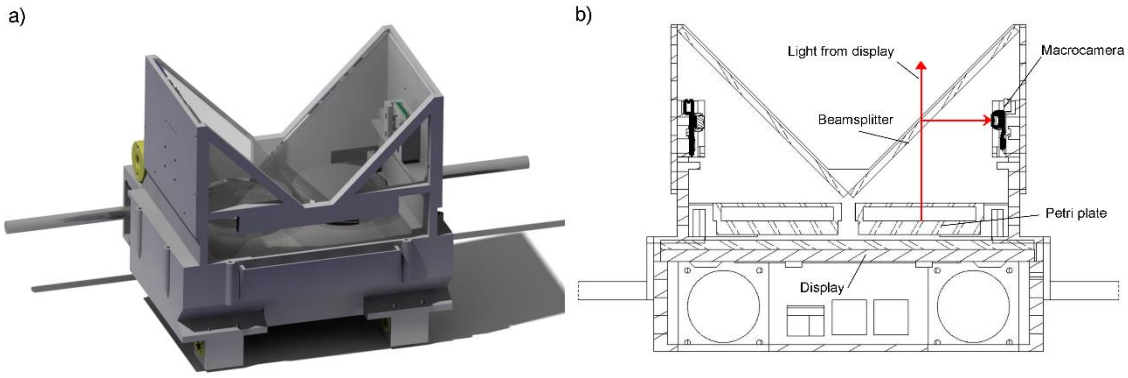

Figure 5.2. The XY carriage. (a) the whole carriage (b) a section view to see parts in detail.

Active vision

Active vision is used to control lighting, thereby the intensity and light colour that each worm receives can be regulated by the following methodology: the macrocamera and the display form a closed control loop, which makes all the pixels in the image reach the same reference. See [42] to know how to calibrate the camera with respect to the display, in order to find the transformation matrix correlating each texel display with each camera pixel (in this case the macrocamera). When there is a Petri dish between display and camera, the light received by the camera has different grey level due to worm shadows. The controller will illuminate more intensely the texels associated to those darker image pixels than the reference detected; and when pixels are brighter than the reference, then the intensity will be reduced to the associated texels.

The head

The head (Figure 5.3a, b) has both microcameras and the laser, to know the head position with respect to the carriage, assembled thereon. It has two cameras, thus enabling stereovision. The cameras have a certain angle (8°) to be able to take various perspectives, which makes it possible to orientate both cameras to capture the same region of interest (where the worm is). And, on the other hand, this angle causes a necessary space between the lenses, where a laser can be set, whose light falls orthogonally on the Petri dish surface. The laser projects a point on the

macroimage, which gives the head position (microcameras) with respect to the macrocamera. In this way, the carriage position can be corrected, and thus microcameras can capture a desired worm-target selected from global information captured by the macrocamera. The microcameras are adjusted in such a way that the laser pointer is right in the centre of each image, thus when the laser pointer is in the target worm position, this worm will be displayed at both image centres.

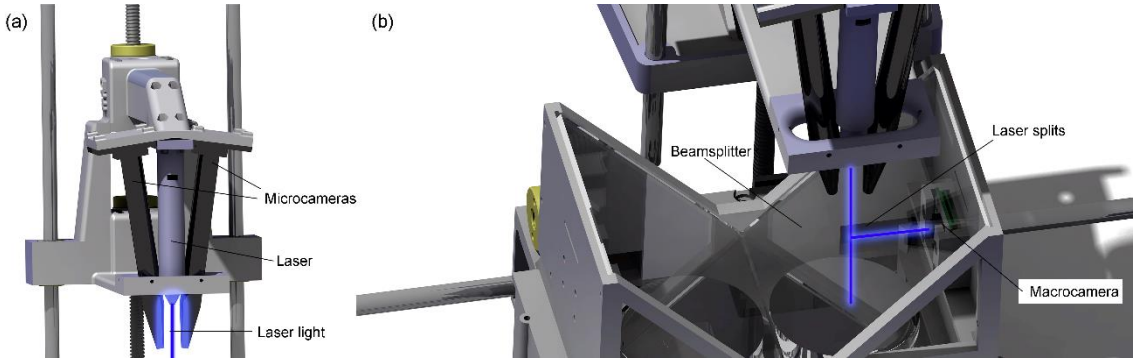

Figure 5.3. The head. (a) The head has two microcameras and one laser. (b) The head and de carriage are assembled, where the laser light trajectory is shown.

Control system

The algorithms have been developed in C ++, with the Robotic Operating System (ROS) which is a tool for distributed systems and the computer vision library is OpenCV. The Operating System is Ubuntu, a Ubiquity distribution runs on the Raspberry Pi4 that has the ROS installation. The Master is launched on a Desktop Computer where UBUNTU 18.04.5 LTS and ROS melodic are installed and running.

The ROS structure is shown in Figure 5.4. The Master has both nodes of image processing and control. At least the same number of Raspberries Pi as cameras are required, so each camera will have its ROS node running on a Raspberry Pi, which will publish the image. One Raspberry has a ROS node, which connects via serial to a Teensy 3.6, this node subscribes to a topic where the movement steps are published by another node (Macroprocessing_Node and/or Microprocessing_Node). And another Raspberry Pi launches other node that executes the display driver and subscribes to the display image.

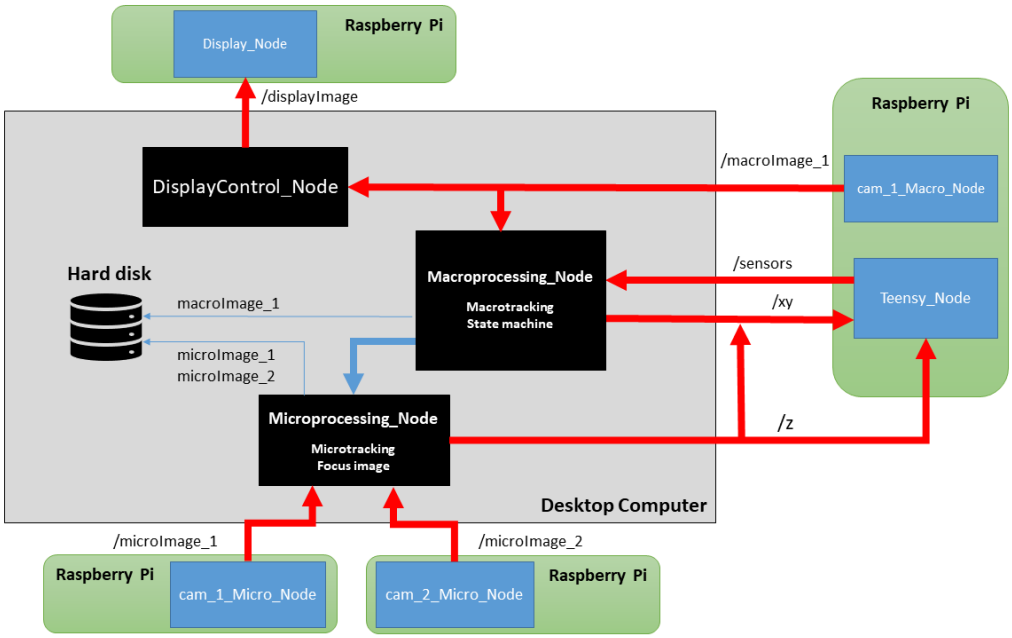

Figure 5.4. ROS diagram. Black squares are ROS nodes running on desktop computer, green squares are the four Raspberries Pi and blue squares are ROS nodes running on Raspberries Pi. Macroprocessing_Node implements the macroimage processing, macrotracking and state machine. Microimage_Node implements both microimage processing, microtracking and microimage focus (by changing Z axe). The nodes: cam_1_Micro_Node, cam_2_Micro_Node and cam_1_Macro_Node, execute the camera driver, take the image and publish the images into /microImage_1, /microImage_2 and /macroImage_1 respectively

Finally, the processing and control nodes are launched in the Master:

- DisplayControl_Node is the one that controls the display lighting. This is subscribed to the macroimage topic, it performs the macrocamera calibration, the image transformation, compensates the lighting to obtain the reference level and publishes the lighting pattern calculated into /displayImage, thereby its subscriber (Display_Node) can draw the illumination pattern on the display.
- Macroprocessing_Node subscribes to the macroimage topic (macrocamera). This node processes the image, locates the targets, makes the framing on worm selected with macroimage information and contains a state machine, which sequences the tasks. The image processing consists of three steps; (1) an adaptative threshold is used for image segmentation; (2) the objects are classified by size; and (3) the object identification is tracked by the

minimum distance between the last object locations to the current locations. Further details of the image processing are shown in Supplementary Figure 1.

- Microprocessing_Node, subscribed to the both microcameras, does the image processing, focusing the image via publishing Z variable and also performs the microtracking by publishing on XY variable, which is made with microimage information. Further details of the image processing are shown in Supplementary Figure 2.

The state machine (Figure 5.5) sequences all the tasks: all worms constant macrotracking (1) worm selection and worm-goal acquisition (2) selected worm microtracking (2.1) selected worm focus in microcameras (2.2) both microimage capture.

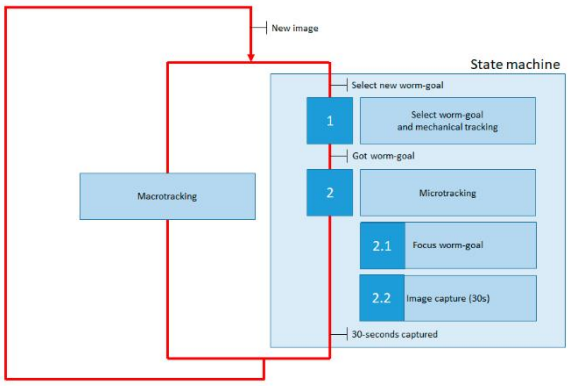

Figure 5.5. State machine. This flowchart shows the tasks of the state machine. Macrotracking is running constantly (it is software tracking), while state machine executes 1) when the worm has been selected. The 2-state starts when worm-goal has been achieved (the worm selected is framed). And when a 30-second sequence has been captured, then the mechanical tracking ends and the loop restarts.

The distance between the plate and the macrocamera is fixed, thus the relationship between the pixels and the motor steps can be known, by calculating the needed step number to move a certain pixel number. This model may have a small variability due to the agar height variability, 1 *mm* in Z (height) produces an error of 0.338 *mm* in X and Y, as shown in Equation (5.1), where the half of view field is $\alpha = 41.41°/2 = 20.7°$. With this small error, this model is a good approximation, which can be corrected with a proportional regulator.

$$\nabla x = \nabla z \cdot tan\,\alpha \qquad (5.1)$$

Tracking is carried out at two levels (1) macrotracking and (2) microtracking. Macrotracking constantly locates all the worms on the plate and identifies them using software, providing data on which worms have been tested and which have not (Supplementary Video 1). Among all worms, one is selected (worm selection state), whose centroid in pixels is known just as the laser position. The error is calculated and multiplied by the *pixel/step* ratio, the result is the necessary step number to reach the worm position, which is sent to the motor controllers. In one or two iterations the target is reached and when the error is small ($e < 15\ pxl$) the state is switched to microtracking. For microtracking, the laser is unnecessary, because the worm occupies a large image part and remains centred on it. What is more, the laser also impoverishes the image quality because it emits another light component besides backlight; furthermore, it saturates a small spot on the microimage. For these reasons, the designed sequence is as follows: the laser is turned off, the worm centroid is obtained and it is carried to its centre as the nematode moves. While microtracking is performed, two sequentially subroutines are executed: first the nematodes are placed in focus and, second, the microimages are captured at 2fps for 30 seconds (in our case). For this other tracking we also calculate a model to approximately determine the *pixel/step* ratio (1.14).

Experiment design

We prepared three conditions with three different mutant strains, the wild type (N2 Bristol) strain is the control condition, the study condition is RVM66, and as a negative control with a mutant with obvious mobility problems (*unc-1*). The biggest differences are observed in Young Adult stage (YA), therefore experimental results focus on that day.

Culture and maintenance of *C. elegans* strains

All worms were maintained in standard dishes measuring 55mm at 20°C degrees as described elsewhere [1]. Wild type animals (i.e. the Bristol N2

strain) were obtained from the Caenorhabditis Genetics Center (CGC, Minneapolis, MN, USA). Uncoordinated animals contain a nonsense mutation, *vlt10*, in the *unc-1* gene that alter locomotion significantly [95]. In this work, we have developed a strain, RVM66, which carries two copies of the transgene *vltIs66[unc-25p::144CAG]; myo-2p::mCherry*. Untranslated CAG expansion produces CAG transcripts that induce dysfunction of GABAergic neurons. The transgene has been inserted into a known site of the *C. elegans* genome using the MosSCI technology [96]. This strain shows a much subtler motor defect compared to *unc-1* mutants. Nematodes were grown in NGM (Nematode Growth Medium) petri dishes and *E. coli* OP50 were used as a food source.

Manual motility assay

To evaluate worm motility capacity (i.e. fitness and locomotion-based healthspan) we collected data from a locomotion phenotype, the so-called thrashing assays. Briefly, synchronized L1 worms ware incubated in NGM plates until they reached the young adult stage. In this phase, we picked individual animals from the NGM plate and put them into a well of a cell culture 24-well-plate, which was filled with M9 buffer (a physiological solution). After acclimation for 30 seconds, we counted the number of thrashes (head and tail movement simultaneously) for 1 minute manually. We analysed at least 30 animals for each strain and we performed each experiment three times.

Automated motility assay

For the automatized locomotion assays, we cultured the animals in NGM plates from L1 to the young adulthood stage. An experiment consists of three plates per condition with about 30 worms each plate, that is, n=90. We replicated the experiment four times. The capture method: we place a Petri plate in the plate support of the device. From this instant on, a macroimage sequence is taken at 1 *fps*. While the macroimage sequence is taken, one 30-second microimage sequence at 2 *fps* (60 images) is taken worm by worm. Once the microimage sequences of all the worms have

been taken, the macroimage sequence capture is stopped and the current Petri plate is exchanged for another new plate, and so on.

We calculated several indices, all of them from the control actions (x and y shifting) at each instant *k*, for which the index that gave us significant differences in all cases was one based on the displacement modules, ``M'', obtained from Equation (5.2), shown in Figure 5.6.

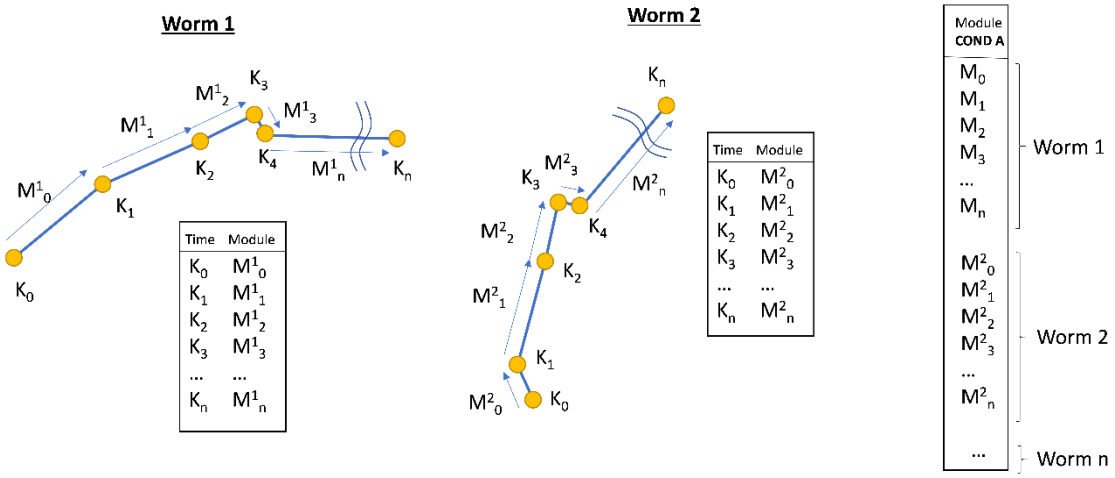

Figure 5.6. Module index. Every worm movement of every time instant is recorded (worm 1, worm 2… worm n).

$$M_x = \left|\overrightarrow{AB}\right| = \sqrt{(x_k - x_{k-1})^2 + (y_k - y_{k-1})^2} \qquad (5.2)$$

Results

In worms, neuronal or muscular defects may be translated into movement dysfunction. Hence, to test our system we used three strains of *C. elegans* that shows no motor phenotype (wild type animals, N2 Bristol), worms showing a very mild phenotype (transgenic worms with slightly impaired GABAergic neurons) and *unc-1* mutants, which are severely impaired for movement. These *unc-1* mutants have altered electrical synapse and produce uncoordinated movement in worms [95], [97]. We analysed the motor performance of these strains using the so-called thrashing assays, which consist of counting every movement of the whole body made by each animal while swimming. Our manual analyses showed that *unc-1* mutants have, as expected, a severe motor defect compared to wild type

worms Figure 5.7. The worms expressing CAG expansions in GABAergic neurons show mild motor phenotype, compared to *unc-1* mutants Figure 5.7. This mild phenotype of the transgenic worms is attractive to optimise an automated system of locomotion since, for example, a strain showing subtle phenotypes represents a challenge for drug screening.

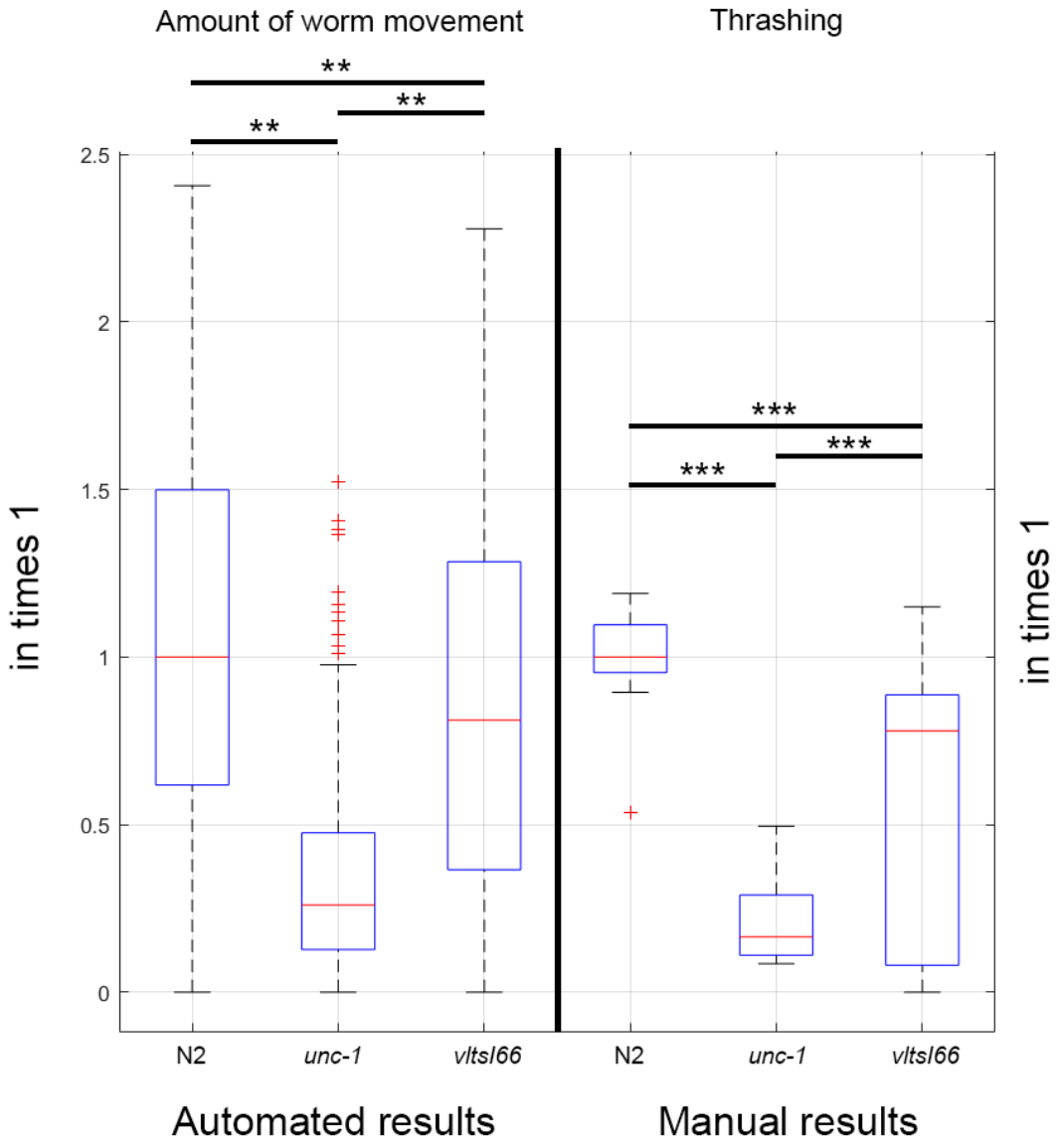

Figure 5.7. The module index for automated inspection and the thrashing index for manual inspection are shown, which are both transformed into percentages to facilitate visual comparison. On the left is the module sum index. On right, is the graphical output of the manual analysis of the movement capacity. Strains for both experiments are wild type and mutant worms. Wild type (N2 Bristol), *unc-1* mutants and transgenic worms expressing CAG expansions in GABAergic neurons show very different motor capacity in liquid. ** means

p−value < 0.05, with Wilcoxon rank sum test. *** means *p*-value<0.001, in ANOVA test with Tukey's post-hoc test.

The automated system results. The macroimage allows the tracking of all worms on the Petri plate and also controls the device-head positioning, which is achieved by capturing the blue laser point position on the captured image. However, there is a problem with the laser spot, since its beam splits when passing through the beamsplitter: 50% is transmitted and reaches the Petri dish and the other 50% is reflected. Thus, the macrocamera captures the laser pointer twice in the same position at two different magnifications, because these are at different distances: one laser spot capture is further away, which is reflected on the agar surface (small spot) and another closer one is reflected on the beamsplitter (large spot). On the small image area where the laser spot is projected, the laser intense lighting saturates this small area and makes segmentation difficult. We have minimized this point size and it does not cause problems as long as the mechanical tracking movements are quite fast ($v_{max} = 8000\ stp/s$ and $a_{max} = 25000\ stp/s^2$) and accurate.

The luminance control means that the macroimage has the same grey levels throughout the image. In this way, the image quality is higher and the light intensity received by the worms is also controlled [42]. However, microcameras require greater light intensity, for this reason we have implemented a high intensity illumination circle with the centre at the worm-goal position. This circle produces illumination gradients, and thus to solve the image segmentation problem we used two techniques (1) adaptive threshold and (2) a function to generate this lighting circle to soften illumination gradients. This smoothing function is a sigmoidal function that depends on the distance to the circle centre. The result can be seen in the macroimage in Figure Figure 5.8a, b. The sigmoid calculation is made at the image grey level in such a way that the controller corrects the image error to obtain a sigmoid with small gradients (Figure 5.8 and Supplementary Figure 1).

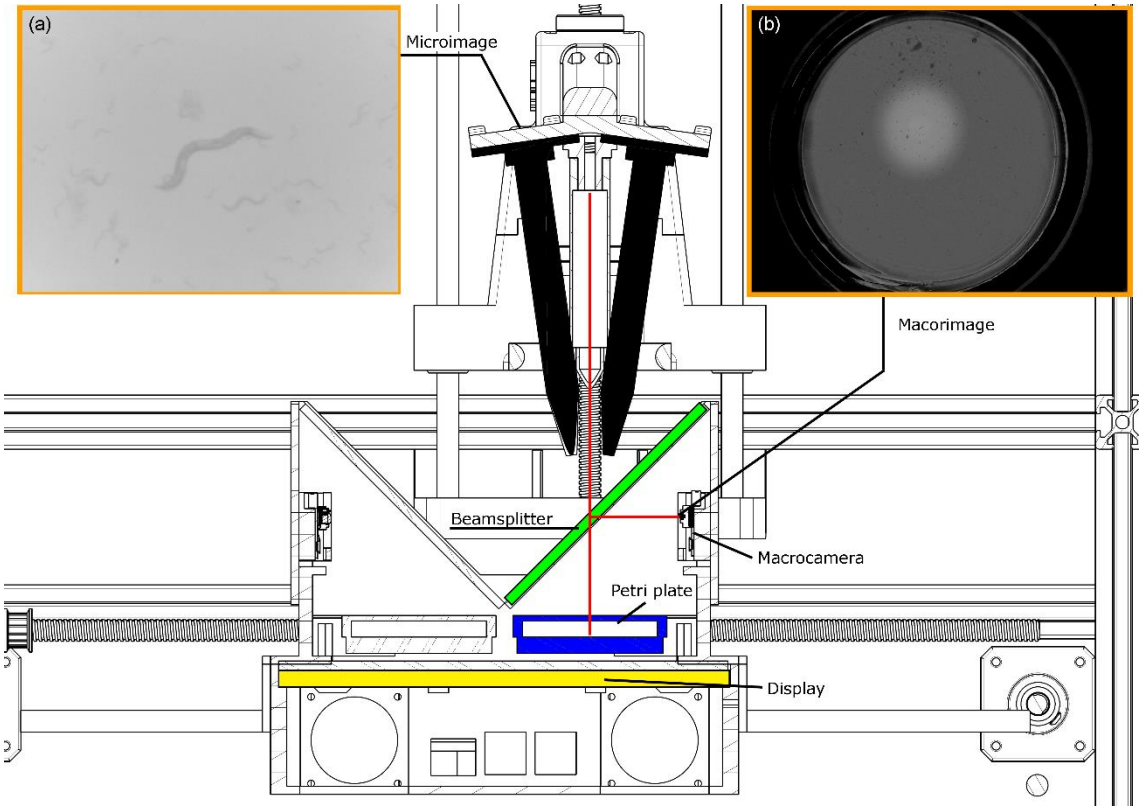

Figure 5.8. Profile view. The head and the carriage assembly are shown and how all components interact. (a) shows a microimage taken from one of both microcamera. (b) shows macroimage taken from macrocamera.

Tracking is achieved as shown in the Supplementary Video 1, with images captured as shown in Supplementary Figure 1. The microtracking control actions were recorded in a file. The images of all the plates were taken one by one. In one iteration, the robot can correct the worm positioning while performing microtracking, to keep it centred in both microcamera images.

The nematodes were young adults, for which the p-value<0.05 was obtained for all four experiments with the Wilcoxon rank sum test. The most repetitive value rank is the [0-1] rank, which means the worm is most provably static, but this probability depends on strain because some strains demonstrate more movement than others. Figure 5.9 shows that the wild type (N2 Bristol) has higher mobility, there are greater frequencies of higher movement modules, that is, there is more probability of longer movements. This is confirmed, observing the relative

frequency of minimum module rank [0-1], which is lower than the other strains. The *unc-1(vlt10)* mutant is markedly different, where all the module frequencies are closer to 0, which obviously means it has shorter movements. While the *vltIs66[unc-25p::144CAG]* mutant closely resembles the wild-type strain N2, although slightly smaller relative frequencies of the modules than the wild type can be observed. P-values demonstrate figure observations; thus, we can affirm *vltIs66[unc-25p::144CAG]* has a statistically significant reduction in mobility. The module index is transformed in Figure 5.7 to allow visual comparison with thrashing method. The module transformation index consists of the module sum for each worm, which provides the amount of movement per worm, and this is expressed in percentage.

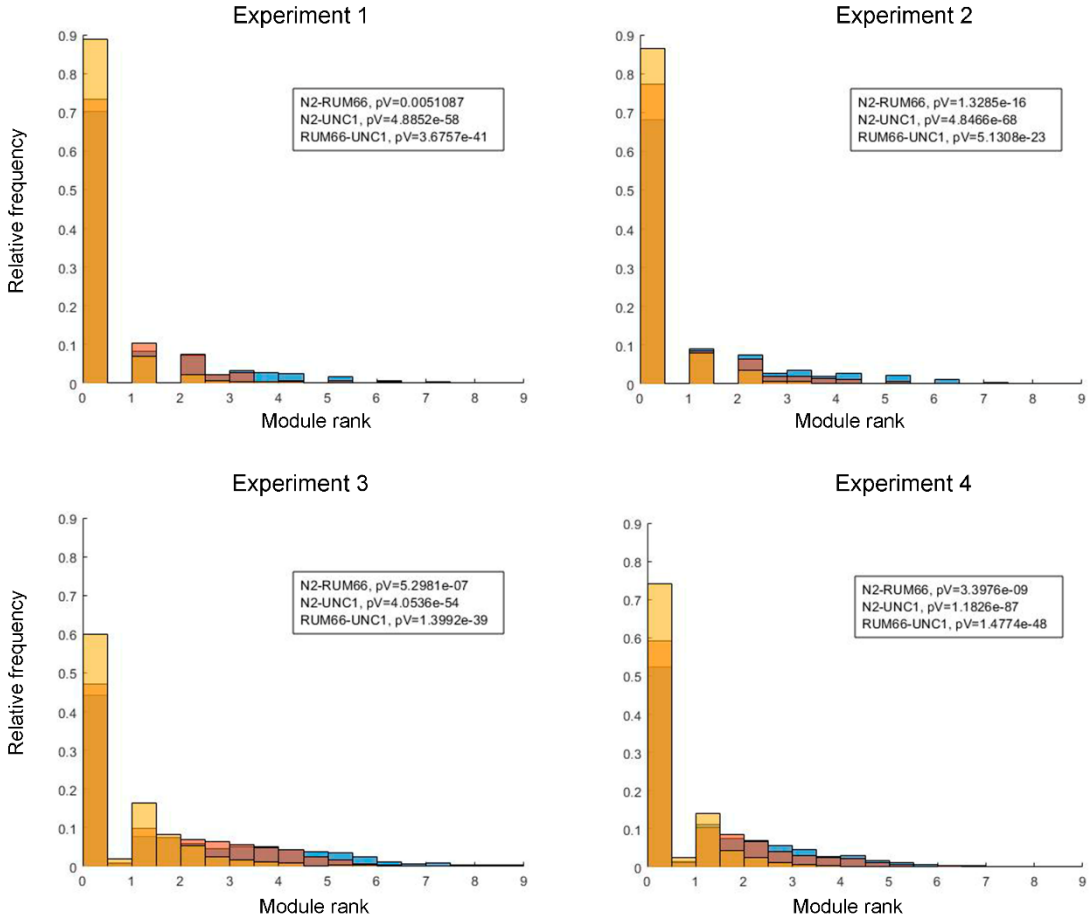

Figure 5.9. Relative frequency of module values. The abscissa axis represents the module value rank. The units are in steps, which in millimetres are 1.09*µm/step*. The blue bars are Wild Type

(N2) strain, the orange bar is *vltIs66[unc-25p::144CAG]* strains and the red one is *unc-1(vlt10)* strain.

We also performed experiments with one-day-old adult worms, but as with the manual study, on day 1 the differences are minimized, and the statistics are not significant. However, this method opens new paths towards achieving analysis that can provide more information than those obtained to date.

Conclusion

We have demonstrated the multi-view Cartesian robot can inspect *C. elegans* in standard Petri dishes and extract information to find statistical differences between *C. elegans* movements, with a simple index based on the position variation modules in each sampling period, k. These differences can be observed between strains with very subtle differences (wild type and *vltIs66[unc-25p::144CAG]*). Multi-view monitoring provides greater data-collection flexibility because it offers more than one resolution, which allows all worms to be tracked at once, while also tracking one animal at high-resolution. This method can also monitor worm movement in standard Petri dishes (55 mm of diameter), which improves negative behavioural alterations caused by smaller spaces.

Contact and interaction with other worms may cause the tracking algorithm to lose the identity of the tracked animal. If the tracked worm identity is lost, some acquired data may require censorship. In our case, where approximately 30 worms were contained in a standard Petri dish measuring 55 mm in diameter, the probability of contact between them is approximately 3% [60].

If there were a greater number of worms in the Petri dish, the probability of contact and interaction between worms would increase. As a future work, it would be interesting to solve the problem of re-identification of worms using the high-resolution images by trying to avoid data cancelation in a future study.

In addition, future work could integrate other locomotion behaviors, such as body bend, forward movement, backward movement and others.

Furthermore, this method has paved the way to solving motion pattern classification problems and other assays using high-resolution images.

New image processing studies will be made possible given this increased amount of available data, facilitating the analysis of *C. elegans* movement characteristics. Possibly, accumulative data collection will shed light on characteristics in the physiognomy, movement or posture of the nematodes that define characteristic group behaviour, which other analyses cannot detect.

This method can also capture the image with two microcameras, thus future works on 3D reconstructions can be made of each worm in the Petri dish.

CHAPTER 3
DISCUSSION

Previous work and objectives

The main objective is to develop new automated methods for inspection with *C. elegans*. The lifespan experiment is the most widespread, it is based on counting live and dead worms, observing if they move, being able to spike them in the last days of life, to check if they are really dead. Healthspan experiment is another of the most widespread experiments, and is based on defining the *C. elegans* health according to the its movement features, such as thrashing or body bends. Manually this inspection is very laborious and time consuming, for that reason we set ourselves the challenge of automating these tests.

Lifespan and healthspan machines can undergo *C. elegans* imaging problems, due to hardware limitation, biological factors or physical events.

- *C. elegans* are **sensitive to light** in two ways, on the one hand it excites them by producing a withdrawal reaction and on the other hand it shortens their life when the wavelengths are short, or the intensities or exposure timing are great. For this reason, the animals must be isolated from the environment and when they are illuminated, it must be known with what type of lighting and for what reason you want to illuminate them. To inspect them, the lighting must be dim, short-lived and configured for red tones.
- Lighting **stimulation** can be useful to observe the nematode movement. *C. elegans* have withdrawal behaviors due to various factors such as certain lighting configurations (phototaxis), vibrations in the environment (vibrotaxis), certain chemical compounds (chemotaxis), etc. Although these responses are minimized with age, even becoming undetectable.
- Another factor that causes reactions to a stimulus to decrease is **habituation and memory**. The greater the stimuli number the more animal remembers it and stops reacting to it, therefore the more times an action is applied the more effectiveness decreases.
- Returning to the irregularity issue in lighting, and the need for its low intensity, difficulties can arise when issues of dirt, occlusions,

condensation or contamination appear. Another problem is the medium darkening over time. These problems can be minimized with better lighting, however if they are significant problems the lighting will not be able to prevent errors in detection. The key is to avoid these effects.

- *C. elegans* stop moving with age, so they reach a lethargy stage before death. Thus, sensitivity in motion detection is important in old age. Stimulation or higher image resolution can be used to determine movement.
- **Aggregation** is the most common problem and difficult to solve, since when several worms connect it becomes very difficult to discern if it is a cluster of worms or it is dirt. In case to be a cluster it is not known how many worms there are and if these are alive or not.
- Lifespan and healthspan machines are usually scanners or cameras attached to microscopes. The scanners have a very low scanning frequency, thus they cannot perform tracking in the first days. The cameras attached to microscopes only frame a small area, therefore they cannot take the entire plate.
- The illumination system is usually a light whose illumination loses intensity radially, so when the intensity is low, the image quality is poor at the image edges.
- The dust particles have sizes and shapes very similar to *C. elegans*, which is why they tend to cause false positives in detection. The ways to avoid these particles are to be into clean rooms, which are not usually used due to the large investment involved; and the other way is to avoid moving the Petri dish once it is placed in the inspection machine, but this solution avoids being able to carry out more than one experiment at once.

According to the above conditions, the following objectives were planned:

- Must have a controllable lighting method, to be able to regulate the light according to interest (minimal excitement or excitement on purpose) that reaches each *C. elegans*.

- Must improve image quality with uniform lighting.
- Must develop a technique that allows classifying *C. elegans* alive or dead, without being affected by changes in position, appearances of dirt, contamination, aggregations, occlusions, condensations.
- Must increase sensitivity by developing an automated method that can stimulate nematodes to move, without modifying the worm's biological factors. Also adjust the stimulus to avoid the habituation effect.
- Must increase sensitivity, by developing a technique that allows multiple resolutions to be used simultaneously.

Contributions

Some of the new contributions established in this thesis are flexible techniques that offer a great variety of possibilities for experimentation and study.

Until now, no method had been designed that would detect *C. elegans* and classify alive or dead in lifespan assays, also allowing to replace standard Petri dishes. This entails various additional identification problems such as the translations and rotations of the nematode positions, in addition to introducing fluff on the lid. Once these problems have been solved, the detection software method is very useful to allow the same vision system to inspect as many Petri dishes as desired, this entails being able to automate the system for placing and replacing the plates.

Another of these flexible contributions is intelligent lighting, because by being able to illuminate point to point with a variety of three wavelengths, it allows the application of an infinite number of control strategies. It also allows drawing lighting gradients or flashes that can cause a flight reaction (phototaxis) of *C. elegans*, this allows experiments to evaluate if the nematode can be controlled to make it go to a desired location, perform learning and memory tests or simply to verify that they are alive in lifespan trials.

The vibrotaxis method has been shown to improve live or dead grading in the lifespan assay. It can be used as a substitute for the manual skewer in automated tests, as it causes this flight reaction, and also applies the same intensity and duration at the same time to all the animals on the plate. This method also provides flexibility, since the time or intensity or duration parameters can be modified, it can be used for learning and memory experiments, adaptation or cognitive function.

The multiview robot opens a new way in which to analyze in greater detail those characteristics in *C. elegans* that can provide information that classifies their behaviors. It also allows us to compare two images of different resolutions simultaneously and this can lead us to relate the characteristics of high resolution with those of low.

General evaluation

The *C. elegans* inspection in standard Petri plates poses a challenge because there are certain objects with shapes and sizes that can be very similar to nematodes causing false positives.

In addition, these animals have biological characteristics that can alter their life, so it occurred to us that both problems could be addressed by controlling lighting.

Let's start with the image quality improvement. It was important to analyse all the lighting factors that could affect image quality. For example, in our case, achieving a pure backlight illumination improve quality. For this reason, a box was used to isolate the system from outside ambient lighting, and the interior was cover with materials little reflective to reduce the illumination system light bounced off on the box walls. This allows reducing the grey levels of worms, which went from 13 low levels to low ones of zero.

Different reflections and refractions appeared on the standard Petri plate walls. Reflections could produce a mirror effect on the wall to show that reflected worms were near the walls. Regarding refractions, some light beams that passed through the Petri walls did not arrive at the camera,

which produced dark circles near the walls. These areas were about 6% of the inspected area, which means that it was unlikely that a worm would be found in that areas because an *E. coli* lawn was strategically placed in the middle of the plate. Moreover, special segmentation software solutions can be applied for these areas.

All these issues are very important to capture an image with the least possible interference. The image is the output matrix of the feedback control loop, so interference can cause the system to be uncontrollable. Having reduced these possible sources of errors, then the calibration between the camera and the illumination display is possible.

Every time that system was booted, homography calibration was performed. Once calibrated, the plate was inserted into the system, this new media provoked small refractions that increased the calibration errors, what produce small intensity waves on the image. An alternative procedure would be to calibrate homography for each plate, but the experiments showed that calibration with no plate was robust enough.

In terms of control, after a stable lighting pattern was achieved in a certain number of iterations *k* of the control loop, the lighting pattern tends to a composition of maximum (white) and minimum (black) values. However, to allow an effective wavelengths control strategy, the control action was fixed earlier when the control error was low. For this reason, a detection event strategy was defined to fix the control action, but other strategies can be used.

As stated, the wavelengths near the ultraviolet are more detrimental for *C. elegans*' survival, hence the strategic order (R, G, B) upon the control action was chosen. Therefore, blue light proved more detrimental than green light, and green light was more detrimental than red light [32]. Given this strategy, most of the plate was illuminated with light that was close to red and some green (255, 190, 0). The maximum control action (255, 255, 255), was applied automatically, but only to opaque zones (Petri walls and strong contamination) and worms. To detect worms in opaque zones was not possible, thus applying blue light to these zones is a

very interesting strategy because worms tend to avoid blue-illuminated zones [33]. In addition, this withdrawal by blue light could improve lifespan results of the whole plate. In our case, the maximum intensity level of the blue light was applied to worms because the monitoring process lasted only few seconds. Depending on the application, other control strategies can also be implemented by applying light as desired.

In order to avoid control instabilities due to calibration errors, stable PIDs regulators were introduced and a diffuser was added to the display. It is possible to emulate a diffuser by measuring output (y_k) as the average of 30 pixels, which was related to the same texel. However, if we used a diffuser, the computational load required to calculate the averages would be avoided. But if diffuser is used, another problem could appear due to the texel lighting affecting not only the pixels associated with it in calibration, but also those associated with neighbouring texels. Hence it became a coupled system by conferring interactions in the control. In order to fix these interactions, a controller with a small k_p was designed.

This method compensates automatically different illumination changes. For example, media transparency changes on all the assay days, whose mean image grey level can vary from 70 to 55; also, may exist changes in ambient conditions, such as smooth condensation on lids, whose mean image grey level can vary by 18 grey levels; light derivatives of the illumination source during its lifetime. Therefore, the control technique simplifies the worm segmentation problem by reaching near uniform illumination throughout the image. As Fisher index shows the contrast is increased (from 0.2049 ± 0.0267 to 0.8636 ± 0.1427), this might both increase the quality in all areas (by reducing information loss) and obtain constant illumination in the whole area (by allowing fixed threshold image segmentation).

This image improvement can be significant in some Petri dish areas, in such a way that it can improve the classification between dust, precipitation, depositions, contamination, which can camouflage or be confused with a *C. elegans*. But even so the possibilities that these causes

prevent the correct animal detection, we define the software techniques based on movement and the filtering of outlier values.

The post-processing filter was applied to minimise final count errors, which took into account the probability of errors occurring on different days by applying various error correction strategies. The optimal corrective action considered that all the errors on the first assay days were false-negatives and all the errors on the last days were false-positives. False-negatives probability was higher on the first assay days, therefore was assumed all errors were false-positives on this period, and the last assay days was better approach to correct errors on by considering them all to be false-positives.

The post-processing reduced the automated counting errors from 0.32±1.4 individuals to 0.06 ± 0.9 individuals per plate, and the survival curve error reduced from 4.62 ± 2.01% to 2.24 ± 0.55%. Outliers were alleviated, hence provided more robustness to plate displacements and dirty environments, and helped to ease typical occlusion problems due to aggregation, hiding, contamination or condensation. The automated counting errors of live worms is a Gaussian distribution, therefore the larger the sample, the fewer errors on the lifespan curve. Nevertheless, by reducing errors with post-processing, the population required for a given error is smaller, which implies shorter experimentation and analysis times, and cheaper costs in relation to plates, animals, storage, etc.

To reduce the negative errors caused by occlusions (wall shadows, aggregation, etc.) were developed the following methods: The motion analysis was applied to wall zones to detect live worms despite occluded dark rings. On the other hand, the probability of three-worm aggregations came close to zero when using 10 to 15 worms on a 27.5 mm-radius plate. When a two-worm aggregation was detected (probability of 1.09%), an optimisation process was applied in an attempt to disaggregate them.

Two strains with different lifespan, N2 and *daf-2*, were assessed by this method. The post-processing method is a good lifespan approach method for any nematode strain, even for a long lifespan during which dirt and

contamination progressively increase. It may also be suitable to set the mean lifespan as an optimum day to change the correction strategy.

To integrate all of the above together and verify that there are no alterations in the animal behavior, a device is designed that also facilitates the experiment handling.

A SiViS prototype has been designed, developed and validated for lifespan assays. For lifespan assays is a good approach in automated worm-count, without significantly statistical differences between automated and manual counts. In addition, its repeatability is good because no significant differences were found between independent measurements. The experiments were performed for strains with different lifespan, which are the N2 strain, and N2 with metformin treatment or to other strains (*daf-2* and *daf-16*). Therefore, the methods are suitable for a variety of lifespan assays.

Considering that SiViS is a satisfactory measuring system, it has several other advantages. The first, it relates to the possibility of replacing the Petri plates during the experiment, thus enabling the monitoring of any plate at any moment. Another advantage is its small size, thus it can be easily scaled up by increasing device number. In addition to this, plate replacement could be automated to achieve a fully autonomous lifespan assay process.

It is a flexible system because, in addition to lifespan assays, it can be used to measure other *C. elegans* phenotypes, such as those related to dispersion, healthspan, memory or food preferences, among others, by simple code modification.

The above methods are designed to try to achieve maximum reliability in detecting the life of *C. elegans*. However, errors continue to exist that make it necessary to increase the detection sensitivity. As the techniques are based on motion detection, the increase in sensitivity will depend on this variable. To better quantify the movement, it can be achieved in two ways or by increasing the camera resolution, or by stimulating the animal. It was decided to opt for stimulation because the appropriate hardware is

not always available, and also because in traditional manual methods they are also stimulated by poking them individually with a spike.

In previous bibliography it was possible to verify that vibrotaxis produced this withdrawal response, therefore we carried out the appropriate experimentation to confirm that applying this stimulus improves the detection of *C. elegans*.

Vibrotaxis improves live worm detection, which is achieved by worm motion response rates of more than 93%. What demonstrates this is an effective stimulation method and, in some cases, the sensitivity for lifespan of the automated systems under the same conditions even doubled (from 2.6% to 1.2%), and the error variance per plate reduced by half (from ±1 individual to ±0.6). According to the findings obtained, vibration did not statistically alter *C. elegans* life expectancy (wild-type strain).

Therefore, this new simple automated inspection system increases throughput over manual methods and improves sensitivity in detection for automated methods. Worms can be stimulated all together, which releases the expert from these repetitive tasks. Therefore, to reduce the sample size for the same error value is possible, thus time and costs are reduced. Moreover, worms react to vibration rapidly. Hence sufficient motion leads to more rapid motion detection, which in turn allows for a shorter monitoring period.

Worms have memory, thus can remember past non-threatening situations and recognise similar ones, this recall causes animal habituation, what reduces its movement. Although, high vibration makes nematode difficult to remain still. Thereby, an overstimulation causes habituation what can be a limitation to improve lifespan results. Accordingly, stimulation needs to be as infrequent as possible, so stimulation should be initiated on days when worms begin to slightly move.

Smooth condensation problems can be alleviated by our technique given both the position change and or image grey level variation.

Once the previous methods had been explored and their possibilities for the analysis of behavior studied, a new line is opened that would allow us to increase the image information, by increasing the resolution and the zoom of the images. Our motivation was to analyse what is really happening with the low-resolution images which is been working with. Therefore, the multi-view robot was developed to take simultaneous images at different scales. This development in itself was more complex, so we raised a first manageable challenge based on the most basic principle of the robot, which is tracking.

The multi-view Cartesian robot can inspect *C. elegans* in standard Petri dishes and extract information to find statistical differences between *C. elegans* movements. These differences can be observed between strains with very subtle differences (wild type and *vltIs66[unc-25p::144CAG]*). These different image resolution and simultaneous tracking allows monitor worm movement in standard Petri dishes (55 mm of diameter), with no need to restrict the nematode movement by containing them in microchambers, micropillars or small multi-well plates. This bigger area improves negative behavioural alterations caused by smaller spaces.

Aggregation with other worms may cause the tracking algorithm to lose the identity of the tracked animal. To try to avoid worm clusters, the worm number per plate (55 mm) was approximately of 30 worms, the probability of contact between them is approximately 3% [60].

This new line opens up new and interesting research possibilities.

CHAPTER 4
CONCLUSIONS

Goal accomplishment

An extensive study of the state of the art has been carried out based on previous publications, in addition to the information transmitted by the collaboration with the ADM Biopolis and La Fe research groups.

Those approaches to the problems of automation of the experiments have been successfully resolved. The resolution to the Lifespan and Healthspan trials, plus a new and innovative way that opens up new possibilities.

Future works

The multi-view Cartesian robot integrates almost all the techniques announced in this thesis, so it is a perfect future line. This generates good images with which to extract subtle characteristics, however it can happen that the classification of some behaviors is very difficult, because even at the human level it is not able to discern difference. Therefore, Computational Neural Networks (NN) can be used to find these differences automatically. Studies with NN have already been initiated in methods such as the live or dead classification for lifespan[3] experiments with optimal results, so these techniques can be improved to be able to classify types of movements. The trajectories of the movements can show signs of neuronal, muscular or health problems; so a line of the future is the recognition of patterns in the movement to identify neurodegenerative diseases in *C. elegans*.

With the NN, one could even try to find a relationship between the high-resolution images with the low-resolution ones, in such a way that thanks to the high-resolution images they help us to classify determining details in the low-resolution images that, without that extra information, could have been previously overlooked. Besides if there were a greater number of worms in the Petri dish, the probability of contact and interaction between worms would increase. As a future work, it would be interesting

[3] García Garví, A.; Puchalt, J.C.; Layana Castro, P.E.; Navarro Moya, F.; Sánchez-Salmerón, A.-J. Towards Lifespan Automation for Caenorhabditis elegans Based on Deep Learning: Analysing Convolutional and Recurrent Neural Networks for Dead or Live Classification. Sensors 2021, 21, 4943. https://doi.org/10.3390/s21144943

to solve the problem of re-identification of worms using the high-resolution images by trying to avoid data cancelation in a future study.

In addition, this robot can perform all the experiments mentioned in this thesis: lifespan, healthspan, learning and memory, adaptation and cognitive function, so based on this, new techniques can be improved or designed: computational (such as the Neural Networks previously described), robotic, image capture...

PAPER BIBLIOGRAPHY

[1] S. Brenner, “THE GENETICS OF CAENORHABDITIS ELEGANS,” *Genetics*, vol. 77, no. 1, pp. 71–94, 1974.

[2] H. A. Tissenbaum, “Using C. elegans for aging research,” *Invertebrate Reproduction & Development*, vol. 59, no. sup1, pp. 59–63, 2015, doi: 10.1080/07924259.2014.940470.

[3] C. J. Kenyon, “The genetics of ageing,” *Nature*, vol. 464, p. 504, Mar. 2010.

[4] L. Guarente and C. Kenyon, “Genetic pathways that regulate ageing in model organisms,” *Nature*, vol. 408, p. 255, Nov. 2000.

[5] D. W. Walker, G. McColl, N. L. Jenkins, J. Harris, and G. J. Lithgow, “Evolution of lifespan in C. elegans.,” *Nature*, vol. 405, no. 6784, pp. 296–297, 2000, doi: 10.1038/35012693.

[6] F. R. G. Amrit, R. Ratnappan, S. A. Keith, and A. Ghazi, “The C. elegans lifespan assay toolkit,” *Methods*, vol. 68, no. 3, pp. 465–475, 2014, doi: 10.1016/j.ymeth.2014.04.002.

[7] M. R. Klass, “Aging in the nematode Caenorhabditis elegans: Major biological and environmental factors influencing life span,” *Mechanisms of Ageing and Development*, vol. 6, pp. 413–429, 1977, doi: https://doi.org/10.1016/0047-6374(77)90043-4.

[8] L. Aitlhadj and S. R. Stürzenbaum, “The use of FUdR can cause prolonged longevity in mutant nematodes,” *Mechanisms of Ageing and Development*, vol. 131, no. 5, pp. 364–365, 2010, doi: https://doi.org/10.1016/j.mad.2010.03.002.

[9] R. Hosono, “Age dependent changes in the behavior of Caenorhabditis elegans on attraction to Escherichia coli,” *Experimental Gerontology*, vol. 13, no. 1, pp. 31–36, 1978, doi: https://doi.org/10.1016/0531-5565(78)90027-X.

[10] R. Hosono, “Sterilization and growth inhibition of Caenorhabditis elegans by 5-fluorodeoxyuridine,” *Experimental Gerontology*, vol. 13, no. 5, pp. 369–373, 1978, doi: https://doi.org/10.1016/0531-5565(78)90047-5.

[11] B. Onken and M. Driscoll, “Metformin Induces a Dietary Restriction–Like State and the Oxidative Stress Response to Extend C. elegans Healthspan via AMPK, LKB1, and SKN-1,” *PLOS ONE*, vol. 5, no. 1, pp. 1–13, 2010, doi: 10.1371/journal.pone.0008758.

[12] S. A. Keith, F. R. G. Amrit, R. Ratnappan, and A. Ghazi, “The C. elegans healthspan and stress-resistance assay toolkit,” *Methods*, vol. 68, no. 3, pp. 476–486, 2014, doi: 10.1016/j.ymeth.2014.04.003.

[13] J.-H. Hahm *et al.*, “C. elegans maximum velocity correlates with healthspan and is maintained in worms with an insulin receptor mutation,” *NATURE COMMUNICATIONS*, vol. 6, Nov. 2015, doi: 10.1038/ncomms9919.

[14] M. Hertweck and R. Baumeister, “Automated assays to study longevity in C. elegans,” in *Mechanisms of Ageing and Development*, 2005, vol. 126, no. 1, pp. 139–145. doi: 10.1016/j.mad.2004.09.010.

[15] N. A. Swierczek, A. C. Giles, C. H. Rankin, and R. A. Kerr, “High-throughput behavioral analysis in C. elegans,” *Nature Methods*, vol. 8, no. 7, pp. 592-U112, 2011, doi: 10.1038/nmeth.1625.

[16] N. Stroustrup, B. E. Ulmschneider, Z. M. Nash, I. F. López-Moyado, J. Apfeld, and W. Fontana, “The Caenorhabditis elegans Lifespan Machine.,” *Nature methods*, vol. 10, no. 7, pp. 665–70, 2013, doi: 10.1038/nmeth.2475.

[17] T. Puckering, J. Thompson, S. Sathyamurthy, S. Sukumar, T. Shapira, and P. Ebert, “Automated Wormscan,” *F1000Research*, vol. 6, p. 192, Sep. 2017, doi: 10.12688/f1000research.10767.2.

[18] E. Fontaine, J. Burdick, and A. Barr, “Automated Tracking of Multiple C. Elegans,” in *2006 International Conference of the IEEE Engineering*

in Medicine and Biology Society, 2006, pp. 3716–3719. doi: 10.1109/IEMBS.2006.260657.

[19] S. K. Jung, B. Aleman-Meza, C. Riepe, and W. Zhong, "QuantWorm: A comprehensive software package for Caenorhabditis elegans phenotypic assays," *PLoS ONE*, vol. 9, no. 1, 2014, doi: 10.1371/journal.pone.0084830.

[20] N. Roussel, C. A. Morton, F. P. Finger, and B. Roysam, "A Computational Model for C. elegans Locomotory Behavior: Application to Multiworm Tracking," *IEEE Transactions on Biomedical Engineering*, vol. 54, no. 10, pp. 1786–1797, 2007, doi: 10.1109/TBME.2007.894981.

[21] M. D. Mathew, N. D. Mathew, and P. R. Ebert, "WormScan: A Technique for High-Throughput Phenotypic Analysis of Caenorhabditis elegans," *PLOS ONE*, vol. 7, no. 3, Mar. 2012, doi: 10.1371/journal.pone.0033483.

[22] N. Otsu, "A Threshold Selection Method from Gray-Level Histograms," *IEEE Transactions on Systems, Man, and Cybernetics*, vol. 9, no. 1, pp. 62–66, 1979, doi: 10.1109/TSMC.1979.4310076.

[23] C. Wählby *et al.*, "An image analysis toolbox for high-throughput C. elegans assays.," *Nature methods*, vol. 9, no. 7, pp. 714–6, 2012, doi: 10.1038/nmeth.1984.

[24] W. Chen *et al.*, "Segmenting Microscopy Images of Multi-Well Plates Based on Image Contrast," *Microscopy and Microanalysis*, vol. 23, no. 5, pp. 932–937, 2017, doi: DOI: 10.1017/S1431927617012375.

[25] D. Kainmueller, F. Jug, C. Rother, and G. Myers, "Active Graph Matching for Automatic Joint Segmentation and Annotation of C. elegans BT - Medical Image Computing and Computer-Assisted Intervention – MICCAI 2014," 2014, pp. 81–88.

[26] T. R. Raviv *et al.*, "Morphology-Guided Graph Search for Untangling Objects: C. elegans Analysis BT - Medical Image Computing and Computer-Assisted Intervention – MICCAI 2010," 2010, pp. 634–641.

[27] G. Tsechpenakis, L. Bianchi, D. N. Metaxas, and M. Driscoll, “A novel computational approach for simultaneous tracking and feature extraction of C. elegans populations in fluid environments,” *IEEE Transactions on Biomedical Engineering*, vol. 55, no. 5, pp. 1539–1549, 2008, doi: 10.1109/TBME.2008.918582.

[28] C. J. Cronin *et al.*, “An automated system for measuring parameters of nematode sinusoidal movement,” *BMC GENETICS*, vol. 6, Feb. 2005, doi: 10.1186/1471-2156-6-5.

[29] C. Restif, C. Ibáñez-Ventoso, M. M. Vora, S. Guo, D. Metaxas, and M. Driscoll, “CeleST: Computer Vision Software for Quantitative Analysis of C. elegans Swim Behavior Reveals Novel Features of Locomotion,” *PLoS Computational Biology*, vol. 10, no. 7, 2014, doi: 10.1371/journal.pcbi.1003702.

[30] W. Geng, P. Cosman, J.-H. Baek, C. C. Berry, and W. R. Schafer, “Quantitative Classification and Natural Clustering of Caenorhabditis elegans Behavioral Phenotypes,” *Genetics*, vol. 165, no. 3, pp. 1117 LP – 1126, Dec. 2003.

[31] W. Geng, P. Cosman, C. C. Berry, Z. Feng, and W. R. Schafer, “Automatic tracking, feature extraction and classification of C. elegans phenotypes,” *IEEE Transactions on Biomedical Engineering*, vol. 51, no. 10, pp. 1811–1820, 2004, doi: 10.1109/TBME.2004.831532.

[32] C. D. De Magalhaes Filho, B. Henriquez, N. E. Seah, R. M. Evans, L. R. Lapierre, and A. Dillin, “Visible light reduces C. elegans longevity,” *Nature Communications*, vol. 9, no. 1, 2018, doi: 10.1038/s41467-018-02934-5.

[33] S. L. Edwards *et al.*, “A novel molecular solution for ultraviolet light detection in Caenorhabditis elegans,” *PLOS BIOLOGY*, vol. 6, no. 8, pp. 1715–1729, 2008, doi: 10.1371/journal.pbio.0060198.

[34] K. H. Lee and M. Aschner, “A Simple Light Stimulation of Caenorhabditis elegans,” in *Current Protocols in Toxicology*, John Wiley & Sons, Inc., 2001. doi: 10.1002/0471140856.tx1121s67.

[35] M. A. Churgin, S.-K. Jung, C.-C. Yu, X. Chen, D. M. Raizen, and C. Fang-Yen, “Longitudinal imaging of Caenorhabditis elegans in a microfabricated device reveals variation in behavioral decline during aging.,” *eLife*, vol. 6, May 2017, doi: 10.7554/eLife.26652.

[36] C. Ricolfe-Viala and A.-J. Sanchez-Salmeron, “Camera calibration under optimal conditions.,” *Optics express*, vol. 19, no. 11, pp. 10769–10775, 2011, doi: 10.1364/OE.19.010769.

[37] G. Percoco, F. Lavecchia, and A. J. S. Salmerón, “Preliminary study on the 3D digitization of millimeter scale products by means of photogrammetry,” in *Procedia CIRP*, 2015, vol. 33, pp. 257–262. doi: 10.1016/j.procir.2015.06.046.

[38] J. Juchem, S. Lefebvre, T. Mac Thi, and C.-M. Ionescu, “An analysis of dynamic lighting control in landscape offices,” in *Preprints of the 3rd IFAC Conference on Advances in Proportional-Integral-Derivative Control (PID)*, 2018, pp. 232–237.

[39] R. De Keyser and C. Ionescu, “Modelling and simulation of a lighting control system,” *Simulation Modelling Practice and Theory*, vol. 18, no. 2, pp. 165–176, 2010, doi: https://doi.org/10.1016/j.simpat.2009.10.003.

[40] S. Maldonado and R. Weber, “A wrapper method for feature selection using Support Vector Machines,” *Information Sciences*, vol. 179, no. 13, pp. 2208–2217, 2009, doi: https://doi.org/10.1016/j.ins.2009.02.014.

[41] M. Hertweck and R. Baumeister, “Automated assays to study longevity in C. elegans,” *Mechanisms of Ageing and Development*, vol. 126, no. 1, pp. 139–145, 2005, doi: 10.1016/j.mad.2004.09.010.

[42] J. C. Puchalt, A.-J. Sánchez-Salmerón, P. Martorell Guerola, and S. Genovés Martínez, “Active backlight for automating visual

monitoring: An analysis of a lighting control technique for Caenorhabditis elegans cultured on standard Petri plates," *PLOS ONE*, vol. 14, no. 4, p. e0215548, Apr. 2019.

[43] T. Stiernagle, "Maintenance of C. elegans," *The C. elegans Research Community, WormBook*, 2006. https://www.ncbi.nlm.nih.gov/books/NBK19649/?report=classic

[44] P. T. McGrath *et al.*, "Quantitative Mapping of a Digenic Behavioral Trait Implicates Globin Variation in C. elegans Sensory Behaviors," *Neuron*, vol. 61, no. 5, pp. 692–699, 2009, doi: https://doi.org/10.1016/j.neuron.2009.02.012.

[45] M. G. Sterken, L. B. Snoek, J. E. Kammenga, and E. C. Andersen, "The laboratory domestication of Caenorhabditis elegans," *Trends in genetics : TIG*, vol. 31, no. 5, pp. 224–231, May 2015, doi: 10.1016/j.tig.2015.02.009.

[46] C. Kenyon, J. Chang, E. Gensch, A. Rudner, and R. Tabtiang, "A C. elegans mutant that lives twice as long as wild type," *Nature*, vol. 366, no. 6454, pp. 461–464, 1993, doi: 10.1038/366461a0.

[47] J. B. Dorman, B. Albinder, T. Shroyer, and C. Kenyon, "The age-1 and daf-2 genes function in a common pathway to control the lifespan of Caenorhabditis elegans.," *Genetics*, vol. 141, no. 4, pp. 1399–1406, 1995.

[48] H. A. Zariwala, A. C. Miller, S. Faumont, and S. R. Lockery, "Step response analysis of thermotaxis in Caenorhabditis elegans.," *The Journal of neuroscience : the official journal of the Society for Neuroscience*, vol. 23, no. 10, pp. 4369–77, 2003.

[49] C. H. RANKIN and B. S. BROSTER, "FACTORS AFFECTING HABITUATION AND RECOVERY FROM HABITUATION IN THE NEMATODE CAENORHABDITIS-ELEGANS," *BEHAVIORAL NEUROSCIENCE*, vol. 106, no. 2, pp. 239–249, 1992, doi: 10.1037//0735-7044.106.2.239.

[50] E. M. HEDGECOCK and R. L. RUSSELL, “NORMAL AND MUTANT THERMOTAXIS IN NEMATODE CAENORHABDITIS-ELEGANS,” *PROCEEDINGS OF THE NATIONAL ACADEMY OF SCIENCES OF THE UNITED STATES OF AMERICA*, vol. 72, no. 10, pp. 4061–4065, 1975, doi: 10.1073/pnas.72.10.4061.

[51] P. A. Kralchevsky and K. Nagayama, “Capillary interactions between particles bound to interfaces, liquid films and biomembranes,” *Advances in Colloid and Interface Science*, vol. 85, no. 2, pp. 145–192, 2000, doi: https://doi.org/10.1016/S0001-8686(99)00016-0.

[52] Y. Cheon, H. Hwang, and K. Kim, “Plasticity of pheromone-mediated avoidance behavior in C. elegans,” *Journal of Neurogenetics*, vol. 34, no. 3–4, pp. 420–426, 2020, doi: 10.1080/01677063.2020.1802723.

[53] T. Yoshimizu, H. Shidara, K. Ashida, K. Hotta, and K. Oka, “Effect of interactions among individuals on the chemotaxis behaviours of Caenorhabditis elegans,” *Journal of Experimental Biology*, vol. 221, no. 11, 2018, doi: 10.1242/jeb.182790.

[54] S. Park, H. Hwang, S.-W. Nam, F. Martinez, R. H. Austin, and W. S. Ryu, “Enhanced Caenorhabditis elegans Locomotion in a Structured Microfluidic Environment,” *PLOS ONE*, vol. 3, no. 6, pp. 1–5, 2008, doi: 10.1371/journal.pone.0002550.

[55] S. R. Lockery *et al.*, “Artificial Dirt: Microfluidic Substrates for Nematode Neurobiology and Behavior,” *Journal of Neurophysiology*, vol. 99, no. 6, pp. 3136–3143, 2008, doi: 10.1152/jn.91327.2007.

[56] M. Rahman *et al.*, “NemaLife chip: a micropillar-based microfluidic culture device optimized for aging studies in crawling C. elegans,” *Scientific Reports*, vol. 10, no. 1, p. 16190, 2020, doi: 10.1038/s41598-020-73002-6.

[57] B. Xian *et al.*, “WormFarm: a quantitative control and measurement device toward automated Caenorhabditis elegans aging analysis,” *AGING CELL*, vol. 12, no. 3, pp. 398–409, Jun. 2013, doi: 10.1111/acel.12063.

[58] W.-J. Kuo and H.-S. Chuang, “Development of an Image-Based Algorithm for the Motility Characterizations of the Nematode Caenorhabditis Elegans,” in *1ST GLOBAL CONFERENCE ON BIOMEDICAL ENGINEERING & 9TH ASIAN-PACIFIC CONFERENCE ON MEDICAL AND BIOLOGICAL ENGINEERING*, 2015, vol. 47, pp. 107–110. doi: 10.1007/978-3-319-12262-5_30.

[59] M. S. Gill, A. Olsen, J. N. Sampayo, and G. J. Lithgow, “An automated high-throughput assay for survival of the nematode Caenorhabditis elegans,” *FREE RADICAL BIOLOGY AND MEDICINE*, vol. 35, no. 6, pp. 558–565, Sep. 2003, doi: 10.1016/S0891-5849(03)00328-9.

[60] J. C. Puchalt, A.-J. Sánchez-Salmerón, E. Ivorra, S. Genovés Martínez, R. Martínez, and P. Martorell Guerola, “Improving lifespan automation for Caenorhabditis elegans by using image processing and a post-processing adaptive data filter,” *Scientific Reports*, vol. 10, no. 1, p. 8729, 2020, doi: 10.1038/s41598-020-65619-4.

[61] F. Cabreiro *et al.*, “Metformin retards aging in C. elegans by altering microbial folate and methionine metabolism.,” *Cell*, vol. 153, no. 1, pp. 228–239, Mar. 2013, doi: 10.1016/j.cell.2013.02.035.

[62] W. Luyten *et al.*, “Ageing with elegans: a research proposal to map healthspan pathways,” *Biogerontology*, pp. 1–12, 2016, doi: 10.1007/s10522-016-9644-x.

[63] S. C. Lin, M. H. Lin, P. Horvath, K. L. Reddy, and R. V Storti, “PDP1, a novel Drosophila PAR domain bZIP transcription factor expressed in developing mesoderm, endoderm and ectoderm, is a transcriptional regulator of somatic muscle genes.,” *Development (Cambridge, England)*, vol. 124, no. 22, pp. 4685–4696, Nov. 1997.

[64] S. Ogg *et al.*, “The Fork head transcription factor DAF-16 transduces insulin-like metabolic and longevity signals in C. elegans.,” *Nature*, vol. 389, no. 6654, pp. 994–999, Oct. 1997, doi: 10.1038/40194.

[65] J. Chen *et al.*, “Kinetochore inactivation by expression of a repressive mRNA,” *eLife*, vol. 6, p. e27417, Sep. 2017, doi: 10.7554/eLife.27417.

[66] L. A. Herndon *et al.*, “Stochastic and genetic factors influence tissue-specific decline in ageing C. elegans,” *Nature*, vol. 419, p. 808, Oct. 2002.

[67] B. C. Petzold, S.-J. Park, E. A. Mazzochette, M. B. Goodman, and B. L. Pruitt, “MEMS-based force-clamp analysis of the role of body stiffness in C. elegans touch sensation,” *INTEGRATIVE BIOLOGY*, vol. 5, no. 6, pp. 853–864, 2013, doi: 10.1039/c3ib20293c.

[68] Md. A. Islam *et al.*, “Probabilistic Reachability Analysis of the Tap Withdrawal Circuit in Caenorhabditis elegans,” in *2016 IEEE INTERNATIONAL HIGH LEVEL DESIGN VALIDATION AND TEST WORKSHOP (HLDVT)*, 2016, pp. 170–177.

[69] A. S, K. K, and H. R, “Hierarchy of habituation induced by mechanical stimuli in Caenorhabditis elegans.,” *Zoological Science*, 1999, doi: 10.2108/zsj.16.423.

[70] S. R. Wicks and C. H. Rankin, “The integration of antagonistic reflexes revealed by laser ablation of identified neurons determines habituation kinetics of the Caenorhabditis elegans tap withdrawal response,” *JOURNAL OF COMPARATIVE PHYSIOLOGY A-SENSORY NEURAL AND BEHAVIORAL PHYSIOLOGY*, vol. 179, no. 5, pp. 675–685, Nov. 1996, doi: 10.1007/BF00216131.

[71] S. R. WICKS and C. H. RANKIN, “INTEGRATION OF MECHANOSENSORY STIMULI IN CAENORHABDITIS-ELEGANS,” *JOURNAL OF NEUROSCIENCE*, vol. 15, no. 3, 2, pp. 2434–2444, Mar. 1995.

[72] M. Chalfie, “Modulation of C. elegans Touch Sensitivity Is Integrated at Multiple Levels,” *Journal of Neuroscience*, vol. 34, no. 19, pp. 6522–6536, 2014, doi: 10.1523/JNEUROSCI.0022-14.2014.

[73] P. G. Childs *et al.*, “Use of nanoscale mechanical stimulation for control and manipulation of cell behaviour,” *ACTA BIOMATERIALIA*, vol. 34, no. SI, pp. 159–168, 2016, doi: 10.1016/j.actbio.2015.11.045.

[74] R. Meyhöfer and J. Casas, “Vibratory stimuli in host location by parasitic wasps,” *Journal of Insect Physiology*, vol. 45, no. 11, pp. 967–971, 1999, doi: http://dx.doi.org/10.1016/S0022-1910(99)00060-8.

[75] T. Sugi, E. Okumura, K. Kiso, and R. Igarashi, “Nanoscale Mechanical Stimulation Method for Quantifying C-elegans Mechanosensory Behavior and Memory,” *ANALYTICAL SCIENCES*, vol. 32, no. 11, SI, pp. 1159–1164, Nov. 2016.

[76] M. CHALFIE, J. E. SULSTON, J. G. WHITE, E. SOUTHGATE, J. N. THOMSON, and S. BRENNER, “THE NEURAL CIRCUIT FOR TOUCH SENSITIVITY IN CAENORHABDITIS-ELEGANS,” *JOURNAL OF NEUROSCIENCE*, vol. 5, no. 4, pp. 956–964, 1985.

[77] C. H. Rankin, C. D. O. Beck, and C. M. Chiba, “Caenorhabditis elegans: A new model system for the study of learning and memory,” *Behavioural Brain Research*, vol. 37, no. 1, pp. 89–92, 1990, doi: https://doi.org/10.1016/0166-4328(90)90074-O.

[78] W. Zhou *et al.*, “Ultrasound neuro-modulation chip: activation of sensory neurons in Caenorhabditis elegans by surface acoustic waves,” *Lab Chip*, vol. 17, no. 10, pp. 1725–1731, 2017, doi: 10.1039/C7LC00163K.

[79] A. Ward, J. Liu, Z. Feng, and X. Z. S. Xu, “Light-sensitive neurons and channels mediate phototaxis in C. elegans.,” *Nature neuroscience*, vol. 11, no. 8, pp. 916–22, 2008, doi: 10.1038/nn.2155.

[80] K. Lee and M. Aschner, “A Simple Light Stimulation of Caenorhabditis elegans,” *Current protocols in toxicology / editorial board, Mahin D. Maines (editor-in-chief) ... [et al.]*, vol. 67, pp. 11.21.1-11.21.5, 2016, doi: 10.1002/0471140856.tx1121s67.

[81] G. Nagel, M. Brauner, J. F. Liewald, N. Adeishvili, E. Bamberg, and A. Gottschalk, “Light Activation of Channelrhodopsin-2 in Excitable Cells of Caenorhabditis elegans Triggers Rapid Behavioral Responses,”

Current Biology, vol. 15, no. 24, pp. 2279–2284, 2005, doi: https://doi.org/10.1016/j.cub.2005.11.032.

[82] D. H. Mitchell, J. W. Stiles, J. Santelli, and D. R. Sanadi, "Synchronous growth and aging of Caenorhabditis elegans in the presence of fluorodeoxyuridine.," *Journal of gerontology*, vol. 34, no. 1, pp. 28–36, Jan. 1979.

[83] A. Jushaj, M. Churgin, B. Yao, M. de La Torre, C. Fang-Yen, and L. Temmerman, "Optimized criteria for locomotion-based healthspan evaluation in C. elegans using the WorMotel system," *PLOS ONE*, vol. 15, no. 3, p. e0229583, Mar. 2020, [Online]. Available: https://doi.org/10.1371/journal.pone.0229583

[84] J. A. Rollins, A. C. Howard, S. K. Dobbins, E. H. Washburn, and A. N. Rogers, "Assessing Health Span in Caenorhabditis elegans: Lessons From Short-Lived Mutants," *The Journals of Gerontology: Series A*, vol. 72, no. 4, pp. 473–480, 2017, doi: 10.1093/gerona/glw248.

[85] S. D. Buckingham and D. B. Sattelle, "Fast, automated measurement of nematode swimming (thrashing) without morphometry," *BMC neuroscience*, vol. 10, p. 84, Jul. 2009, doi: 10.1186/1471-2202-10-84.

[86] A. P. Gómez-Escribano *et al.*, "Synergistic activation of AMPK prevents from polyglutamine-induced toxicity in Caenorhabditis elegans," *Pharmacological Research*, vol. 161, p. 105105, 2020, doi: https://doi.org/10.1016/j.phrs.2020.105105.

[87] J. N. Pitt *et al.*, "WormBot, an open-source robotics platform for survival and behavior analysis in C. elegans," *GeroScience*, vol. 41, no. 6, pp. 961–973, 2019, doi: 10.1007/s11357-019-00124-9.

[88] K. N. Le, M. Zhan, Y. Cho, J. Wan, D. S. Patel, and H. Lu, "An automated platform to monitor long-term behavior and healthspan in Caenorhabditis elegans under precise environmental control," *Communications Biology*, vol. 3, no. 1, p. 297, 2020, doi: 10.1038/s42003-020-1013-2.

[89] A. L. Hsu, Z. Feng, M. Y. Hsieh, and X. Z. S. Xu, “Identification by machine vision of the rate of motor activity decline as a lifespan predictor in C. elegans,” *Neurobiology of Aging*, vol. 30, no. 9, pp. 1498–1503, 2009, doi: 10.1016/j.neurobiolaging.2007.12.007.

[90] K. Chung *et al.*, “Microfluidic chamber arrays for whole-organism behavior-based chemical screening,” *Lab on a chip*, vol. 11, no. 21, pp. 3689–3697, Nov. 2011, doi: 10.1039/c1lc20400a.

[91] B. P. Gupta and P. Rezai, “Microfluidic Approaches for Manipulating, Imaging, and Screening C. elegans,” *Micromachines*, vol. 7, no. 7, 2016.

[92] D. Lange, C. W. Storment, C. A. Conley, and G. T. A. Kovacs, “A microfluidic shadow imaging system for the study of the nematode Caenorhabditis elegans in space,” *Sensors and Actuators B: Chemical*, vol. 107, no. 2, pp. 904–914, 2005, doi: http://dx.doi.org/10.1016/j.snb.2004.12.039.

[93] C. B. Rohde, F. Zeng, R. Gonzalez-Rubio, M. Angel, and M. F. Yanik, “Microfluidic system for on-chip high-throughput whole-animal sorting and screening at subcellular resolution,” *Proceedings of the National Academy of Sciences*, vol. 104, no. 35, pp. 13891–13895, 2007, doi: 10.1073/pnas.0706513104.

[94] M. Rahman *et al.*, “NemaLife: A structured microfluidic culture device optimized for aging studies in crawling C. elegans,” *bioRxiv*, 2019, doi: 10.1101/675827.

[95] A. P. Gómez-Escribano *et al.*, “Multiple hormonal signalling pathways function cell-nonautonomously to control protein homeostasis in Caenorhabditis elegans,” *bioRxiv*, p. 551580, Jan. 2019, doi: 10.1101/551580.

[96] C. Frøkjær-Jensen, “Transposon-Assisted Genetic Engineering with Mos1-Mediated Single-Copy Insertion (MosSCI) BT - C. elegans: Methods and Applications,” D. Biron and G. Haspel, Eds. Totowa, NJ: Humana Press, 2015, pp. 49–58. doi: 10.1007/978-1-4939-2842-2_5.

[97] B. Chen, Q. Liu, Q. Ge, J. Xie, and Z.-W. Wang, “UNC-1 Regulates Gap Junctions Important to Locomotion in C. elegans,” *Current Biology*, vol. 17, no. 15, pp. 1334–1339, 2007, doi: https://doi.org/10.1016/j.cub.2007.06.060.